Alma Mater Studiorum – Università di Bologna

DOTTORATO DI RICERCA

Science for Conservation

Ciclo XXII

Settore scientifico disciplinare di afferenza: CHIM/12

TITOLO TESI

MULTI-POLLUTANTS IMPACT ON MODERN CEMENT BUILT HERITAGE

Presentata da: **Izabela Joanna Ozga**

Coordinatore Dottorato	**Relatori**
Prof. Rocco Mazzeo	**Prof.ssa Cristina Sabbioni**
	Prof. Luciano Morselli

Esame finale anno 2009

Acknowledgements

Index

Introduction

The rapid industrial and urban development occurred in recent decades has influenced the regional air quality by increasing the emission in the atmosphere of gaseous pollutants and aerosols from combustion processes. It is now well known that air pollution has impact not only on the human health but also accelerates the deterioration of building's façade, monuments and outdoor statues located in urban areas. The dry and wet deposition of air pollutants is demonstrated to be the most important damage factor in building material deterioration; in particular, aggressive airborne particulate matter has been proved to have a driving role in soiling of monument surfaces. The phenomenon of air multi-pollutants deposition has been extensively studied focusing on natural stones, especially marble and limestone, considering their wide use in the construction of many famous European monuments. The research performed on the deterioration of the built cultural heritage due to atmospheric pollutants indicates that SO_2 and particulate matter, primarily from the combustion of fossil fuels, are the most dangerous agents in case of marbles, limestone and dolostones. However, the decrease of SO_2 emission from industry and domestic fuel burning in recent years in many parts of Europe and the increase in traffic (raising the atmospheric concentration of nitrogen compounds, ozone and particles) have created a new multi-pollutant situation. Only recently, a special attention has been given to the dark component of aerosols, referred to black carbon (soot), which causes aesthetic impairment (blackening) of the building façade in areas protected from rain run-off. The formation of the so called black crusts effects in increase of material roughness and retention of particulate matter by building surfaces.

Despite many studies dedicated to the environmental damage of cultural heritage, in case of cement mortars, commonly used in the 20th century architecture, the deterioration due to air multi-pollutants impact is still not well explored and requires deeper investigation.

The present work centers on cement material-environment interaction, focusing on the investigation of the damage of the 20th century architecture induced by air multi-pollutants. For this purpose three European sites, exposed in different urban areas, have been selected for sampling and analysis of damage layers: Centennial Hall, Wroclaw (Poland), Chiesa dell'Autostrada del Sole, Florence (Italy), Casa Galleria Vichi, Florence (Italy).

Through the analytical studies of the samples collected at the buildings under consideration, the complete characterization of damage layer formed on cementitious monuments was achieved for the first time. The results from experimental work allowed the identification and prioritization of the air pollutants responsible for the surface deterioration considering the location of the buildings under study. The comprehensive diagnosis of damage layer and identification of the anthropogenic pollutants influencing its formation, represents a prerequisite for the sustainable protection and conservation of the modern built cultural heritage. The knowledge achieved during this research will be also useful in the construction sector for investigating the durability of modern building materials.

1. Impact of multi-pollutants on modern cement built heritage

The 20th century architecture, characterized by concrete constructions such as high buildings and gigantic bridges, seems to be indestructible. However, it has now been recognized that many modern buildings undergo rapid deterioration, especially in areas with high concentrations of air pollutants. It is demonstrated that the deposition of gaseous multi-pollutants and aerosols plays a major role in causing the deterioration of monuments and built cultural heritage in European cities.

The deposition of air pollutants (SO_2, NO_x, O_3, aerosols, etc.) on building materials can be divided into two sub-processes: dry and wet deposition: (1) dry deposition by the transport of particulate and gaseous contaminants from the atmosphere onto surfaces in the absence of precipitation (Davidson and Wu, 1989) (2) wet deposition by transfer of trace gases and particles occurring in an aqueous form (rain, fog, snow). Dry deposition is slow and continuous, whereas wet deposition delivers sudden and infrequent pollutants in dilute solution (Morselli et al., 2003). The most studied process, in case of building material deterioration especially marble, limestone, sandstone, is dry- and wet- deposition of SO_2, which cause growth of gypsum crystals. The major pathways of acid deposition, for example of SO_2, can be summarized as follow: SO_2 oxidized mainly by reaction with OH radicals leading to the formation of sulphuric acid (H_2SO_4), which rapidly nucleate to form aqueous H_2SO_4 droplets, acting themselves as condensation nuclei as cloud droplets. The aqueous phase formation of H_2SO_4 proceeds via absorption of SO_2 in cloud droplets or moist particles and subsequent oxidation reaction. Finally, the aerosol sulphate and gaseous SO_2 are subjected to below cloud scavenging by rainfall, removing a large fraction of atmospheric SO_2 by acid precipitation (Steiger, 2003). The dry deposit of atmospheric sulphur components involves the gaseous SO_2 and particulate sulphate. The overall rate of dry deposition depends on the material properties such as chemical composition and surface wetness, and the reactivity of the atmospheric trace gas of interest (Steiger, 2003).

In order to determine and compare the effects of atmospheric deposition on different building materials (stones and mortars) and the mechanism of degradation that occurs on construction materials, exposure tests were performed by Zappia et al., (1998). For the exposure tests, samples of different stones (Carrara marble, Travertine, Trani and Portland

limestone) and mortars (lime, pozzolan and cement mortars) were exposed for 6, 12 and 24 months in two sites: Milan (as an example of urban site) and Ancona (as an example of maritime site).

The results obtained can be summarized as follows:

1. Sulphation is the main process of degradation that occurs on both stones and mortars specimens.

2. The exposed materials showed different degrees of sulphation (Figure 1.1), highlighted the reactivity to SO_2 of stones and mortars exposed. Considering the total sulphur detected on the samples, mortars have been demonstrated to be more reactive than stones. This is mainly due to the micro-structural properties such a porosity, in fact mortars have a higher porosity than stones, and therefore higher potential of interaction with pollutants.

3. Taking into account the exposition to the rain run-off, the highest amount of airborne ion concentrations (sulphate, sulphite, nitrate, nitrite, chloride, fluoride, oxalate) respect to the bulk material, was observed in the areas completely protected.
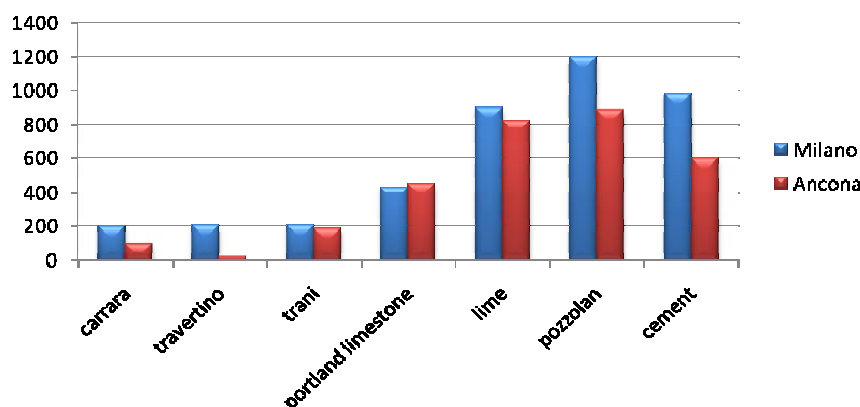
Figure 1.1. Total sulphur (μg cm^{-2}) measured on stones and mortars exposed for 12 months in Ancona and Milan (Zappia et al., 1998).

The literature contains numerous studies on the environmental degradation of building materials, such as natural stone and brick (Sabbioni, 1995; Riontino, et al., 1998), but very few data are available on the impact of air pollutants on mortars, in particularly cement mortar, which is the sign of the modern architecture. Only in recent years have been published a series of works, which have filled in part this gap.

1.1. Cement mortars

Cement mortars belongs to hydraulic mortars group, characterized by the capacity to set and harden under water.

The first evidence of humans using a form of "hydraulic" mortars, was discovered during the excavation of the underground aqueduct of Megara (500 B.C.), where a reservoir was coated with a pozzolanic mortar. This was a lime based mortar, made with an additive of volcanic ash, which gave to it hydraulic properties. The development of hydraulic mortars and theirs application was observed in ancient Greece; the Greek employed pozzolanic mortar obtained by adding volcanic ash from the Thira or Nisiros islands in Greece or from Dikearchia (Pozzuoli) in the Greek colony in Italy. However, it was the Romans, who improved the use and methods of this type of mortars; they substitute the ordinary sand in lime mortar into sand of volcanic origin from the village Pozzuoli close to Vesuvius. This village gave the name to mortars known as pozzolanic mortar and cement (van Balen et al., 2003, Werynski, 2006). The hydraulic properties of this mortars are principally due to presence in pozzolan of aluminium oxide (alumina) and silicon oxide (silica), that thanks to their amorphous, vitreous state and high specific surface area react with lime and water to form calcium silicates and aluminates hydrates (van Balen et al., 2003). The same effect was achieved by later Romans, using rich in silica and alumina ground fired clay (chamotte) or "cocciopesto" (finely ground bricks or tiles) instead of pozzolana. One of the first important works of Romans is the ancient theatre of Pompeii accommodating 20000 spectators (in 75 BC). Numerous works, which are admirable from both technical and architectural perspective follow, such as Coliseum (82 BC), Pantheon (123 BC) and several water reservoirs, like the one in the city of Nimes in France (150 AD). Worth mentioning is the written text "De architectura Libri Decem" by Marcus Vitruvius Polioin (13 B.C.), giving directions to architects for the preparation of a mortar which sets both in air and in water.

In medieval times there was no development of the art of making hydraulic mortar. In the middle of 1700 's AD, an English engineer John Smeaton discovered the hydraulic reaction during observation that lime mortars with lime, which were produced from the burning of

limestone containing clay (silica and alumina), could set both in the air as well as – more importantly - in water. This observation is considered to be the first essential step for the production of cement in the form in which it is produced today. Similar developments of that period were achieved by L. J. Vicat and Lesage in France.

The fundamental step for the creation of cement in the form it is used today, is attributed to the English engineer Joseph Aspdin, who took out a patent in 1824 for "Portland Cement", which mixed with water and sand gives Portland cement mortar (often known simply as cement or OPC mortar). This name was given because the colour of hardened cement was very similar to the colour of rocks in Portland.

The Portland cement is one of the most common sorts of cement used to produce mortars and concrete since 20th century. First step in Portland cement production is preparation of clinker, through the heating of blended limestone, clay and marlstone. Clinker (95 %), mainly composed of CaO, SiO_2, Al_2O_3 and Fe_2O_3, is mixed with calcium sulphate (anhydrite, hemihydrate, dihydrate (2-5 %)) and ground to form the cement powder - Portland cement (Czarnecki et al., 1996, Werynski, 2006). The chemical and mineralogical composition of it is presented in Table 1.1 and Table 1.2.

Table 1.1. Chemical composition of Portland cement (Czarnecki et al., 1996).

Chemical formula	Notation	Chemical name	Mass (%)
CaO	C	Calcium oxide	62-68
SiO_2	S	Silicon oxide	18-25
Al_2O_3	A	Aluminium oxide	4-8
Fe_2O_3	F	Ferric oxide	3-4
MgO	M	Magnesium oxide	0.5-2.5
Na_2O+K_2O	N+K	Alkali	0.4-3
SO_3		Sulfur trioxide	0.8-3

Table 2.2. Mineralogical composition of Portland cement (Czarnecki et al., 1996).

Mineral	Chemical formula	Notation	Chemical name	Mass (%)
Alite	$3CaO·SiO_2$	C_3S	Tricalcium silicate	30-65
Belite	$2CaO·SiO_2$	C_2S	Dicalcium silicate	15-45
Celite	$3CaO·Al_2O_3$	C_3A	Tricalcium aluminate	5-15
Ferrite	$4CaO·Al_2O_3·Fe_2O_3$	C_4AF	Tetracalcium aluminoferrite	5-15
Gypsum	$CaSO_4·2H_2O$		Calcium sulfate dihydrate	2-5

The addition of water to the clinker causes the process called cement hydratation, during which in the same time undergo two types of reactions: hydration and hydrolysis. Hydration reactions of typical constitutes of Portland cement (alite, belite, celite, ferrite) are presented in Table 1.3. The most abundant hydration products are calcium silicon hydrate (C-S-H) around 70 % and calcium hydroxide $Ca(OH)_2$ around 20 %. The amount of calcium hydroxide results in highly alkaline (pH between 12.5 and 13) and is responsible for material durability.

Table 1.3. Hydratation reactions of typical constitutes of Portland cement (Werynski, 2006).

Mineral:	Hydratation reactions:	Comments:
Alite	$2(3CaO \cdot SiO_2) + 6H_2O \rightarrow 3CaO \cdot 2SiO_2 \cdot 3H_2O + 3Ca(OH)_2 + Q^*$	really fast, cause setting and strength development in the first few weeks
Belite	$2(2CaO \cdot SiO_2) + 5H_2O \rightarrow 3CaO \cdot 2SiO_2 \cdot 4H_2O + Ca(OH)_2 + Q$	slower than of alite, this reaction is responsible for strength growth.
Celite	$2(3CaO \cdot Al_2O_3) + 21H_2O \rightarrow 4CaO \cdot Al_2O_3 \cdot 13H_2O + 2CaO \cdot Al_2O_3 \cdot 8H_2O + Q$	the fastest among all hydration reactions
Ferrite	$4CaO \cdot Al_2O_3 \cdot Fe_2O_3 + CaSO_4 + 16H_2O \rightarrow Ca_4 \cdot (AlO_3 \cdot)_2SO_4 \cdot 12H_2O + Ca(OH)_2 + 2Fe(OH)_3$	starts quickly as water is added, but then slows down

* heat

All hydration reactions are exothermal, the biggest amount of heat (Q) is produced in hydration of $3CaO \cdot Al_2O_3$ and the smallest of $3CaO \cdot SiO_2$ (Werynski, 2006).

The hydration of cement is a complicated process taking into account all reactions between water, different phases of clinker and gypsum, which is added to regulate time of setting. At the beginning of this process, when water is put into cement, big amount of alkalis, calcium ions, sulphates, and smaller amount of silica, iron and aluminium ions go into solution. Gypsum starts to react with $3CaO \cdot Al_2O_3$ in the following reaction:

$$3CaO \cdot Al_2O_3 + 3CaSO_4 \cdot 2H_2O + 26H_2O \rightarrow 3CaO \cdot Al_2O_3 \cdot 3CaSO_4 \cdot 32H_2O,$$

causing formation of hexacalcium aluminate trisulfate hydrate called ettringite, which belongs to the minerals group known as AFt phases. Gypsum undergoes to a total

transformation into ettringite in first 24 hours of reaction. Alite begins fast reaction with water producing calcium hydroxide. Ettringite and calcium hydroxide are the first products of cement hydratation. In the first 24 hours basic microstructure form appears, consisting of C-S-H needles and C-S-H leafs playing role of connection among separate cement particles. During further hydratation the density of microstructure rises, hardening increases with decreasing speed (Werynski, 2006).

When the source of sulphate (gypsum) is finished the ettringite subsequently starts to react with $3CaO \cdot Al_2O_3$ in reaction:

$$3CaO \cdot Al_2O_3 \cdot 3CaSO_4 \cdot 32H_2O + 3CaO \cdot Al_2O_3 + 4H_2O \rightarrow 3Ca_4 \cdot (AlO_3 \cdot)_2 SO_4 \cdot 12H_2O,$$

producing monosulfate from minerals group called "AFm phases".

Duration and progress of hydratation process depends on different factors. The most important are chemical and mineralogical composition of cement, water/cement ratio, temperature of hydratation, different supplements adding during or in the beginning of hydratation. It is assumed that 70 % of cement paste volume is composed of hyratation products and around 30 % of pores (Werynski, 2006).

1.2. Impact of air pollutants on cement mortars

The studies dedicated to the concrete construction corrosion are mainly focused on the interaction of the cement components with chlorides and sulphates from ground waters (Petri and Kawalec, 1998), while few works have been performed towards the understanding of the interaction of cement matrix with atmospheric multi-pollutants.

Buildings, especially in urban areas, exposed to acid rain precipitation undergo faster deterioration, which in case of cement materials can be observed by white or yellow efflorescence, micro cracks, surface swelling (Petri and Kawalec, 1998). Deterioration of Portland cement mortar, caused by acid deposition, was investigated by several laboratory and field tests performed in different conditions, summarized in Table 1.4 and 1.5. Laboratory and exposure experiments showed that acid rain dissolves calcium hydroxide, the dissolved amount increase with the increase in the acidity of simulated acid rain solution and the decrease in the flow rate (Okochi et al., 2000). A field exposure experiment, carried out for two years indicated that the carbonation of calcium hydroxide and the formation of other corrosion products, such as chloride, nitrate, and sulphate were limited to the surface of mortar specimens. The neutralization progressed more deeply in mortar specimens sheltered from rainwater than in those washed by rainwater (Okochi et al., 2000; Derry et al., 2001).

Rainwater with high concentration of ions such as SO_4^{2-}, NO_3^-, Cl^-, dissolves easily calcium hydroxide $Ca(OH)_2$, which is responsible for durability of cement. The typical neutralization reaction of $Ca(OH)_2$ can be presented as following:

$$2HCl + Ca(OH)_2 \rightarrow 2H_2O + CaCl,$$
$$2H^+ + Cl^- + Ca(OH)_2 \rightarrow 2H_2O + Ca^{2+} + 2Cl^-.$$
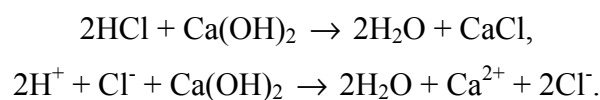
Salts, which are formed during this process, can be dissolved and washed out by rain water, or penetrate with water to inner part of surface. During this process, pH of concrete decreases and deterioration rises, in case of reinforced concrete, corrosion of the reinforcing steel additionally occurs.

The literature dedicated to modern hydraulic mortars deterioration due to the atmospheric multi-pollutants deposition has indicated the following points as requiring further investigation: CO_2/H_2CO_3 (carbonation), SO_2/H_2SO_4 (sulphation), NO_x/HNO_3-cement components interaction (Marinoni et al., 2003; van Balen et al., 2003). It is known that the deposition of air pollutants and aerosols on carbonate stone materials, in areas sheltered from rain run-off, causes formation of black damage layer (Bonazza et al., 2005); this phenomenon in case of cementitious material is still not investigated.

1.2.1. The carbonation process

Carbonation process is defined as interaction between CO_2 and concrete components. This mechanism is based on absorption of carbon dioxide, which converts calcium hydroxide and also hydrated calcium silicates and aluminates into calcium carbonate, that process is restricted by presence of water and relative humidity 40-70 % (Yates, 2003; Alexander et al., 2007; Pede and Guimareas, 2007). Calcium carbonate appears as white efflorescence on concrete surface and it is easily washed out by rain water. Process of carbonation can be presented in reactions:

$$Ca(OH)_2 + H_2O + CO_2 \rightarrow CaCO_3 + 2H_2O;$$
$$10\ (C\text{-}S\text{-}H) + 17CO_2 \rightarrow 17CaCO_3 + 10SiO_2 + 40\ H_2O.$$
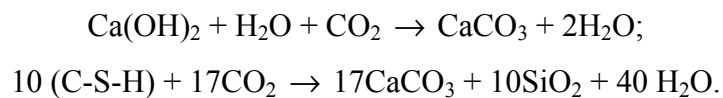
The process of carbonation can cause also decomposition of ettringite, which acts as binder in cement paste, into gypsum, calcium carbonate and alumina gel in the following reaction (Nishikawa et al., 1992; Grounds et al., 1988):

$$3CaO{\cdot}Al_2O_3{\cdot}3CaSO_4{\cdot}32H_2O + 3CO_2 \rightarrow 3CaCO_3 + 3CaSO_4{\cdot}2H_2O + Al_2O_3{\cdot}xH_2O +$$
$$(26\text{-}x)H_2O.$$
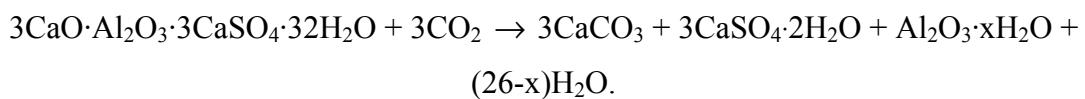
The carbonation reactions result in lowering of the pH and destabilizing all the cement hydration products. The decrease of the pH causes the decrease of the Ca/Si ratio of hydrated calcium silicate. It is assumed that 50 % of the CaO present in C-S-H of non-carbonated paste with pH ranging from 13 to 14, will transform into $CaCO_3$ in carbonated concrete reducing pH to 9 (Chang and Chen, 2006). The lower pH has also impact on

stabilities of ettringite and monosulphate: ettringite become unstable below pH of 10.7, while monosulphate below 11.6 (Gabrisova et al., 1991; Zivica and Bajza, 2001).

The carbonation of concrete depends mainly on environment condition, such as CO_2 concentration, relative humidity (RH), ambient temperature and pressure, as well as properties of cement: porosity and permeability, water/cement ratio, hydratation condition, age and moisture content (Zivica and Bajza, 2001).

1.2.2. The sulphation process

Interaction between buildings materials and SO_2 is assumed to be one of most important factor in buildings materials deterioration. The investigation by laboratory and field exposure test (Table 1.4 and 1.5), and historical buildings built in OPC, show that sulphation is the most common deterioration process on the cement mortars. According to the studies presented in Tables 1.4 and 1.5, in general, the process of SO_2 on cement mortars produces effect similar to the effect of CO_2: sulphur dioxide converts components of cement paste into soluble salts, which are subsequently leached away eroding the surface and increasing porosity. The diffusion of SO_2 through the exterior layer into the interior of the concrete and subsequently dissolution of SO_2 in the pore liquid leads to formation of sulphite acid; than to the formation of calcium sulphurous, and its oxidation under the formation of calcium sulphate or gypsum. Products of this reaction (such as gypsum) have significantly higher volume than the starting calcium compounds, therefore within the pores it causes enormous stresses and then swelling and cracking (Sabbioni et al., 2001; Zivica and Bajza, 2001; Sabbioni et al., 2002).

The interaction between atmospheric SO_2 and materials of the buildings is via the well-known processes of dry and wet deposition (acid deposition). The studies performed using micro-chambers to study the effect of dry and wet deposition on the cement mortars (Martinez-Ramirez, 1998), reports that sulphur dioxide in dry forms has little impact on Portland cement mortars. It has been shown that in case of dry deposition SO_2, the chemical reaction between the mortar components and the gases increases attending the following order:

$$SO_2 < SO_2 + O_3 < SO_2 + H_2O < SO_2 + O_3 + H_2O.$$
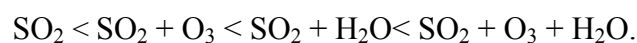
The author also shows that the conversion of SO_2 to $SO_4^=$ increases, when the cement/H_2O ratio decreases.

The investigation by laboratory and field exposure tests, reported in Tables 1.4 and 1.5, show that sulphation process is restricted by the concentration of SO_2, relative humidity and the properties of material, such as Al_2O_3 content and total porosity (Martinez-Ramirez, 1999; Martinez-Ramirez et al., 2002; van Balen et al., 2003).

The products of sulphation process on the cement mortars due to the atmospheric sulphur components or to the sulphate from the ground waters are gypsum ($CaSO_4 \cdot 2H_2O$), ettringite ($3CaO \cdot Al_2O_3 \cdot 3CaSO_4 \cdot 32H_2O$) and thaumasite ($CaSiO_3 \cdot CaSO_4 \cdot CaCO_3 \cdot 15H_2O$).

Gypsum ($CaSO_4 \cdot 2H_2O$) is the first product formed during the hydraulic mortar–SO_2 interaction, it is formed during reaction of SO_2 with calcium hydroxide in the following reaction:

$$Ca(OH)_2 + SO_2 + \frac{1}{2} O_2 + H_2O \rightarrow CaSO_4 \cdot 2H_2O.$$
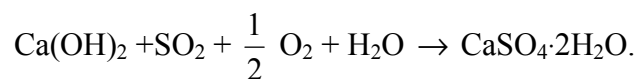
Gypsum is characterized by higher solubility and volume than $Ca(OH)_2$, and its formation effects in loss of strength and durability of cement paste. The problems generated by the formation of gypsum depends on different situations: first, after its formation on the surface, it can be easily washed away from the areas exposed to precipitation, eroding the surface and increased porosity due to its high solubility compared to the compounds of the original materials. On the other hand, the sulphation leads to the formation of black crusts on the surface of low porosity materials (marble and compact limestone) or occurs inside the pores in materials with high porosity, such as mortars and sandstones (Riontino et al., 1998; Sabbioni et al., 1998; Marinoni et al., 2003).

Ettringite is a mineral formed due to the reaction between sulfates, calcium aluminates and water. It can be found in cement materials in three forms: primary ettringite, delayed ettringite formation (DEF) and secondary ettringite. Primary ettringite is a product of hydratation and it is not hazardous (described in Chapter 1.1).

Table 1.4. a Laboratory chamber tests on cement mortars.

Cement characteristic		Type of chamber	RH (%)	T	Exposure time	SO$_2$ (ppm)	O$_3$ (ppm)	others	References
Water/ cement ratio	Water/ sand ratio								
0.4	1:3	Atmospheric flow chambers	84 $\pm$ 2	292 $\pm$ 2 (K)	4 weeks	2.5	2.5	Flux of water 10.6$\times$10^{-7}l/(m·s)	Martinez-Ramirez et al. (2002)
		Atmospheric flow chambers	95	25 °C	6 months 12 months	0.3			Van Balen et al. (2003)
0.5	1:3	1st Flow chamber	50		36 days			CO$_2$ enviroment	Van Balen et al. (2003)
		2nd Flow chamber	95	5 °C	6 months 12 months				Van Balen et al. (2003)
0.5	1:3	1st Flow chamber	95	25 °C	2 days	300			Blanco-Varela et al. (2003)
		2nd Flow chamber	95	5 °C	6 months 12 months				Blanco-Varela et al. (2003)
0.65	1:2	1st Spray chamber rain, pH=4.7		Room temp.	2 h				Okochi et al. (2000)
		2nd Spray chamber rain, pH=3		3 groups[1] 1) room temp. 2) heated (70 °C) 3) cold (2 °C)	2 h				Okochi et al. (2000)

Table 1.4. b Laboratory chamber tests on cement mortars.

Cement characteristic		Type of chamber	RH (%)	T	Exposure Time	SO$_2$ (ppm)	O$_3$ (ppm)	others	References
Water/cement ratio	Water/sand ratio								
0.4	3:1	Spray chamber rain, pH = 4		35 °C[2]	90 days				Martinez-Ramirez and Thompson (1999)
		Spray chamber	100	Room temp.	1cycle: (24h in solution /24h drying)				Sersale et al. (1998)
					1cycle: (120h spraying / 48h drying)				Sersale et al. (1998)

[1] 1st group at room temperature until next exposure
2nd group for 4 hours at room temperature, then heated at 70 °C 4 hours, and again at room temperature until next exposure
3rd cooled about –2 °C for 4 hours and then at room temperature until next exposure
[2] dry and wet cycling with spraying of the acid rain fine mist for 2 hours followed by drying at 35 °C for 2 hours

Table 1.5. Field exposure experiments of cement mortars.

Material	Water/cement ratio	Water/sand ratio	Site	Time of exposure	Exposure side to rain water:			References
					not sheltered	partly sheltered	completely sheltered	
Portland cement	0.65	1:2	Kanagawa University in Yokohama City, urban area in Japan.	2 years	yes	no	yes	Okochi et al. (2000)
Portland Cement	0.8	1:4	City centre site: Southwark, London. Suburban site: Horsted, Chatham, Kent	April – November in one year	yes	no	yes	Derry et al. (2001)
Modern hydraulic mortars		1:3	City centre, large industrial area: Milan, Ancona	6 months 12 months 24 months	yes	yes	yes	Zappia et al. (1998)

There has been many studies dedicated to delayed ettringite formation which is associated with damaging sulphate attack. Its formation occurs when primary ettringite it is subjected to temperatures between 70 °C and 90 °C and undergoes decomposition into monosulphate, then, during the temperature drop, monosulphate reacts with water (moisture) and sulphate, and ettringite (DEF) is formed again. This reformation of ettringite causes the new crystal growth inducing stresses in materials and subsequently cracking. The process is limited by moisture conditions and internal sulphate sources (Stark and Bollmann, 2002; Collepardi, 2003; Ekolu et al., 2006). The secondary ettringite is formed due to external sulphate sources. However, whilst the formation of secondary ettringite due to sulphate from ground water is well understood, the process due to atmospheric sulphur component is not well investigated. This type of ettringite is produced in reaction between gypsum and calcium aluminates hydrate (van Balen et al., 2003):

$$3\ CaSO_4 \cdot 2H_2O + 3CaO \cdot Al_2O_3 \cdot 6H_2O + 20\ H_2O \rightarrow 3CaO \cdot Al_2O_3 \cdot 3CaSO_4 \cdot 32H_2O.$$

This reaction is regulated by access to water (relative humidity), temperature, concentration of SO_2 and materials properties such as Al_2O_3 content and porosity. The crystal growth in the voids of cement matrix results in expansion effect (Collepardi, 2003). Thaumasite (calcium silicate carbonate sulphate hydrate) is a third mineral after gypsum and ettringite found as product of sulphate attack in cement modern construction. Naturally, thaumasite occurs mainly in metamorphic rocks, having crystallizes in the hexagonal system and needle-shaped, that is similar to ettringite structure. The formation of thaumasite in cement-based materials depends on the presence of ions, such as carbonate, sulphate and silicate, associated with calcium cations, and is limited by access to water (Crammond, 2002; Romer, 2003; van Balen et al., 2003; Collett et al., 2004; Ma et al., 2006; Bellman and Stark, 2007). The process of its formation can be presented in formula:

$$CaSO_4 \cdot 2H_2O + CaCO_3 + CaSiO_3 \cdot H_2O + 12\ H_2O \rightarrow CaSiO_3 \cdot CaSO_4 \cdot CaCO_3 \cdot 15H_2O.$$
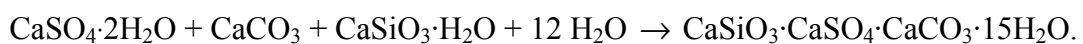
The destructive effect of thaumasite formation consists of the decomposition of C-S-H compounds, which creates "mushy concrete" and decreases the strength of the material.

However, while there has been performed a lot of studies mainly linked to formation of this mineral due to groundwater, this process is still not well understood. The research on the thaumasite form of sulphate attack (TSA) has been carried out by "Thaumasite Expert Group" (TEG) (1999). Through the investigation, the risk factors responsible for thaumasite formation were defined as presence of sulphates ions, ground water, carbonate (in coarse and fine aggregates) and low temperature (<15 ºC). Anyhow, further researches lifted up this theory, showing that among this four factors, sulphate source must be always present (external or internal) and in conditions to penetrate into the cement matrix from outside (i.e. high concentration of SO_2 in atmosphere). In fact, the presence of ground or mobile water is not required, the low temperature accelerate thaumasite formation, but it can be also found in warm climate, carbonate can come from external sources not just from aggregates (Sims et al., 2004). It has been also revealed that thaumasite can be formed also during transformation of ettringite (van Balen et al., 2003; Köhler et al., 2006).

1.2.3. The cement - NO_x interaction

It is known that in urban areas sulphur dioxide and nitrogen oxides are the most important gases associated with acidity precipitation (Morselli et al., 2008). The effect of NO_x on Portland cement is practically not documented. Nitrogen oxides present in atmosphere under suitable conditions can deposit on concrete surface. NO_2 or nitric acid are relatively unstable and can easily undergo oxidation. Reaction of NO_3 with cement matrix component is analogical with the one of CO_2 and SO_2. The salts (called calcium nitrate) formed during the reaction:

$$Ca(OH)_2 + 2HNO_3 + H_2O \rightarrow Ca(NO_3)_2 \cdot 4H_2O$$

are very soluble, therefore no expansive phenomena occurs. Instead, the leaching appears on the attacked layer when NO_2 comes in the contact with concrete (Zivica and Bajza, 2001). However, it is very difficult to determine the effect of NO_x, which plays also roles as oxidant (for example in sulphation process) and oxidation catalysts (Massey, 1999).

There has been performed some tests of cement paste corrosion in acid solution, which has shown the magnitude of the aggressive effect of three acids solution in following order

$HNO_3 > HCl > H_2SO_4$, anyhow this result are difficult to evaluate in historical building effected by rainwater and acid deposition (Pavlik, 1994; Okochi et al., 2000).

1.2.4. Formation of black crust

The deposition and accumulation of multi-pollutants and products of chemical reactions occurring in material surfaces, in areas protected from rain run-off, leads to formation of the so-called black crust. The formation of the black damage layer results not only in aesthetic impairment (blackening) of the building façade but also causes material loss (Ghedini et al., 2006). The characterization of the black crusts on natural stone has indicated gypsum as main component followed by calcite with embedded airborne particulate matter, including carbonaceous and aluminosilicate particles and also metal particles mainly composed of iron (Del Monte et al., 1981; Sabbioni and Zappia, 1991; Zappia et al., 1993; Ghedini et al., 2000; Bonazza et al., 2005). The carbonaceous particles are responsible for darkening of the surface and, due to heavy metal content, act as catalytic support for the heterogeneous oxidation of SO_2 (Benner et al., 1982; Hutchinson et al., 1992; Sabbioni, 1992).

The black damage layer on cement-based mortars is modestly known in monuments and construction sector. The analyses of black crusts from the indoor walls of a concrete tunnel indicated gypsum as the main components with embedded particulate matter produced by fuel combustion. In particular, embedded in the gypsum matrix were found aluminosilacate particles from coal combustion and carbonaceous particles with oil-derived fuels origin (Marinoni et al., 2003).

The studies performed on black crust on the stone monument indicate that sulphur and carbon are the most important elements of anthropogenic origin present in the damage layers on monuments located in urban areas (Sabbioni and Zappia, 1992; Sabbioni et al., 1998; Ghedini et al., 2000).

Carbon in damage layers of monuments in marble and limestone can have different origins: (1) calcium carbonate deriving from underlying material; (2) deposition of atmospheric particles from combustion sources; (3) biological weathering; (4) decay of organic treatment applied in the past (Zappia et al., 1993). Due to the presence of calcium carbonate in damage layers, the measurement of the total carbon is not sufficient to

quantify the carbon of atmospheric origin, therefore the total carbon (TC) is considered to be composed of two fractions:

$$TC = CC + NCC,$$

where CC is the carbonate carbon (originating from the building materials), and NCC is the non carbonate carbon, which in turn is composed of elemental carbon (EC) and organic carbon (OC):

$$NCC = EC + OC,$$

both EC and OC are closely related to atmospheric pollutants. The EC is a certain tracer for combustion, being entirely due to particles emitted by combustion processes into atmosphere; in monuments deterioration it causes blackening of the surface (Bonazza et al., 2007). The organic carbon (OC) is linked to a number of different and often simultaneous origins, including the atmospheric deposition of primary and secondary pollutants (Saiz-Jimenez, 1993; Turpin and Huntzicker, 1995; Cachier, 1998), biological weathering (Saiz-Jimenez, 1995); and the decay of protective organic treatments (Rossi Manaresi, 1996).

Few works reported the quantitative measurements of the carbon content in the damage layers formed on the stone monuments (Zappia et al., 1993; Ghedini et al., 2000; Bonazza et al., 2005; Ghedini et al., 2006); in case of cementitious materials used in 20th century architecture, this subject is not been explored.

The first data set on carbon fractions in surface damage layers on European stone monuments has been published by Bonazza et al. (2005). During this research, methodology combining thermal and chemical treatments was applied to quantify OC and EC fractions in damage layers on European monuments. This, in order to determine the role of carbonaceous aerosols in surface blackening, in terms of the amount of anthropogenic carbon in black crust composition. The results obtained demonstrate that OC and EC fractions are always present in the damage layers on monuments. In general the OC fraction predominates over the EC one, which was particularly evident in the damage layers collected from the monument sides exposed directly to air pollution due to

traffic. This work demonstrated also that damage layers are a record of the environmental changes occurring over time at each specific site, with their chemical composition reflecting that of the atmospheric combustion sources. In particular, they act as cumulative markers of the historical sequence of sources producing the atmospheric pollution responsible for their formation (Bonazza et al., 2005).

2. Presentation of the selected sites

The aim of this work is to evaluate the impact of air multi-pollutants on modern built heritage; for this purpose three buildings from 20th century architecture exposed in different urban atmospheres were selected: Centennial Hall (Wroclaw, Poland), Chiesa dell'Autostrada del Sole (Florence, Italy) and Casa Galleria Vichi (Florence, Italy).

2.1. Centennial Hall, Wroclaw (Poland)

The Centennial Hall (Figures 2.1, 2.2, 2.3) is located in the urban area of Wroclaw, situated in one of the most industrialized and polluted regions of Poland, called Silesian Coal Basin. In this area in 1992 was produced 23 % of Poland's total SO_2 emission, though it occupies only 2 % of the country's area. In the past, Poland was a country having large heavy and power industry based on coal as a primary energy source. Since 1990, due to the Government's effort through legislative, regulatory and economic means, considerable improvements have been achieved in reducing air pollution in the country's industrial areas (Nagy et al, 2006). The Centennial Hall is located in close neighbourhood of coal power stations; the closest one is just 5 km away from the monument.

The hall was built in 1913 according to the plans of Max Berg, to commemorate the 100th anniversary of victory over Napoleon in the Liberation Wars of 1813-15. In 2006 it was added to UNESCO's prestigious list of World Heritage Sites, as one of the most important achievements of 20th century architecture.

Figure 2.1. Centennial Hall, Wroclaw (Poland).

Centennial Hall is a landmark in the history of reinforced concrete architecture; it was one of the world's biggest dome-like structure. This is a pioneering construction of modern architecture, which shows an important interchange of influences in the early 20th century, becoming a key reference in the later development of reinforced concrete structures. The building has the form of a symmetrical quatrefoil (Figure 2.3), with an inner diameter of 69 m and a height of 42 m, creating a vast circular central space, with seating for up to 6000 people.

Figure 2.2. Centennial Hall, Wroclaw (Poland).

Figure 2.3. Centennial Hall, Wroclaw (Poland) source:
http://foto.poland.gov.pl/cache/imgs/_w800/gallery/image/1_HalaLudowa_S.Klimek_010.jpg

2.2. Chiesa dell'Autostrada del Sole, Florence (Italy)

Chiesa dell'Autostrada del Sole (Church of the Highway of the Sun) is situated West of Florence (Italy), between Autostrada del Sole (Highway of the Sun) and the A11 Firenze-Mare highway. The Autostrada del Sole or Autostrada A1 is the longest Italian motorway which connects Milan with Naples through Bologna, Florence and Rome, and it is considered the "spinal cord" of the country's road network.

The Chiesa dell'Autostrada del Sole was built between 1960 and 1963 according to plan of architect Giovanni Michelucci with intention to honor the workers who had died constructing Italy's highways, and was also intended for use by people traveling those highways.

The project of the church reflects both modern and traditional church design. The "cross" floor plan and stone facing are meant to induce a traditional sense while the tent-like vertical elements and copper roofing reflect modern design tastes. The church stands 27.5 m high.

Building maintenance is performed in regular cleaning program; last restoration work was performed two years before sampling.

Figure 2.4. Chiesa dell'Autostrada del Sole, Florence (Italy).

Figure 2.5. Chiesa dell'Autostrada del Sole, Florence (Italy).

2.3. Casa Galleria Vichi, Florence (Italy)

Casa Galleria Vichi (Figures 2.6 and 2.7) is located in the historic centre of Florence (Italy), where traffic is the most significant source of air pollution. The palace is directly exposed to vehicle traffic pollutants emitted from road adjacent.

The Casa Galleria Vichi was designed by architect Giovanni Michelazzi in 1911, commissioned by Argia Marinai Vichi as home and gallery and it still serves this purpose today. The concrete palace was built in the style of art *nouveau* and is the unique example of liberty style in the centre of Florence. The eccentric narrow façade encloses structural and sculptural fantasy motif composed by a mix of artificial stone, steel and glass. Every floor is characterized by a central stained glass window designed following the typical line curve "a colpo di frusta" cut in horizontal elements. The ground and first floor (Figure 2.6) are utilized for commercial use and are more fanciful ornamented with sculptures and reliefs, for example with the eagle holding the lamp, while upper floors to residential use, are less decorated with pilasters around the central windows. The crown of the façade is decorated with two dragons (Figure 2.8).

Figure 2.6. Casa Galleria Vichi, Florence (Italy).

Figure 2.7. Casa Galleria Vichi, Florence (Italy).

Figure 2.8. Dragon on the crown of the façade, Casa Galleria Vichi (Florence).

3. Experimental work

3.1. Sampling

The investigation of the impact of air multipollutants on the 20th century architecture was performed through the laboratory analyses on samples collected from three buildings described in Chapter 2. The sampling sessions were performed taking into account the different levels of the buildings and the protection from rain: sheltered, partly sheltered and exposed areas. Following the analysis criteria, the damage layer was sampled in the form of incoherent deposit for chemical analyses, and in fragments for morphological observation and mineralogical characterization. The samples of damage layer were collected using a brush. In case of coherent crust, strongly attached to the surface, was applied a scalpel to scrape it away, limiting removal of the undamaged material. The fragments were collected using scalpel and hummer taking into account the minimum invasiveness of the operations.

3.1.1. The Centennial Hall – sampling

The samples, in form of damage layer and fragments, were collected taking into account the height from ground level and the protection from rain run-off, on different sides of the Centennial Hall. The plan of the building with sampling points is shown in Figure 3.1. During sampling the dark damage layer appeared in areas protected from rain wash out (Figures 3.2 and 3.3), with maximum thickness in the highest part of the building (Figure 3.4). In some cases the crust was strongly attached to the surface (coherent crust), making it difficult to scrape away. The samples collected with a brief description are listed in Tables 3.1. a and b.

Table 3.1.a. List of samples collected on Centennial Hall, Wroclaw (Poland).

Sample	Height (m)	Side/ sampling area	Protection from rain	Description
CH1	1.5	North	partly sheltered	fragment (substrate + damage layer)
CH2	1.5	North	sheltered	grey coherent crust
CH3	1.5	North	partly sheltered	grey coherent crust
CH4	1.5	South	partly sheltered	fragment (substrate + damage layer)
CH5	1.5	South	sheltered	grey crust
CH6	1.5	North-East	sheltered	grey coherent crust
CH7	12	East	sheltered	fragment (substrate + damage layer)
CH8	12	East	partly sheltered	fragment (substrate + grey damage layer)
CH9	12	East	partly sheltered	grey coherent crust
CH10	12	East	sheltered	fragment (substrate + grey damage layer)
CH11	12	East	sheltered	fragment (substrate + damage layer)
CH12	12	South-East	partly sheltered	crust from yellow area
CH13	14	South-East	partly sheltered	grey crust
CH14	14	South	partly sheltered	grey coherent crust
CH15	14	East	partly sheltered	dark crust
CH16	14	North	unsheltered	coherent crust from yellow area
CH17	14	South-East	partly sheltered	dark coherent crust
CH18	14	North	sheltered	dark crust
CH19	14	South	sheltered	fragment (substrate + damage layer)
CH20	14	South-East	sheltered	fragment (substrate + damage layer)
CH21	14	East	partly sheltered	fragment (substrate + damage layer)

Table 3.1.b. List of samples collected on Centennial Hall, Wroclaw (Poland).

Sample	Height (m)	Side/ sampling area	Protection from rain	Description
CH22	12	South	sheltered	fragment (substrate + damage layer) from the building on the second floor
CH23	12	South	sheltered	fragment (substrate + damage layer) from the building on the second floor
CH24	12	South	partly sheltered	grey coherent crust from the wall of the building on the second floor
CH25	27	East		fragment found on the floor
CH26	27			substrate
CH27	27			substrate
CH28	27	West	partly sheltered	fragment (substrate + damage layer)
CH29	27	West	partly sheltered	fragment (substrate + damage layer)
CH30	27	West	partly sheltered	grey crust
CH31	27	North	partly sheltered	crust from yellow area
CH32	27	South-East	partly sheltered	crust from yellow area
CH33	27	South-East	sheltered	fragment (substrate + damage layer)
CH34	40	North-East	sheltered	dark coherent crust
CH35	40	North-East	partly sheltered	coherent crust from yellow area
CH36	40	North-East	sheltered	fragment (substrate + dark damage layer)
CH37	40	North	sheltered	fragment (substrate + dark damage layer)
CH38	40	North-West	sheltered	thick dark crust with rough surface
CH39	40	East	sheltered	fragment (substrate + damage layer)
CH40	40	East	sheltered	fragment (substrate + damage layer)
CH41	40	North-East	sheltered	fragment (substrate + damage layer)
CH42	12	North West	sheltered	grey coherent crust
CH43	12	North-West	sheltered	fragment (substrate + damage layer)

sheltered area,   partly sheltered,   unsheltered
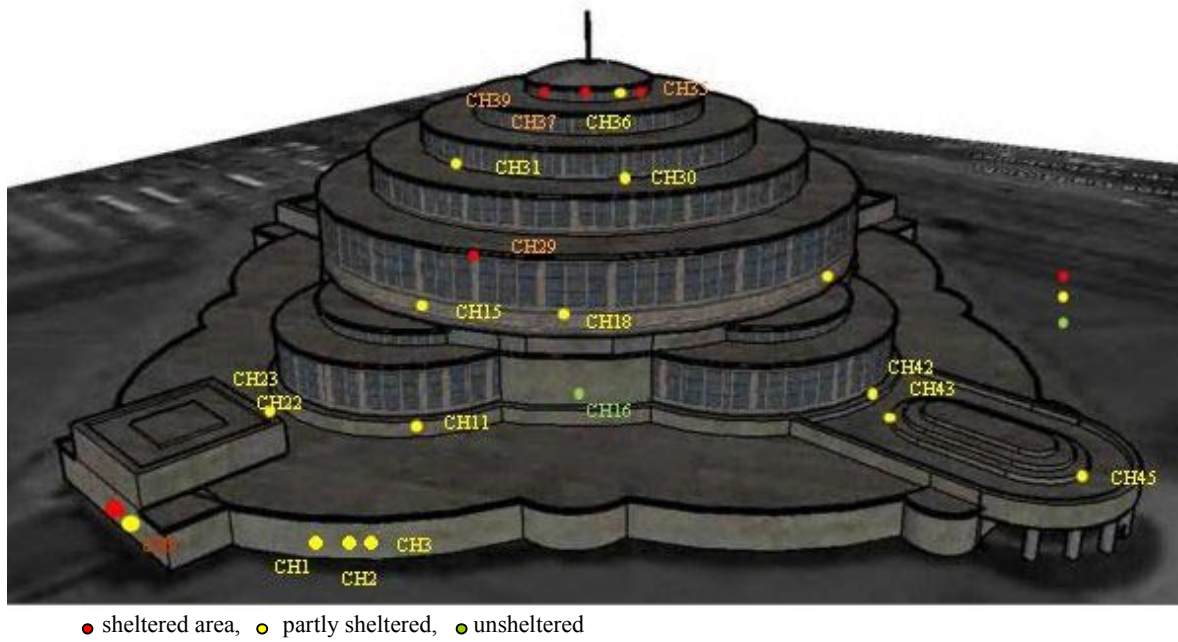
Figure 3.1. Plan of the Centennial Hall (North-West), sampled areas within the red, yellow, green circles.

Figure 3.2. Centennial Hall (Wroclaw), there are observable areas with black crust.

Figure 3.3. Centennial Hall, sampled areas with black crust.

Figure 3.4. Centennial Hall, black thick crust in area protected from rain run-off.

3.1.2. Chiesa dell'Autostrada del Sole - sampling

Samples were collected from the concrete wall on the northern part of Chiesa dell'Autostrada del Sole as it is shown in Figures 3.5, 3.6 and 3.7. This part as well as the whole Church, was restored (cleaned) two years before sampling. Under visual assessment, the damage layer was not observed on the jointing mortars and on the concrete parts of the church. The samples collected in form of fragments for subsequent analysis are listed with short description in Table 3.2.

Sample	Height (m)	Side/sampling area	Protection from rain	Description
FIC_sub		North, concrete wall	unsheltered	substrate
FIC1	0.5	North, concrete wall	unsheltered	fragment (substrate + damage layer)
FIC2	1.70	North concrete wall	unsheltered	fragment (substrate + damage layer)
FIC3	1.50	North concrete wall	unsheltered	fragment (substrate + damage layer)

Table 3.2. Samples collected on the Chiesa dell'Autostrada del Sole (Florence).

Figure 3.5. The concrete wall[*] in the northern part of the Chiesa dell'Autostrada del Sole (Florence).
[*]The concrete wall appears black because the picture was taken in a rainy day and the wall was wet.

Figure 3.6. Chiesa dell'Autostrada del Sole (Florence), sampled area.

Figure 3.7. Sampling on Chiesa dell'Autostrada del Sole (Florence).

3.1.3. Casa Galleria Vichi - sampling

The samples were collected on the facade (South-West) of Casa Galleria Vichi (Florence, Italy) by scalpel or brush, moving on a platform lift as it is shown in Figure 3.8. Sampling was started from above, at a height of 19 m on the left side, then moved to the centre and went to the right side. The same pattern, with horizontal bands, was repeated at other levels as it is presented in Figure 3.9.

Under visual assessment, the damage layer appeared in areas protected from rain run-off. There were distinguished two types of damage layers; dark coherent crust strongly attached to the surface (Figure 3.10), and incoherent grey deposit with powder consistency (Figure 3.11). In addition fragments with black crust and substrate were collected. The list of the collected samples with their position and brief description is reported in Table 3.3.

Table 3.3. List of samples collected at Casa Galleria Vichi (Florence).

Sample	Height (m)	Side/ sampling area	Protection from rain	Description
BOS1	19	dragon of the left	sheltered	dark coherent crust, rough surface
BOS2	19	central part	sheltered	fragment (substrate + damage layer)
BOS3	19	dragon on the right	partly sheltered	dark coherent crust, probably biological
BOS4(2)	19	dragon on the right		substrate
BOS5	19	central part	sheltered	grey incoherent deposit
BOS6	15	shell on the left	sheltered	dark coherent material, smooth surface
BOS7	15	mask on the left		substrate
BOS8	15	mask on the left	sheltered	dark grey incoherent deposit
BOS9	15	frame	partly sheltered	grey incoherent deposit
BOS10	15	mask on the right	sheltered	dark coherent crust, smooth surface
BOS11	15	frame on the right	partly sheltered	grey incoherent deposit
BOS12	11	frame	sheltered	grey incoherent deposit
BOS13	7	mask on the right	sheltered	dark incoherent crust
BOS14	5	sculpture on the right	partly sheltered	dark coherent crust, rough surface
BOS1516	5	sculpture on the left	partly sheltered	dark coherent crust, rough surface
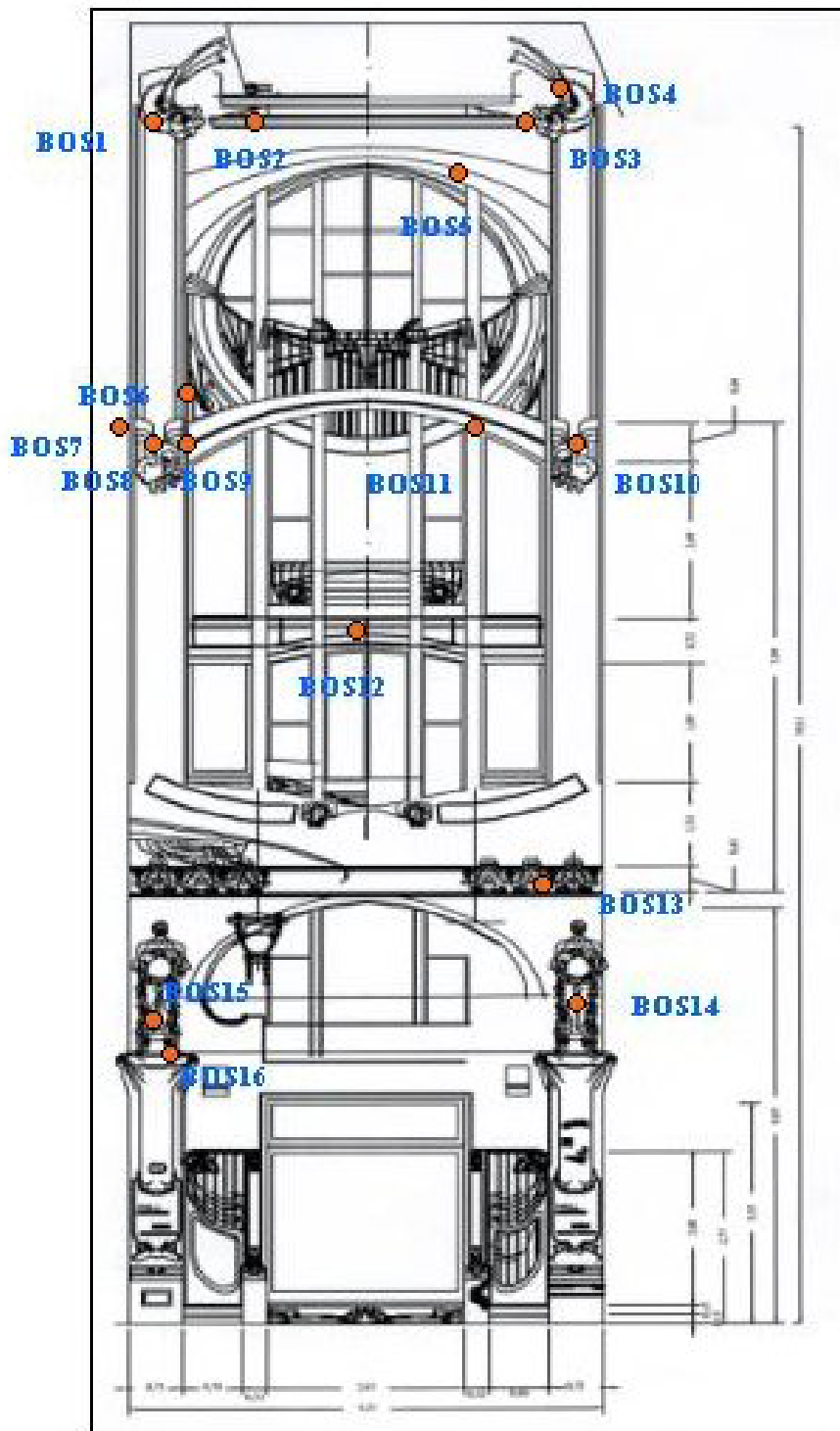
Figure. 3.8. Plan of façade of the Casa Galleria Vichi, sampled area within the red circles.

Figure 3.9. Sampling: (a) platform lift, (b) collection of the black crust from area protected from rain ran-off.

Figure 3.10. (a), (b) Sampling points of coherent black crust, Casa Galleria Vichi (Florence).

Figure 3.11. Casa Galleria Vichi. Sampling point, (a) and (b) incoherent grey deposit, easily collected by brush

3.2. Analytical techniques

3.2.1. Optical Microscopy

The textural and petrographical features of the samples collected from Centennial Hall, Wroclaw (Poland), Chiesa dell'Autostrada del Sole, Florence (Italy) and Casa Galleria Vichi, Florence (Italy) were observed in transversal thin section using an Olympus BX51 microscopy, equipped with a scanner and the MICROMAX software "Primoplus_32" vers.8.11.02. The aim is the characterisation of the damage layers sampled and of the underlying building material by the mineralogical and petrographical point of view.

3.2.2. Scanning Electron Microscopy

Scanning electron microscopy (SEM) with energy dispersive X-ray analyser (EDX) is a method generally employed for high-resolution imaging of surfaces of the sample and identification of its elemental chemical composition. The SEM scans the sample surface with a high-energy beam of electrons in a raster scan pattern. The advantages of SEM over optical microscopy include higher magnification (over 100000 times) and greater depth of field up to 100 times that of optical microscopy. The EDX method allows a fast and non-destructive chemical analysis with a spatial resolution in the micrometer regime. It is based on the spectral analysis of the characteristic X-ray radiation emitted from the sample atom upon irradiation by the focussed electron beam of SEM.

The SEM instrument has many application across different industrial sectors; taking into account the high magnification together with localised chemical information, it becomes an useful tool for solving a great deal of common conservation issues, such as soot particle analysis and identification of material defects.

The morphological and elemental characterization of surface damage layers collected from the buildings under study were performed by scanning electron microscope equipped with an energy-dispersive analyser - SEM-EDX Philips XL 20. Samples were mounted on aluminium stubs and coated with a thin layer of graphite to allow surface conductivity. The

application of graphite films is necessary for the correct identification of the emission spectrum of sulphur.

3.2.3. X-ray Diffractometry

X-ray diffractometry (XRD) is a widely used technique to identify crystalline phases, based on their crystal structure. Working principle of XRD is based on the detection of the scattered intensity of a X-ray beam diffracted at angles determined by the spacing of the planes in the crystals and the type and arrangement of the atoms.

XRD is applied in conservation sciences in determining the nature of pigments, deterioration and alteration products both for buildings materials and metal objects.

The X-ray diffractometery in this case was used to identify the main crystalline phases of the damage layers and underlying material collected from the selected buildings. The powdered samples (minimum 3 g) distributed on a Plexiglas stub were analysed by Philips PW 1730 diffractometer equipped with a copper anticathode and a nickel filter. The measurement conditions have a diffraction interval of 2 θ, between 5 ° and 50 °, and a 2 °/minute step at 40 kV voltage and 30 mA current intensity.

This analytical methodology permits the acquisition of qualitative and semiquantitative data on the crystalline phases present in a concentration of at least 3-4 %.

3.2.4. Differential and Gravimetric Thermal Analysis

Thermal analysis techniques determine changes on physical properties and reaction products when a substance is heated under controlled condition. Differential thermal analysis (DTA) monitors changes in thermal properties, either exothermic or endothermic, by detecting the differences in temperature between the sample and inert reference standard. The DTA curve provides data on the transformations that have occurred, such as phase transitions, crystallization, melting and sublimation. Peaks produced during heating are characteristic for specific materials, while the area under the peaks is a measure of the quantity of active material (material, which gives exothermal or endothermal changes in the sample). Thermal gravimetric analysis (TGA) measures the weight loss of material as

function of temperature. The two techniques, DTA and TGA, complement each other to record weight changes and differential thermal analysis curves.

DTA-TGA has long been applied mainly at the study of minerals and polymers and also is commonly used in environmental research.

In this case the DTA-TGA analyses were performed in order to quantify gypsum, carbonates and portlandite in the collected samples by the instrument METTLER TOLEDO TGA/SDTA 851, equipped with a TSO 800GC1 programmable gas switch. The 25-80 mg of powdered sample, placed in 150 microlitre capacity aluminium crucibles, was analysed at constant oxygen flow, temperature ranging between 25-1100 °C and thermal gradient equal to 10 °/min.

3.2.5. Ion Chromatography

Ion chromatography (IC) is a form of liquid chromatography that uses ion-exchange resins to separate atomic or molecular ions based on their interaction with the chromatographic system. Its greatest utility is for analysis of anions, cations and biochemical species such as amino acids and proteins. Most ion-exchange separations are done with pumps and metal columns. Ion chromatography has been widely used to analyse the anionic and cationic components in waters related to acid rain. It is also the most popular and powerful tool for analysis of environmental samples, because of its high accuracy and reliability.

The ion chromatographic analyses are carried out using the Dionex Chromatograph (4500i model), equipped with: conductivity detector (Dionex CD II), injection *loop* from 5 to 500 μl (inc. 0.010 ID Peek mode), variable wavelength spectrophotometric reader (VDN 2), gradient pump module (GPM-2), micromembrane anion suppressor (Dionex AMMSI), and data acquisition and instrument control (Dionex AL-450 II). As far as sensivity is concerned, the low concentration limit is 0.01 ppm, while for Cl^-, NO_3^- the limit is 0.001 ppm. The instrument is also equipped with an AS14 Ionpac 4mm column for the discrimination and measurement of anions. An Ag 4A-SC Ionpac 4x50mm pre-column and an AS 4A- SC Ionpac 4x250 mm column are required for the measurement of sulphates.

The analysis is suitable for measuring the soluble anions. In this case we focused on the following anions: $SO_4^=$, NO_3^-, NO_2^-, Cl^-, Br^-, CHO_2^-, $C_2H_5O_2^=$, $C_2O_4^=$, in order to understand the acidic deposition on the buildings.

The preparation of the sample and the subsequent analyses includes:

- Prior to analysis, the samples, in form of powder were weighed; the average amount of sample required was ≈ 100 mg. It was put into a glass container, where 50.00 ml of ultra pure (reagent grade) water were added. The container was sealed and put into an ultra sound bath for 30 minutes at a controlled temperature of less than 30 °C.

- The solution obtained was then utilised for the IC anion determination. The amount of ion solution required was 1 ml, which is injected into the instrument by means of a filter of 0.2 μ of porosity.

- A buffer solution Na_2CO_3/ $NaHCO_3$ (1.8 mM : 1.7 mM) in ultrapure water (reagent grade) employed as eluent.

The amount of every ion must be correlated with the quantity of sample weighed, and expressed as a percentage or in ppm.

3.2.6. Carbon Compound Discrimination and Measurements

The carbon fractions present in the damage layers, collected at the selected sites, were discriminated and measured by flash combustion/gas chromatographic analysis using a conductibility detector (CHNSO EA 1108 FISONS Instruments), according to the methodology published by Ghedini et al. (2006).

The procedure is based on the three distinct stages, each performed on a different part of the same damage layer specimen: 1) total carbon is quantified by burning one part of the bulk sample; 2) non carbonate carbon is obtained by the combustion of a second part of the sample after carbonate decomposition and the complete removal of carbon dioxide; 3) elemental carbon is measured by oxidation of the residue obtained after eliminating the inorganic matrix and organic species by means of a chemical treatment.

The quantity of powdered black crust required for the overall procedure is about 1 g.

The procedure is summarized in the following steps:

Step I. Total carbon (TC)

About 10 mg of bulk ground sample, precisely weighed is directly placed into a silver capsule, where it is fully oxidized and quantified by flash combustion/gas chromatographic analysis.

Step II. Non carbonate carbon (NCC)

About 10 mg, exactly weighed, of ground sample is placed in a silver capsule, where it undergoes acidification to remove carbonates by means of maintenance in an atmosphere of HCl concentrate solution until microeffervescence stops. It is then preserved for 12 h in a KOH drier to eliminate CO_2, HCl, and H_2O before being analyzed by the instrument for non carbonate carbon quantification.

Step III. Carbonate carbon (CC)

Carbonate carbon is calculated as the difference between TC and NCC.

Step IV. Elemental Carbon (EC)

The procedure established for elemental carbon quantification can be presented in the following six stages.

1. An exactly weighed quantity of ground black crust, ranging between 200 mg and 1 g, depending on its EC content and the type of preparation equipment, is placed in an airtight tube, and 2 ml of Na_2CO_3 saturated solution is added. The tube is then hermetically sealed and heated at 120 °C for 2 h. The cooled sample is centrifuged at 5.000 revs/min for about 10 min and, after liquid-phase removal, is washed with 2 ml of tepid distilled water and is recentrifuged.

2. Subsequently, the residue is treated, under agitation in an open tube, in steps of 20 ml, with a concentrated solution of HCl (37 %), until the effervescence stops; the complete decomposition of carbonates and the removal of CO_2 are then obtained by heating the suspension to 40−50 °C. After cooling, the residual sample is centrifuged and rinsed as described above.

The treatment with the Na_2CO_3 saturated solution (1) leads to the solubilisation of lowest soluble salts (e.g., $CaHPO_4$, $SrSO_4$, CaC_2O_4) because of the formation of carbonates, which are then removed, together with the carbonates present as mineralogical components of the original sample, using the HCl treatment (2).

3. The residual sample undergoes five alternate digestion steps at 120 °C for 1 h performed with 2 ml HCl 37 % and at 120 °C for 30 min with 2 ml KOH 30 %. Each digestion step is followed by centrifugation and washing with 2 ml of distilled water after the acid digestion and with 2 ml of distilled water, acidified with HCl solution, after the basic one.

The HCl treatments allow the dissolution of basic materials and the decomposition of silicates, while the repeated KOH attacks produce the complete dissolution of the acid

substances, the quartz, and the amorphous silica derived from the HCl action on silicates. The five alternate attacks with HCl and KOH concentrated solutions are indispensable for isolating elemental carbon from particularly complex matrixes.

4. If, after the above steps, the residual sample still reveals the presence of silicates, their complete removal can be obtained by means of a final treatment with $NH_4F \cdot HF$, at 120 °C, until the dissolution of salts, followed by centrifugation and washing with distilled water.

5. For each sample, the liquid phases derived from all treatments, including washing, are collected, mixed, pH adjusted to about 10, added to 25−30 mg of Zn^{2+} (as $ZnCl_2$), and stirred. The soft jellylike mass resulting from the formation of zinc hydroxide, which contains EC, is isolated by centrifugation, is washed, and is added to the residue of the previous treatment.

6. The sample is finally dried at 180 °C until reaching constant weight, after which it is analyzed by combustion (CHNSO) to evaluate the elemental carbon content.

Step V. Organic carbon (OC)

Organic carbon is then calculated as the difference between NCC and EC.

3.2.7. Induce Coupled Plasma-Optical Emission Spectroscopy

Induced coupled plasma-optical emission spectroscopy is an analytical technique used for elemental chemical analyses. The sample to be analysed must be in liquid form, if solid normally is first dissolved or digested before being fed into the plasma.

The procedure is based on conversion of the molecules of the liquid sample to individual atoms and ions using high temperature ratio frequency induced argon plasma. The sample is introduced into plasma as solution. The analyzed sample is pumped to a nebulizer by peristaltic pump. The purpose of nebulizer is to convert the sample to the fine spray and mix with argon in the spray chamber, where only droplets in a narrow size range are carried into the plasma and instantly excited by the high temperature.

A number of atoms pass into the excited state and, when relax to the ground state, emit radiations characteristic for each element. The emitted radiations are easily detected and the elements identified through an optical spectrometer (in general in the UV, Vis or NIR region). The intensity of the radiation is proportional to the concentration of that element within the solution and so can be used for quantitative purposes.

The concentration of elements in damage layer and underlying material collected on the buildings under study was determined using inductively coupled plasma - optical emission spectrometer (ICP-OES), Circular Optical System CIR.O.S.CCD.

Preparation of the sample for ICP-OES analyses:

- Powdered samples were weighed; the average mass of sample required was ≈ 0.1 g.
- The weighted sample was treated with acids mixture: HF (2 ml) + HCl (6 ml) + HNO_3 (2 ml), then the solution was put into the microwave oven in the following conditions: t = 25 min; T = 200 °C; p = 10-15 bar; P = 400 W.
- After heating, to the dissolved samples was added a solution of H_2BO_3 (22 ml) 4 % and filled with H_2O double-distilled till volume of 50 ml.

In order to identify the origin of the elements, the data obtained during ICP-OES analysis were processed with two statistical techniques i.e. student's t-test and principle components analyses, and the enrichment factors were calculated.

- *Student's t - test*

Student's t-test is a one of the most commonly technique used for testing the hypothesis on the basis of the difference between sample means (William at al., 1992). In this case one tailed t-test was applied to the mean concentrations and the corresponding standard deviations of the elements in substrate and damage layer, to find the elements with a significant positive difference in concentration between damage layer and substrate. The following equation was used:

$$t_{calculated} = (\overline{X}_1^2 - \overline{X}_2^2) / \sqrt{\frac{S_{x_1}^2}{n_1} - \frac{S_{x_2}^2}{n_2}} \quad ,$$

where $\overline{X}_1$ and $\overline{X}_2$ are the mean concentrations of element X in damage layers and substrate respectively, S_{x_1} and S_{x_2} are standard deviations of the two means: damage layers and substrate, n is number of measured values (n_1 in damage layer, n_2 in substrate).

Considering the positive differences (X_1-X_2), if the $|t_{calculated}| > t_{table}$, where t_{table} is critical values of t, at level of significance $\alpha=0.05$ and the degree of freedom N= (n_1+n_2-2), we can say that the concentration of the element X in the damage layer is significantly (statistically) higher than in the substrate.

In this case, the element of interest (X) can be ascribed to the atmospheric deposition.

- *Principal components analysis (PCA)*

Principal components analysis (PCA) is an useful statistical technique to uncover unknown trends in data (Gorban et al., 2007). Principal component analysis involves a mathematical procedure (eigenvalue decomposition of a data, covariance matrix of the data) in order to transform a number of possibly correlated variables into a smaller number of uncorrelated variables called principal components. The main aim of PCA is to reduce the dimensionality (number of variables) of the dataset but retain most of the original variability in the data. The first principal component accounts for as much of the variability in the data as possible, and each succeeding component accounts for as much of the remaining variability as possible. The mean elements concentrations of samples under study were subjected to a PCA. Three principal components were extracted, by assigning one principal component (PC) to the x-axis and another PC to the y-axis; maps were generated to visualize the similarity/dissimilarity relationships between the plotted points.

- *Enrichment factor*

The elaboration of obtained data from ICP-OES allows for the first time to evaluate enrichment factor (EF) for cementitious materials. The enrichment factor indicates the association of the elements to the substrate or to the atmospheric deposition. The (EF) was evaluated using the following formula:

$$EF\,(X) = \frac{[X]_{blackcrust} \;/ [Al]_{blackcrust}}{[X]_{substrate} \;/ [Al]_{substrate}} \quad,$$

where [X] and [Al] represent respectively the concentration of element X and Al in the black crusts and substrate. We use aluminum as reference element based on the chemical composition of the Portland cement mortar, assuming minor contribution of the pollutant Al. There was adopted that if the value of EF (X) > 5, the element X is in the crust due to atmospheric deposition, and not belonging to original building material (Geo et al., 2002; Arditsoglou and Samara, 2005).

4. Results and discussion

4.1. Experimental data of Centennial Hall

4.1.1. Optical Microscope Observations

The optical microscope (OM) observations performed on transversal thin section of specimens CH19, CH21, CH29, CH37, CH39 indicated that external surface of samples was covered by no homogenous damage layer, as it is shown in Figures 4.1 and 4.2.
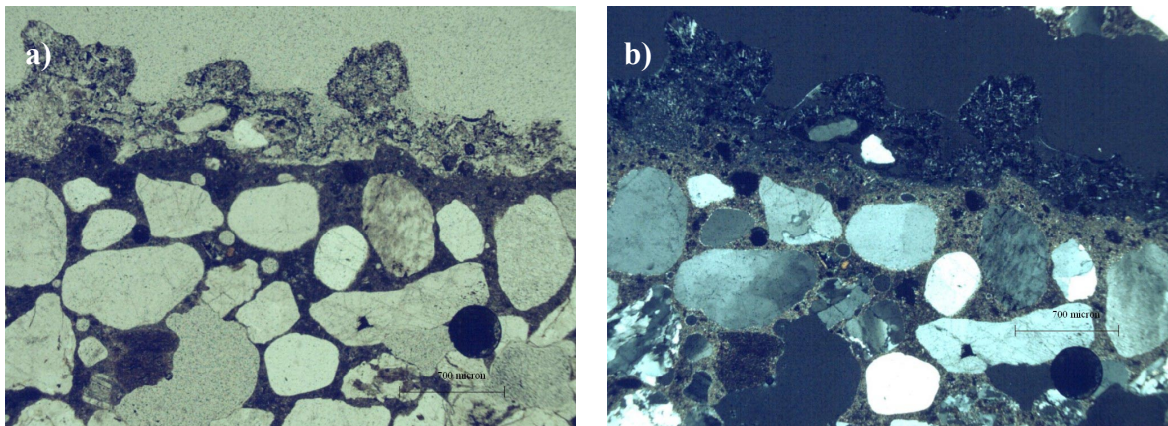
Figure 4.1. Optical micrographs (a) planed-polarised light, (b) cross-polarised light of damage layer in sheltered area (CH37).
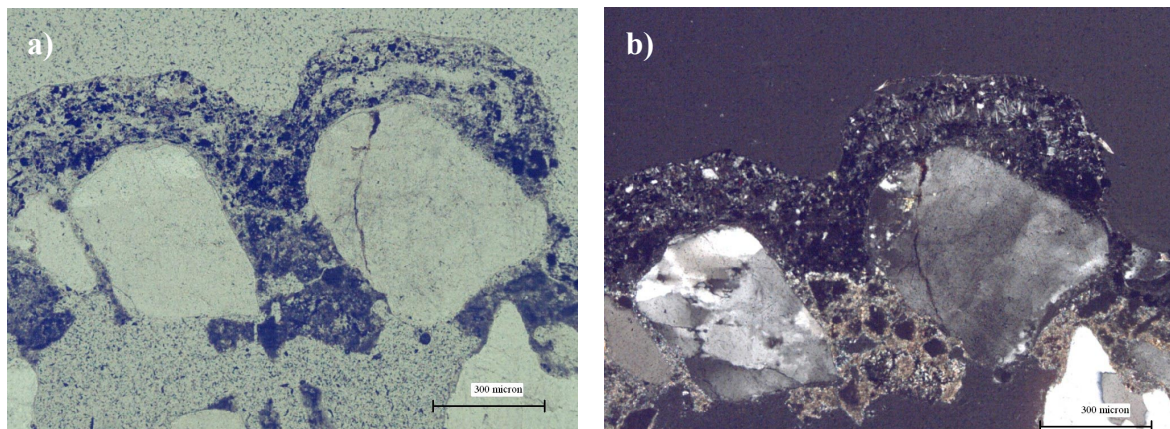
Figure 4.2. Optical micrographs (a) planed-polarised light, (b) cross-polarised light of damage layer in sheltered area (CH19). Black carbonaceous particles are clearly identifiable embedded in the gypsum matrix.
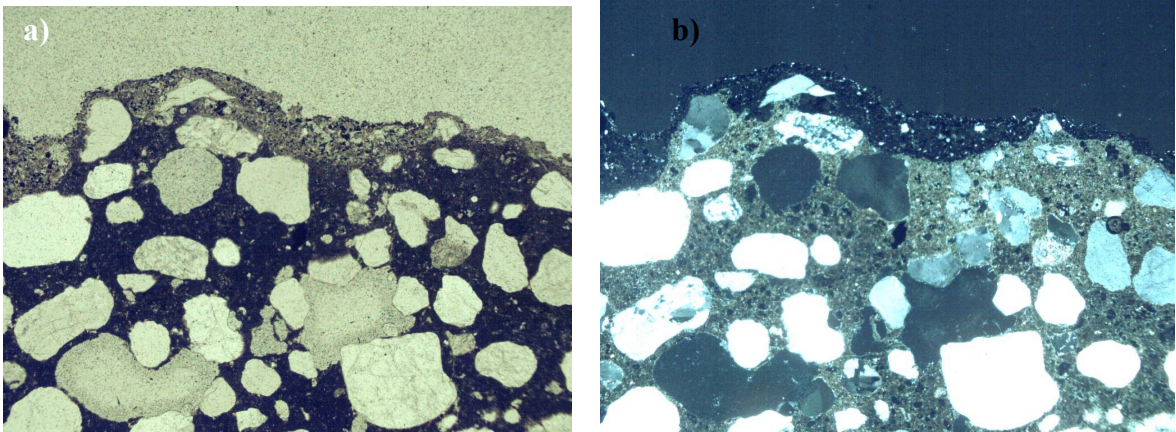
Figure 4.3. Optical micrographs (a) planed-polarised light (b) cross-polarised light of damage layer in partly sheltered area (CH29). Gypsum matrix clearly identifiable.
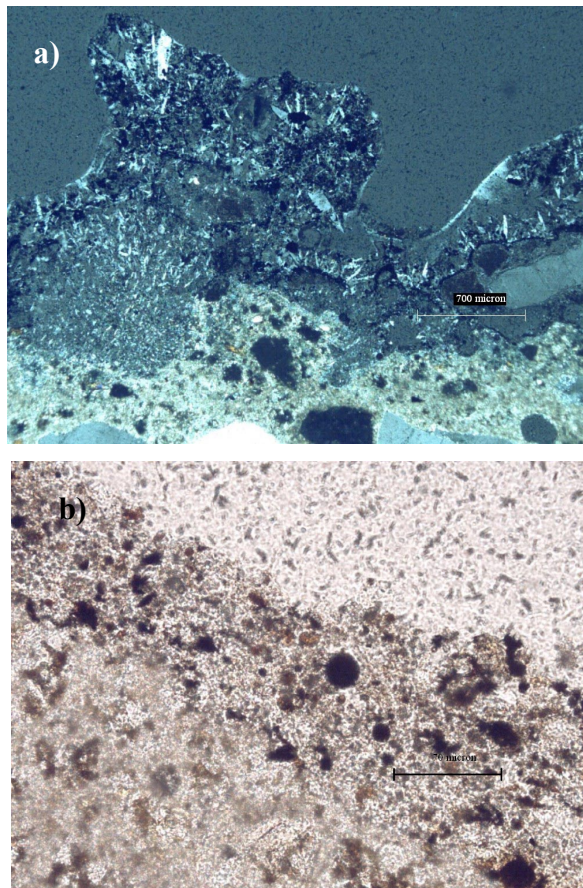
Figure 4.4. Optical micrographs (a) cross-polarised light (b) planed-polarised light of damage layer in sheltered area (CH19), black carbonaceous particles, yellow transparent aluminosilicate particles and orange iron oxides are observable.

The crust appeared in different thickness. In samples from sheltered areas (CH19, CH37, CH39) the thickness of the damage layer was ranging from 200 μm to 850 μm (Figures 4.1 and 4.2), with higher dimension in samples from upper part of the building (CH37, CH39). In case of samples from partly sheltered parts (CH21, CH29) the crust was thinner ranging from 100 μm to 300 μm as it is presented in Figure 4.3.

The damage layer in all samples is composed mainly of gypsum, quartz and iron oxides, presented in Figure 4.4. Along with gypsum matrix, two typologies of particles have been frequently observed: black carbonaceous particles with diameter from 13 μm to 30 μm, and yellow or white transparent aluminosilicate particles, generally 5-7 μm in diameter, presented in Figure 4.4.

The observations performed on the substrate indicated that the material is a cement mortar with a coarse texture and binder presenting the typical mineralogical and morphological features of hydraulic components. The mineralogical composition of the aggregate has been identified as follows: mainly monocrystalline and polycrystalline quartz, fragments of silicatic stones and sporadic feldspar crystals.

4.1.2. Scanning Electron Microscope Observations

The SEM-EDX analysis performed on the sample surfaces CH6, CH8, CH21, CH29, CH37 and CH39 confirmed the presence of gypsum with laminar structure, as it is shown in Figure 4.5. Two typologies of particles were also identified in gypsum matrix: (1) spherical shape particles with smooth surface (Figure 4.6), were characterized by the presence of silicon and aluminium as the main elements, with smaller amounts of Ca, S, K, Mg, Fe, and Ti, typical of aluminosilicate particles from coal combustion (Jabłońska et al., 2003); (2) particles with spongy structure (Figure 4.7) characterized by S as a main element followed by Ca, Si, Al, Fe, K, Cl, Mg, which represented carbonaceous particles from oil combustion (Bacci et al., 1983).
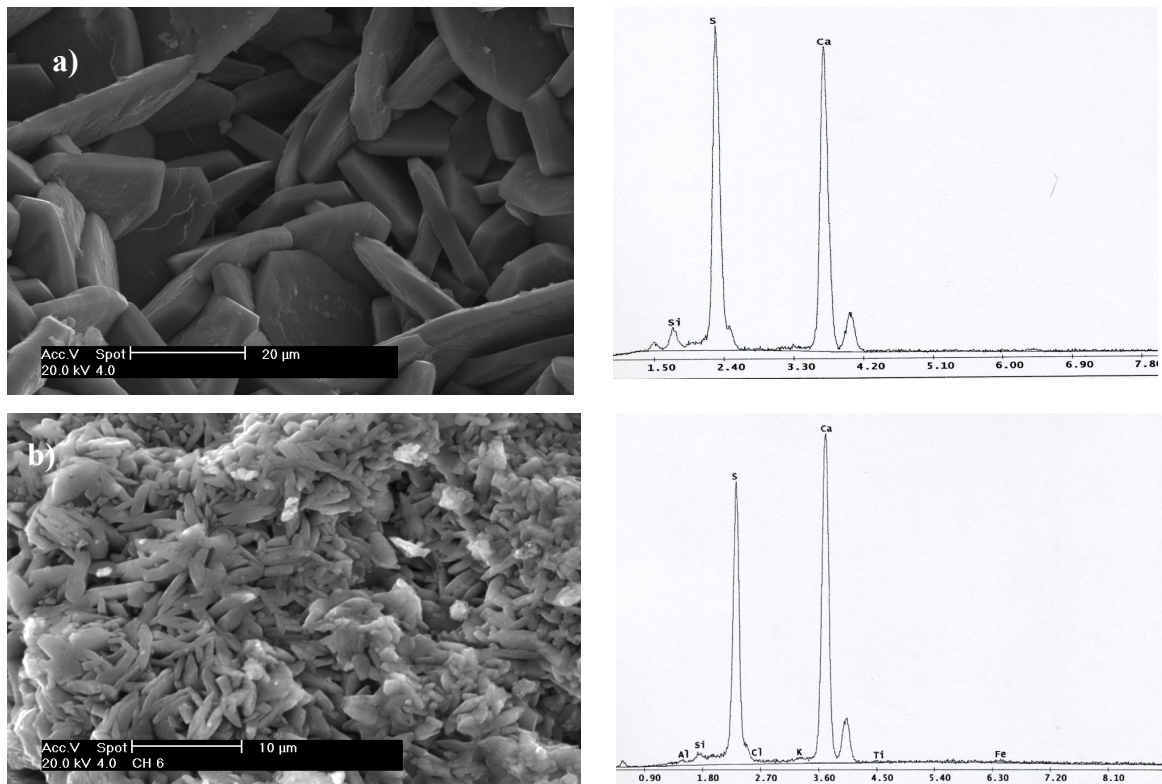
Figure 4.5. Scanning electron micrograph showing surface of damage layer on the left, and relative EDX spectrum on the right from (a) partly sheltered area (CH29) and (b) sheltered are (CH6).

The black carbonaceous particles are responsible for blackening of the surface and can play a catalytic role in sulphation process (Benner et al., 1982; Del Monte et al., 1984).
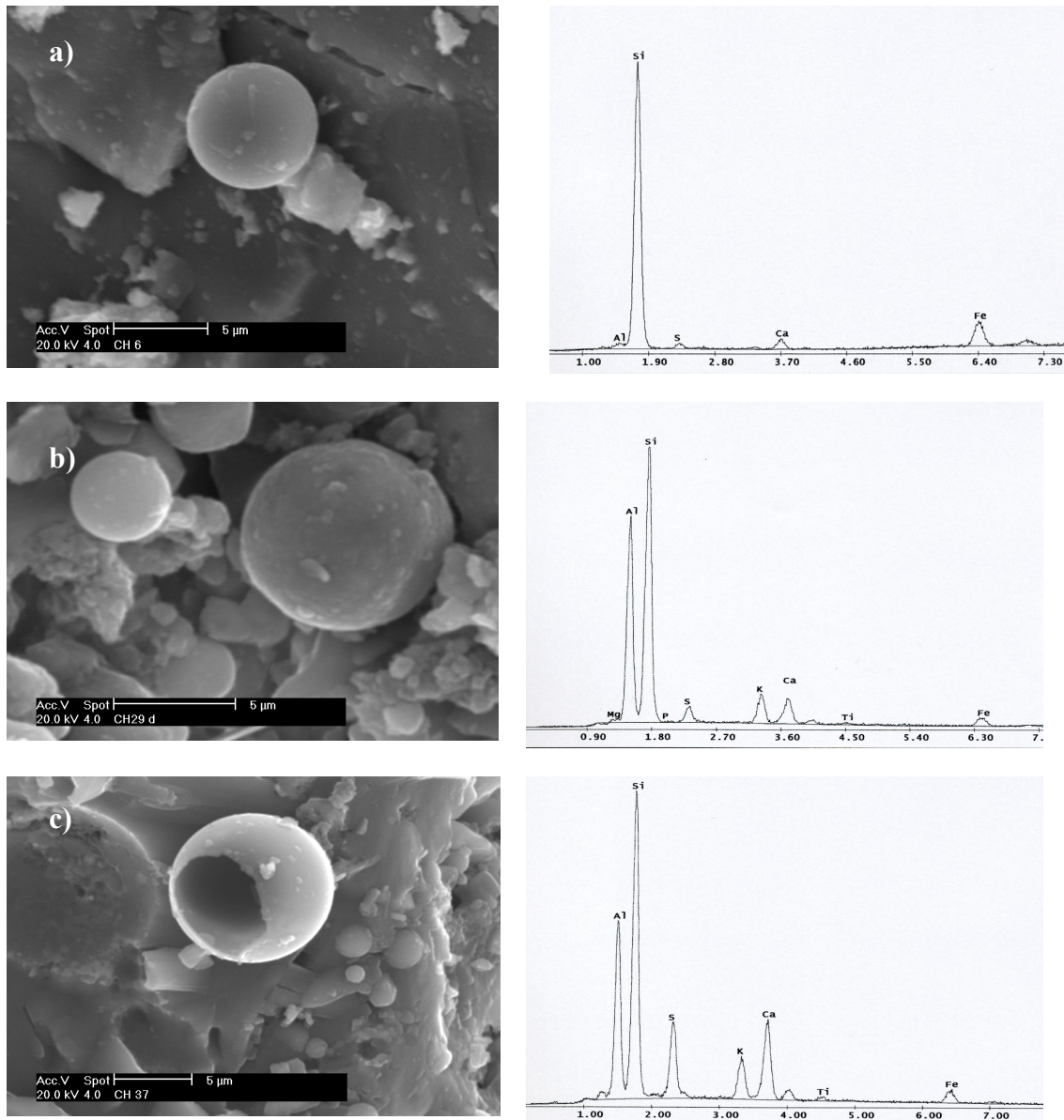
Figure 4.6. Scanning electron micrograph of aluminosilicate particles (a) in sample CH6, (b) in sample CH29, (c) in sample CH37 embedded in laminar gypsum with the EDX spectrum on the right.
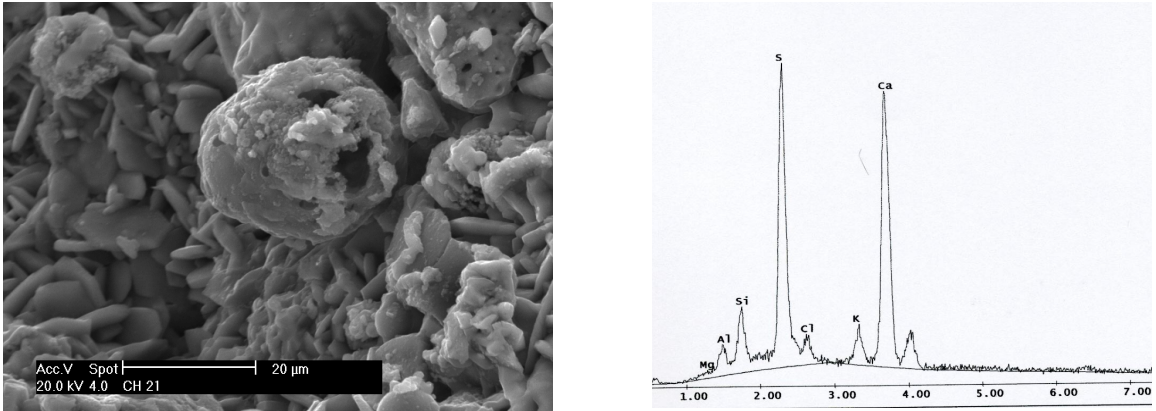
Figure 4.7. Scanning electron micrograph showing the carbonaceous particle embedded in lamellar gypsum with the EDX spectrum on the right.

The results obtained by SEM-EDX confirmed the results from optical microscope observations, highlighting that surface of the damage layer on the Centennial Hall were mainly composed of gypsum and fly ash from coal and oil combustion.

4.1.3. X-Ray Diffraction Analysis

The crystalline phases of damage layers and underlying material were revealed during X-ray diffraction analyses, the results are presented in Table 4.1.

Sample CH27, characteristic of undamaged concrete, was composed of minerals such as quartz with tracers of calcite, portlandite and feldspar (Figure 4.8), which were ascribable to the binder and aggregates of the concrete.

Table 4.1. Main crystalline phases revealed by X-ray diffraction in the analysed crusts and substrate collected on Centennial Hall (Wroclaw).

Sample	Gypsum	Quartz	Calcite	Portlandite	Feldspars	Magnetite	Hematite	Ilmenite	Rutile
CH27[1]		+ + + + +	tr	tr	tr				
CH11		+ + + + +	tr						
CH17	++	+ + + + +	tr				+	tr	tr
CH38	+ + + + +	+					+ +	+	
CH41	tr	+ + + + +	+ +			tr		tr	+

[a] +++++ main mineral present; ++++, +++ very abundant; ++ abundant; + present, tr tracers
[1] substrate

The samples of fragments (containing both damage layer and substrate (CH11, CH41)) show as main crystalline phases quartz and calcite, and traces of gypsum, ilmenite and rutile.

The two specimens of black damage layer, CH38 and CH17 respectively on a sheltered and partly sheltered surface, show gypsum and quartz as the main components followed by hematite, ilmenite, rutile and calcite. In Figure 4.9 is presented the diffractogram of damage layer (CH38).

The presence of quartz and calcite, identified in samples of fragments (CH11, CH41) and of damage layers (CH17, CH38), can be linked to both aggregates of underlying material or atmospheric deposition (solid dust, fly ash). The crystal phases occurring only in damage layers such as gypsum, hematite, ilmenite, magnetite and rutile are related to atmospheric deposition.
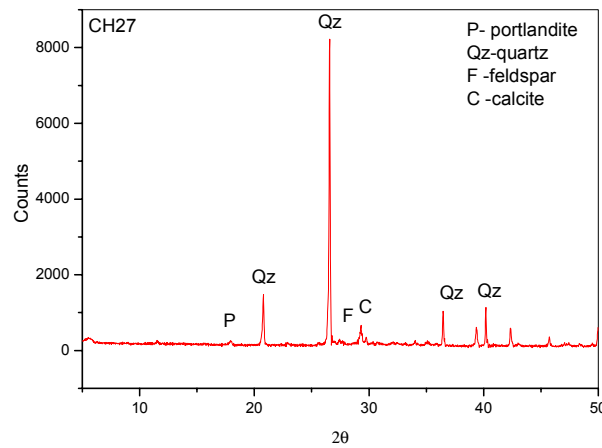
Figure 4.8. X- ray diffractogram of substrate (CH27) sample collected from Centennial Hall, Wroclaw (Poland).
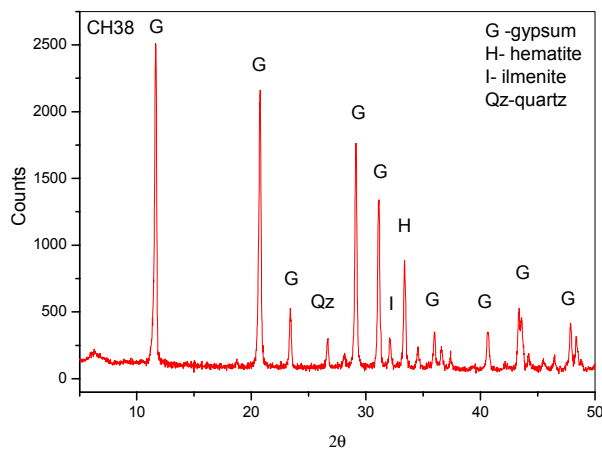
Figure 4.9. X- ray diffractogram of damage layer from sheltered are (CH38), Centennial Hall, Wroclaw (Poland).

Gypsum is formed due to the deposition of atmospheric SO_2/H_2SO_4 and subsequently interaction with cement components (Martínez-Ramírez et al., 1998; Pavlik et al., 2007). The most important man–made sources of sulphur dioxide are fossil fuel combustion, especially coal burning. Taking into account the location of Centennial Hall, the coal power station is the main source of SO_2, and also of tracers of fly ash such as hematite, ilmenite and rutile found in damage layers (Querol et al., 1996).

4.1.4. Differential and Gravimetric Thermal Analysis

The quantitative analysis of gypsum and carbonates were performed by means differential and gravimetric thermal analysis (DTA-TGA).

The results for samples representing the substrate (CH27) show significant mass loss of water up to 230 °C (Figure 4.10). This effect can be ascribe to surface water desorption as well as water loss from C-S-H gel (Gabrovsek et al., 2006). Then the alumino and silicate phases of cement underwent decomposition till temperature 429 °C. The further thermal reaction was the dehydroxylation of smaller portlandite till 520 °C, followed by decarbonation of carbonates up to 776 °C. The percentages of portlandite and carbonates in the sample are presented in Table 4.2.

Table 4.2. Concentrations (%) of gypsum, carbonates and portlandite in samples from Centennial Hall.

Sample	Portlandite[1]	Gypsum[2]	Carbonates[3]
CH27[*]	2.45		7.47
CH38		87.35	
CH42		31.75	

[*] substrate
[1] calculated as $Ca(OH)_2$, [2] calculated as $CaSO_4 \cdot 2H_2O$, [3] calculated as $CaCO_3$
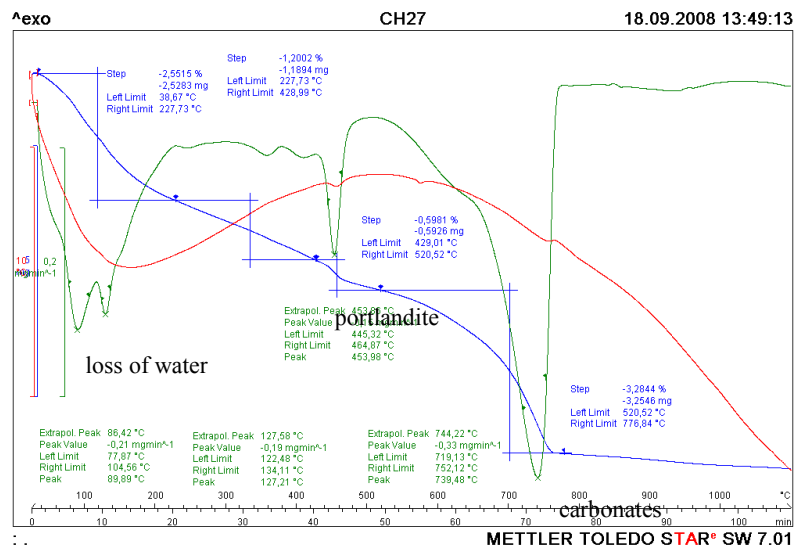
Figure 4.10. DTA-TGA graphs of sample representative substrate (CH27) from Centennial Hall.
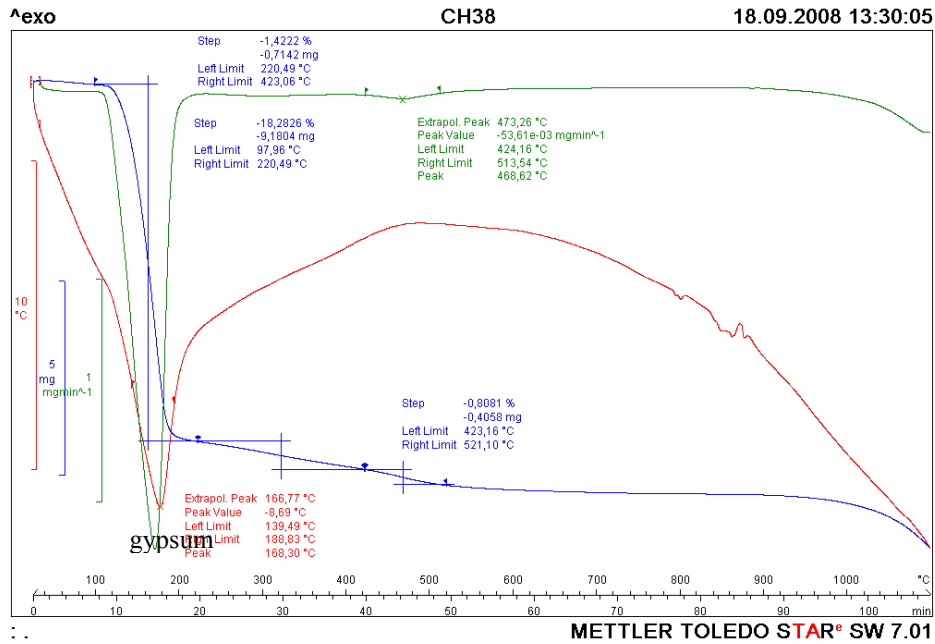
Figure 4.11. DTA-TGA graphs of sample representative of black crust (CH38) from Centennial Hall.

The analysis of damage layer show dehydratation of gypsum between 90 ºC and 220 ºC, with endothermic reaction, as it is presented in Figure 4.11. The quantification of gypsum in crust (Table 4.2) reveals the highest amount of 87 % in sample of thick black crust from sheltered area (CH38). The results confirmed the previous analysis that gypsum is a major mineral in black crust.

4.1.5. Ion Chromatography data

The results obtained by ion chromatography technique on samples collected from Centennial Hall are presented in Table 4.3.

The results show that sulphate ($SO_4^=$) was the most abundant anion, observed in the highest values in samples of black damage layer from sheltered areas e.g. samples CH18 (50 %), and CH38 (41 %). Lower concentrations are observed in samples from partly protected parts, with the minimum of 0,8 % in sample CH15. These results are compatible with optical microscope observation, during which was also revealed thicker damage layer in samples from areas completely sheltered from rain run-off. This fact is connected to the solubility of gypsum, which is removed by rain water in areas partly sheltered.

Table 4.3. Anion concentration (ppm) measured by ion chromatography in damage layer and substrate collected from Centennial Hall.

Sample	$SO_4^=$	NO_3^-	NO_2^-	Br^-	Cl^-	CHO_2^-	$C_2H_3O_2^-$	$C_2O_4^=$
CH27[1]	2779	321	169	n.d	237	226	7684	461
CH2	110685	921	338	673	486	1229	6370	1052
CH3	84269	1004	201	398	673	811	4507	1005
CH4	70903	400	291	333	520	989	3953	457
CH5	27104	174	86	183	171	272	n.d.	n.d.
CH9	39172	700	839	n.d.	137	4799	1659	367
CH14	99623	808	300	808	322	1375	5553	1353
CH15	8228	144	n.d.	n.d.	93	135	n.d.	173
CH18	502320	1751	n.d.	2503	794	5851	n.d.	n.d.
CH38	410361	550	569	2015	664	9020	32948	95
CH42	135684	659	332	394	561	4729	6082	n.d.

[1] substrate

n.d. = not detected.

Small (C1-C2) organic anions such as, acetate ($C_2H_3O_2^-$), formate (CHO_2^-) and oxalate ($C_2O_4^=$), were detected in considerable amount listed in order of abundance. Acetate and formate have the maximum concentration in sample from sheltered area at the highest point of the building, 32948 ppm and 9020 ppm respectively. Oxalate is the less abundant among organic soluble anion with maximum concentration of 1353 ppm.

The role of organic anions in deterioration of cement materials and also in natural stones is still not well understood. The studies dedicated to presence of organic anions on stones,

such as limestone, sandstones, indicate three origins from three different sources: (1) deposition of primary and secondary atmospheric pollutants, (2) biological weathering and (3) restoration treatments (Sabbioni et al., 2003). The special attention has been given to the oxalate patina, which has been found on cultural heritage related to a variety of historic periods and on different materials (Del Monte et al., 1987). The studies are mainly focused on the oxalate patina formed on natural stones and it is mainly ascribed to biological origin (Del Monte and Sabbioni, 1987; Sabbioni and Zappia, 1991). The chemical-physical interaction between colonizing micro-organism secreting oxalic acid and the limestone substrate bring the dissolution of carbonates; calcium cations freed from this process lead to formation of calcium oxalate (Del Monte and Sabbioni, 1983). According to De Santis Allegrini (1989) and Saiz-Jimenez (1989) the presence of oxalic acid can be associated with air pollution deposition. Saiz-Jimenez (1989) hypothesized airborne oxalic acid originated by combustion of fossil fuel. The third hypothesis indicates that organic anions originate from decomposition of organic treatments applied on surface during restorations work (Rampazzi et al., 2004), however, in the case of Centennial Hall there are not information about restoration treatments.

Smaller quantities were detected of NO_3^-, ranging between 144 ppm and 1751 ppm, and NO_2^-, with maximum value of 839 ppm. Nitrates (NO_3^-) and nitrites (NO_2^-), which presence is mainly linked to industrial activity and car emission, however because of the high solubility of nitrogen salts, formed due to the deposition of NO_x/HNO_3, the detected amounts of NO_3^- and NO_2^- cannot be consider as real tracers of the factors causing damage (Derry et al., 2001).

During IC analyses there were also detected significant amounts of Br- and Cl-, which presence in this case could be probably ascribed to fossil fuel combustions (Arditsoglou and Samara, 2005).

4.1.6. Carbon Compound Discrimination and Measurement

The carbon fraction present in black crusts are presented in Table 4.4, where is observed that total carbon (TC) ranges from a minimum of 1 % to a maximum of 3 % of the total mass of sample.

In Figure 4.12 are presented the percentage fractions of total carbon: the non carbonate carbon (NCC) and carbonate carbon (CC). The NCC is an important fraction of TC, ranging from 68 % to 96 % of TC, and predominates in all samples over CC. Indeed CC fraction appears with values below 35 % of TC.

Table 4.4. The TC, NCC, CC, EC and OC concentrations in percentage and OC/EC ratio measured in crusts collected on Centennial Hall.

Sample	TC[1]	CC[3]	NCC[2]	EC[2]	OC[3]	OC/EC
CH9	1.01	0.20	0.81	0.00	0.81	
CH15	1.57	0.31	1.26	0.00	1.26	
CH18	3.12	0.99	2.14	1.26	0.88	0.69
CH38	2.79	0.27	2.52	2.29	0.23	0.10
CH42	0.26	0.01	0.25	0.03	0.22	8.02

[1] measured on substrate, [2] measured on treated samples, [3] calculated
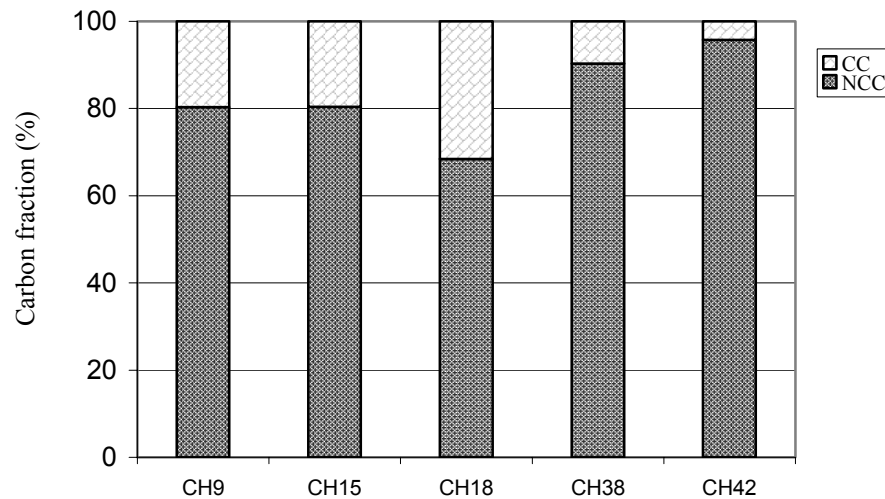
Figure 4.12. The non carbonate carbon (NCC) and carbonate carbon (CC) percentage fraction of total carbon in samples of damage layers collected from Centennial Hall (Poland).
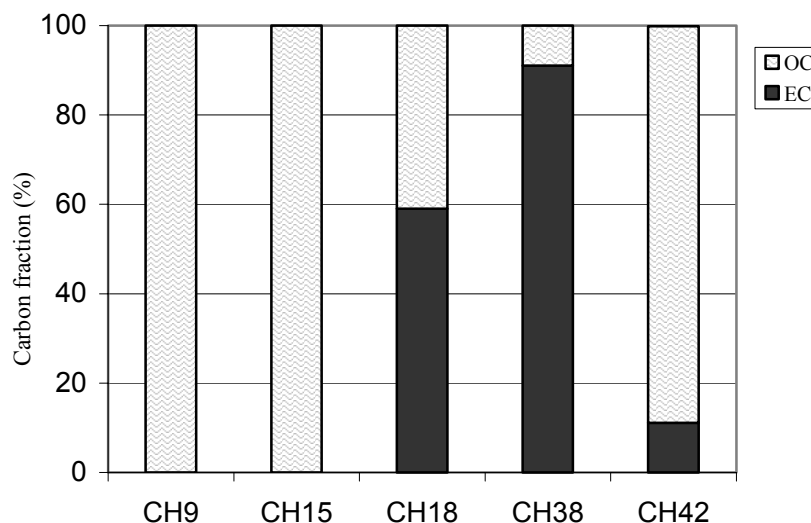
Figure 4.13. The organic carbon (OC) and elemental carbon (EC) percentage fraction of NCC.

Elemental carbon (EC) and organic carbon (OC) percentages with respect to NCC are reported in Figure 4.13, which show very clearly that EC fraction has higher contribution than OC in samples of black crust (CH18 and CH38). This fact is linked to the nature of EC, which constitutes a quantitative index of the black carbonaceous particles embedded in crusts (Lanting, 1986). The elemental carbon comes from combustion–generated aerosols (Kupiainen and Klimont, 2007), which presence in case of Centennial Hall is an effect of fix combustion sources such as coal power station in neighbourhood of the building and coal burning in domestic heating.

Organic carbon predominates over elemental carbon (Figure 4.13) in samples of grey crust (CH9, CH15, CH42), achieving 100 % of NCC in samples CH9 and CH15. Bearing in mind that organic anions (formate, acetate and oxalate) constitute a significant fraction of OC (Sabbioni et al., 2003), this results can be comparable with the one from IC analyses. In fact in case of sample CH9 and CH42 organic anions were detected in significant amounts. The organic carbon (as it was in case of organic anions) can have different origin: primary air pollutants from incomplete combustion of fossil fuels, secondary air pollutants, biological weathering and restoration treatment. For this specific case, it has to be underlined that there are not information available on the restoration works done.

4.1.7. Induce Coupled Plasma-Optical Emission Spectroscopy

The results of elements concentration and corresponding standard deviation from ICP-OES, performed on the samples from Centennial Hall are listed in Table 4.5. The elements with the high concentration were Si, Al, Ca, S, Fe and Na. Sulphur had the highest concentration in sample of black crust (CH38), that reflects results from DTA-TGA, where in this sample was detected the highest amounts of gypsum, and results from IC with high concentration of $SO_4^=$. In Table 4.6 are presented, for each element, the significant positive differences between the concentrations in samples from damage layers and substrate, obtained by one tailed t-test (significant level α=0.05, degree of freedom N=4 for all sample, except sample CH38, where N=3). The critical values of t_{table} are: $t_{(N=4, \alpha=0.05)}$=2.78, and $t_{(N=3, \alpha=0.05)}$=3.18 (Mankiewicz, 2001). The elements with positive significant difference between damage layer and substrate, and therefore with possible origin from atmospheric deposition, were S, Zn, Cu, Pb, Ca, As (in case of As only in sample of thick black crust). The exception in investigation were samples CH22 and CH23, which were collected from wall of small construction on the Centennial Hall, probably built in recent years, but there is lack of information about it. The PCA analyses allowed to extract three principal components accounting for 87 % of the total variance, the 1st principal component explains 44 % of variation, 2nd PC 22 % of variation and 3rd PC 21 %. By assigning one principal component (PC) to the x-axis and another PC to the y-axis, we generated maps to visualize the similarity/dissimilarity relationships between the plotted points, the maps are presented in Figure 4.14. The most important dynamics of the system observed in Figure 4.14 a and 4.14 b was association of As, Ca, Cu, Pb, S, Sn, Zn with samples of damage layers (CH19, CH21, CH29, CH38, CH40) therefore with atmospheric deposition. The elements ascribed to the substrate (sample CH27) were Mg, Na, Al, Mn, Mo, and Fe which are typical for Portland cement. There was also clearly visualized the separation of the two samples CH22 and CH23, that was in agreement with results from t-test and hypothesis that about the different age of those samples.

The values of elaborated enrichment factors are presented in Table 4.7. The elements with EF > 5 and therefore atmospheric origin are As, Cu, Pb, S, Sn, Zn, with exception of sample CH22 and CH23.

Table 4.5. Elemental concentrations (ppm – µg metal/g crust) and corresponding standard deviation, ICP-OES analyses of samples from Centennial Hall (Wroclaw).

Sample	Al	As	Ba	Be	Bi	Ca	Cd	Co	Cr	Cu	Fe	K	Li	Mg	Mn	Mo	Na	Ni	P	Pb	Pt	S	Sb	Se	Si	Sn	Sr	Ti	Tl	V	Zn	Zr
CH27[1]	23795	1	345	13	912	90200	5	118	925	34	31653	8252	8399	15039	602	22	9288	516	1560	10	9	1522	5	259	200236	2	474	3718	-	81	92	83
CH19	14324	4	454	2	210	104629	5	31	198	52	9617	5600	11868	1572	397	-	2568	108	251	206	6	55117	21	58	173547	15	390	581	-	22	1066	25
CH21	12734	21	234	-	730	174142	2	32	731	175	11214	5434	9990	1914	154	-	2390	409	-	128	-	123520	4	136	76646	32	474	684	-	22	174	25
CH22	10434	-	151	-	28	31925	4	4	18	23	4881	4744	8338	710	153	-	1503	10	-	54	4	12082	31	21	240798	6	94	389	-	9	111	36
CH23	10647	-	182	-	260	39825	3	5	256	57	4446	4538	9924	710	77	-	2351	135	-	56	3	16211	33	83	238846	11	122	291	-	10	65	21
CH29	11277	11	207	1	1953	151897	4	55	1996	355	14763	3675	7031	1427	188	9	2694	1078	-	32	-	94796	10	486	139199	-	526	502	-	17	141	20
CH38	5174	16	210	1	32	130204	2	24	27	73	6999	2238	9435	1049	55	-	1056	23	320	225	-	154121	1	-	34748	9	462	537	-	22	140	14
CH40	8938	8	186	-	53	139351	3	16	45	74	6377	4347	11180	1460	169	-	1792	30	136	111	2	83261	15	-	140779	10	498	420	-	20	225	19

Standard deviation

| Sample	Al	As	Ba	Be	Bi	Ca	Cd	Co	Cr	Cu	Fe	K	Li	Mg	Mn	Mo	Na	Ni	P	Pb	Pt	S	Sb	Se	Si	Sn	Sr	Ti	Tl	V	Zn	Zr
CH27[1]	1466	2	8	1	40	1	1	2	40	2	621	826	1	467	25	3	632	22	82	9	1	689	1	10	7933	3	20	83	-	3	1	2
CH19	118	6	6	1	1	2	1	2	1	1	244	25	1	14	1	-	16	2	3	6	1	406	2	9	2843	2	2	1	-	1	6	1
CH21	92	23	2	-	4	2	1	2	7	1	37	31	1	9	3	-	31	4	-	18	-	874	7	35	2092	7	3	3	-	1	1	1
CH22	49	-	1	-	1	1	1	1	1	1	26	30	1	4	1	-	6	1	-	6	1	36	2	9	1013	2	1	1	-	1	1	1
CH23	83	-	2	-	1	1	1	1	1	1	21	23	1	3	1	-	10	1	-	6	1	43	2	8	1367	3	1	1	-	1	1	1
CH29	57	20	1	1	8	1	1	2	15	2	90	13	1	78	2	1	19	10	-	16	-	399	4	26	1721	-	5	9	-	1	1	1
CH38	683	3	6	1	1	1	1	1	1	1	156	242	1	26	1	-	64	2	38	9	-	11084	1	-	7429	3	16	6	-	1	4	2
CH40	53	7	2	-	1	1	1	1	1	1	42	43	1	11	1	-	22	1	6	7	1	622	2	-	2686	3	8	3	-	1	2	1

[1] substrate

Table 4.6. Differences between the mean concentrations of the elements in damage layer and substrate, and corresponding $t_{calculated}$ values calculated for samples from Centennial Hall; in bold are the positive significant differences found by one tailed t-test, α=0.05, N=4 for all samples (t_{table} = 2.78), except for sample CH38, where N=3 (t_{table}=3.18).

Sample	Al	As	Ba	Be	Bi	Ca	Cd	Co	Cr	Cu	Fe	K	Li	Mg	Mn	Mo	Na	Ni	P	Pb	Pt	S	Sb	Se	Si	Sn	Sr	Ti	Tl	V	Zn	Zr
CH19	-9472	3	**109**	-11	-703	**14429**	-1	-87	-727	**18**	-22036	-2652	**3**	-13466	-205	-22	-6721	-409	-1309	**196**	-3	**53595**	**16**	-201	-26689	**14**	-84	-3136	-	-59	**974**	-59
CH21	-11061	19	-111	-13	-182	**83942**	-4	-87	-194	**141**	-20439	-2818	**2**	-13125	-449	-22	-6898	-108	-1560	**118**	-9	**121998**	-1	-123	-123590	**30**	0	-3033	-	-59	**82**	-58
CH22	-13362	-1	-194	-13	-885	-58275	-1	-114	-907	-11	-26772	-3508	-1	-14328	-449	-22	-7785	-506	-1560	**44**	-4	**10560**	26	-238	**40562**	4	-380	-3329	-	-72	**19**	-48
CH23	-13148	-1	-163	-13	-652	-50375	-2	-113	-669	**23**	-27207	-3714	**2**	-14329	-525	-22	-6937	-382	-1560	**46**	-6	**14689**	28	-176	**38610**	9	-352	-3427	-	-71	-27	-62
CH29	-12519	**10**	-138	-12	1041	**61697**	-1	-63	**1070**	**321**	-16890	-4577	-1	-13612	-414	-14	-6594	**562**	-1560	23	-9	**93274**	4	**227**	-61037	-2	**52**	-3215	-	-64	**49**	-63
CH38	-18622	**15**	-135	-12	-880	**40004**	-4	-95	-898	**39**	-24654	-6015	1	-13990	-547	-22	-8232	-493	-1240	**215**	-9	**152599**	-4	-259	-165489	7	-12	-3181	-	-59	**49**	-70
CH40	-14858	**7**	-159	-13	-859	**49151**	-2	-102	-880	**40**	-25275	-3906	**3**	-13578	-433	-22	-7496	-487	-1424	**102**	-6	**81739**	**10**	-259	-59457	8	24	-3298	-	-61	**134**	-64

$t_{calculated}$

Sample	Al	As	Ba	Be	Bi	Ca	Cd	Co	Cr	Cu	Fe	K	Li	Mg	Mn	Mo	Na	Ni	P	Pb	Pt	S	Sb	Se	Si	Sn	Sr	Ti	Tl	V	Zn	Zr
CH19	-11.15	1.04	18.33	-55.57	-30.61	8.80	-3.97	-52.44	-31.76	17.10	-57.19	-5.56	20.33	-49.89	-14.31	-14.45	-18.42	-32.23	-27.63	30.22	-5.92	116.04	15.61	-27	-5.49	6.34	-7.02	-65.33	-	-38.03	282.54	-47.58
CH21	-13.04	1.44	-23.27	-51.52	-7.90	67.05	-5.63	-48.13	-8.35	114.55	-56.89	-5.91	9.25	-48.63	-31.21	-12.68	-18.89	-8.35	-32.59	10.16	-6.50	189.81	-0.28	-6	-26.09	6.76	-0.01	-63.15	-	-33.70	113.05	-47.51
CH22	-15.78	-0.25	-41.71	-62.46	-38.55	-65.96	-10.04	-80.45	-39.63	-10.44	-74.58	-7.35	-0.36	-53.10	-31.38	-14.50	-21.35	-40.02	-32.93	7.02	-19.22	26.50	25.20	-32	8.78	1.86	-32.02	-69.34	-	-47.53	23.80	-38.65
CH23	-15.51	-0.28	-34.32	-65.35	-28.41	-56.10	-12.40	-82.61	-29.22	20.85	-75.81	-7.79	8.97	-53.10	-36.76	-14.20	-19.02	-30.13	-32.86	7.41	-11.79	36.84	22.87	-24	8.31	3.85	-29.66	-71.37	-	-46.69	-34.58	-50.68
CH29	-14.78	0.82	-29.57	-55.82	44.50	53.81	-2.20	-33.97	43.76	205.26	-46.60	-9.60	-8.01	-49.77	-28.89	-8.60	-18.08	40.57	-32.79	2.07	-11.10	202.78	1.94	14	-13.02	-0.39	4.29	-66.60	-	-39.16	59.09	-51.45
CH38	-19.11	6.13	-20.64	-60.00	-38.34	38.89	-12.94	-68.32	-39.24	26.60	-65.69	-11.87	3.86	-51.73	-38.29	-15.08	-22.40	-38.79	-22.77	25.30	-102.55	19.45	-4.53	-47	-23.74	2.60	-0.77	-65.95	-	-37.65	17.79	-54.17
CH40	-17.54	1.56	-32.76	-64.81	-37.42	45.71	-11.42	-75.64	-38.42	35.17	-70.31	-8.18	14.30	-50.31	-30.25	-14.46	-20.55	-38.46	-30.00	15.31	-15.23	152.53	7.46	-32	-12.30	3.36	1.89	-68.65	-	-38.90	100.50	-52.31

Table 4.7. Enrichment factor (EF) (with respect to Al) of samples collected from Centennial Hall (Wroclaw); in bold values of EF > 5.

Sample	Al	As	Ba	Be	Bi	Ca	Cd	Co	Cr	Cu	Fe	K	Li	Mg	Mn	Mo	Na	Ni	P	Pb	Pt	S	Sb	Se	Si	Sn	Sr	Ti	Tl	V	Zn	Zr
CH19	1.0	**7.4**	2.2	0.3	0.4	1.9	1.4	0.4	0.4	2.6	0.5	1.1	2.3	0.2	1.1	-	0.5	0.3	0.3	**34.8**	1.1	**60.2**	6.9	0.4	1.4	**15.1**	1.4	0.3	-	0.5	**19.3**	0.5
CH21	1.0	**37.8**	1.3	-	1.5	3.6	0.6	0.5	1.5	**9.6**	0.7	1.2	2.2	0.2	0.5	-	0.5	1.5	-	**24.3**	-	**151.7**	1.5	1.0	0.7	**34.7**	1.9	0.3	-	0.5	3.5	0.6
CH22	1.0	-	1.0	-	0.1	0.8	1.6	0.1	-	1.5	0.4	1.3	2.3	0.1	0.6	-	0.4		-	**12.5**	1.1	**18.1**	13.9	0.2	2.7	**7.7**	0.5	0.2	-	0.2	2.8	1.0
CH23	1.0	-	1.2	-	0.6	1.0	1.3	0.1	0.6	3.8	0.3	1.2	2.6	0.1	0.3	-	0.6	0.6	-	**12.8**	0.8	**23.8**	14.4	0.7	2.7	**13.9**	0.6	0.2	-	0.3	1.6	0.6
CH29	1.0	**22.3**	1.3	0.2	4.5	3.6	1.6	1.0	4.6	**22.0**	1.0	0.9	1.8	0.2	0.7	0.8	0.6	4.4	-	**7.0**	-	**131.4**	3.9	4.0	1.5	-	2.3	0.3	-	0.4	3.2	0.5
CH38	1.0	**71.9**	2.8	0.5	0.2	**6.6**	1.4	0.9	0.1	**9.8**	1.0	1.2	**5.2**	0.3	0.4	-	0.5	0.2	0.9	**105.4**	-	**465.7**	0.8	0.0	0.8	**23.1**	4.5	0.7	-	1.2	**7.0**	0.8
CH40	1.0	**20.4**	1.4	-	0.2	4.1	1.5	0.4	0.1	**5.8**	0.5	1.4	3.5	0.3	0.7	-	0.5	0.2	0.2	**30.2**	0.7	**145.7**	7.8	0.0	1.9	**15.2**	2.8	0.3	-	0.7	**6.5**	0.6
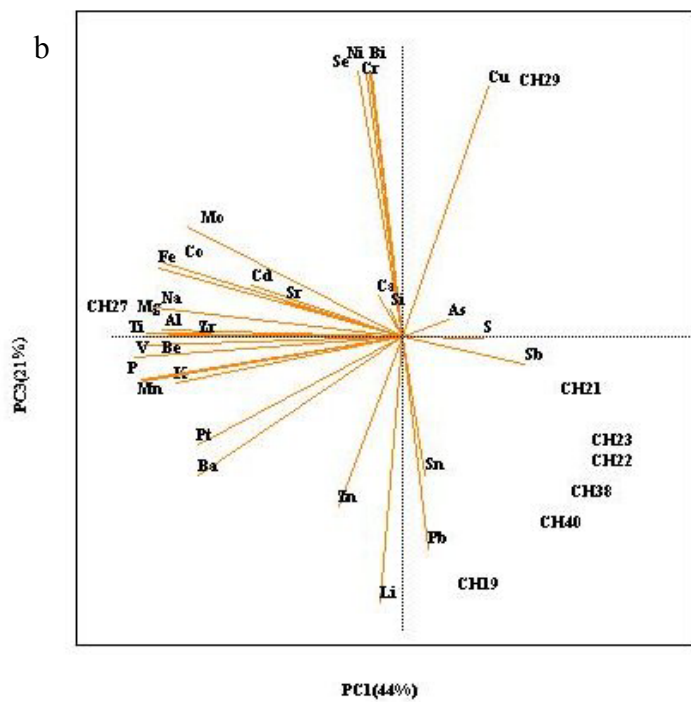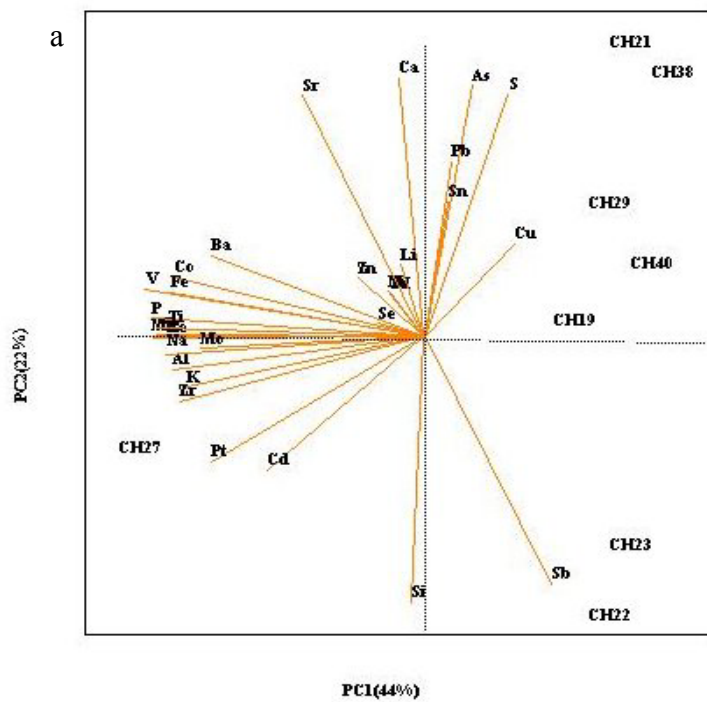
Figure 4.14. Principal Components Analyses, maps generated for results of ICP-OES, Centennial Hall (Wroclaw), a) PC1 verso PC2, b) PC1 verso PC3.

63

Table 4.8. The results from t-test, PCA and EF presenting elements coming from atmospheric deposition.

Method	Elements with atmospheric deposition:
t-test	As, Ca, Cu, Pb, S, Sn, Zn
PCA	As, Cu, Pb, S, Sb, Sn, Zn
EF	As, Cu, Pb, S, Sn, Zn

The results from t-test, PCA and EF are summarized in Table 4.8. An agreement between the results from the PCA and EF methods is observed: the elements linked to the atmospheric deposition and contribution of a variety pollution emissions are As, Cu, Pb, S, Sn, Zn. Considering the location of the Centennial Hall building, sulphur, arsenic and tin can be ascribed to fix combustion sources such as coal power generation, industry and domestic combustion of fossil fuels (Bityukova, 2006; Querol et al., 1995). The finding of Cu, Pb and Zn in damage layer from Centennial Hall can be also attributed to motor exhaust (Caselles et al., 2002).

4.1.8. Concluding remarks

The complete characterization of damage layers formed on cement monument such as Centennial Hall, show that gypsum, due to dry and wet SO_2 deposition, is the main damage product, whose effects lead to the loss of strength and durability of the cement matrix. The highest amounts of gypsum were found in sheltered areas. Such surfaces are not exposed to rain run-off and are therefore the accumulation ground for products of interaction between atmospheric deposition and building material constituents. The lower amount found in the partially sheltered area is connected to the solubility of this mineral. The main sources of atmospheric SO_2, taking into account the location of Centennial Hall, are power generation, industry and domestic combustion of fossil fuels. Moreover, numerous carbonaceous and aluminosilicate particles were found embedded in gypsum matrix. The carbonaceous particles are responsible for the blackening of the surface in areas protected from rain wash out and additionally play a catalytic role in the sulphation process. The quantification of carbon fractions of anthropogenic origin underlines the role of carbonaceous particulate matter in causing an aesthetic damage of the surface (i.e. darkening). The aluminosilicate particles have origin from coal combustion, this underlines the impact of coal power station and coal use in domestic heating on the black crust formation on the Centennial Hall. Additionally, the elaboration of EF showed the atmospheric origin of trace elements accumulated in the black crust, confirming that Centennial Hall deterioration is mainly caused by multi-pollutants emitted by coal combustion.

The results obtained show that the surface deterioration of the Centennial Hall is mainly caused by dry and wet deposition of SO_2 and fly ash from coal combustion, and subsequent interaction with the cement components. These results for the first time demonstrate the impact of coal power stations on black crust formation on cementitious materials.

4.2. Experimental data of Chiesa dell'Autostrada del Sole

4.2.1. Optical Microscope Observations

The optical microscope observations of thin section of sample FIC2 collected from Chiesa dell'Autostrada del Sole indicated the absence of gypsum layer on the surface (Figure 4.15). There were recognizable on the material surface yellow and orange transparent iron oxides, as it is shown in Figure 4.16. This result shows that surface is not affected by sulphation process, this fact is closely connected to the frequent restoration works performed at the building (every 2-3 years).
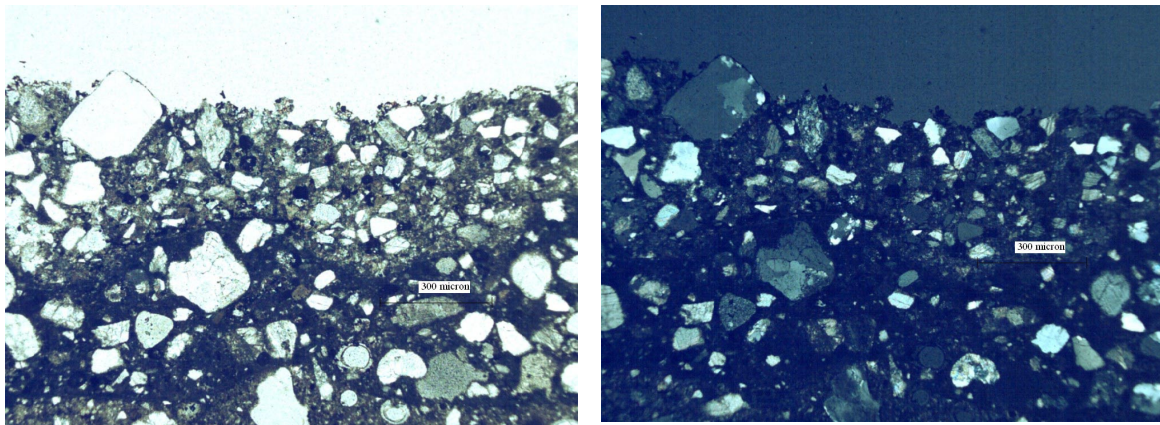
Figure 4.15. Optical micrographs (a) planed-polarised light, (b) cross-polarised light of sample (FIC2) collected from Chiesa dell'Autostrada del Sole. The external surface of sample is not affected by sulphation process.
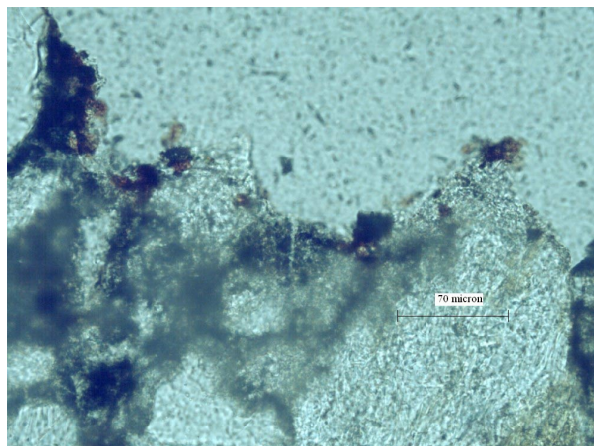
Figure 4.16. Optical micrograph, planed-polarised light of sample (FIC2) collected from Chiesa dell'Autostrada del Sole; yellow-orange iron oxides are observable on the external surface.

The substrate identifiable as cement mortar with binder presenting the typical mineralogical and morphological features of hydraulic components. The aggregate is heterogeneous and poorly sorted. By the mineralogical point of view the aggregate is in order of abundance composed of monocrystalline and polycrystalline quartz, fragments of carbonate stones, calcite, fragments of silicatic rocks and amorphous silica.

4.2.2. Scanning Electron Microscope Observations

The scanning electron micrograph of a sample from Chiesa dell'Autostrada del Sole presented in Figure 4.17, shows that surface is not covered by lamellar gypsum. The EDX analyses indicate that the main elements are Si, Ca, Al and K, typical for Portland cement: this additionally confirms the lack of sulfation process on the surface, that was also revealed during the optical microscope observations.
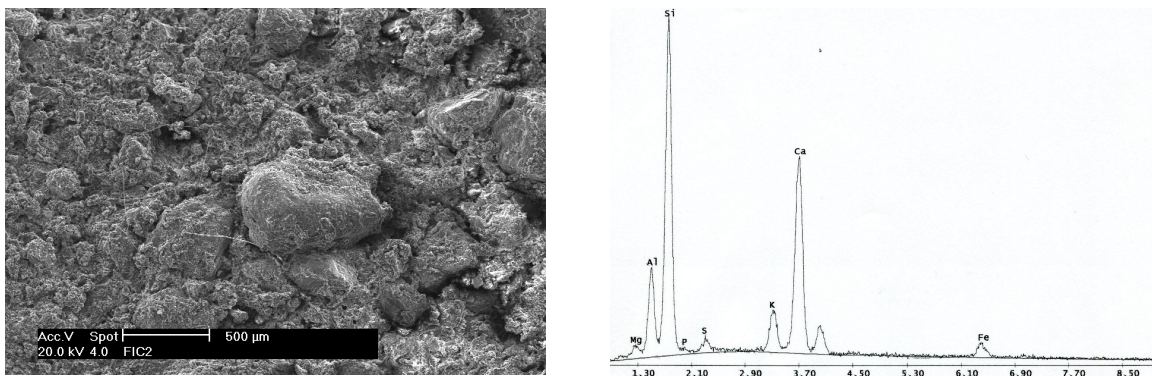
Figure 4.17. Scanning electron micrograph showing the surface of sample from Chiesa dell'Autostrada del Sole, with relative EDX.

Sporadically, on the surface were observed smooth aluminosilicate particles, presented in Figure 4.18. The nature of particles is confirmed by EDX showing Si as major element and Al, Ca, S, K and Ti as minor. Those particles are delivered from combustion processes (Jabłońska et al., 2003).
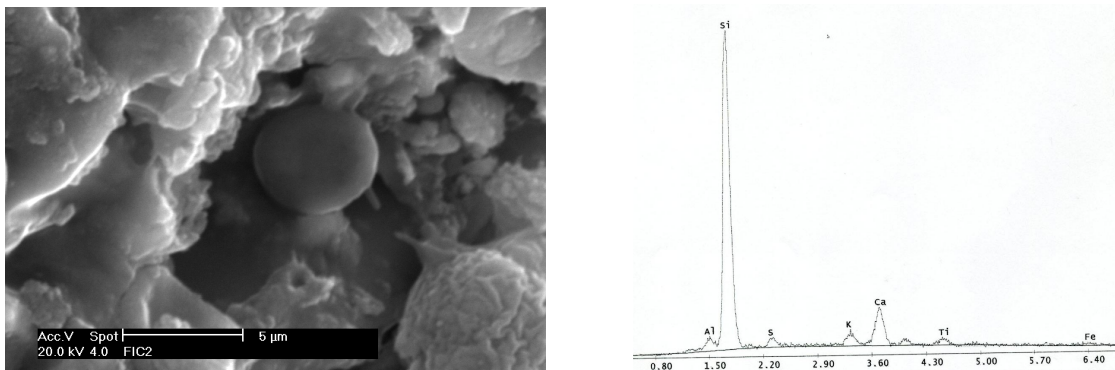
Figure 4.18. Scanning electron micrograph of damage layer surface showing aluminosilicate with the EDX spectrum on the right.

4.2.3. Induce Coupled Plasma-Optical Emission Spectroscopy

The mean concentration of the elements and corresponding standard deviation are reported in Table 4.9. The detected values were very variable, the most abundant elements were Si, Ca, K, Al, Mg, Na, Fe and S. This is also visible on Figure 4.19, presenting the concentration of the elements in substrate (FICsub) and damage layer (samples FIC1+2 (it consist FIC2+FIC2), and FIC3).

Sulphur in this case had higher concentration in underlying material than in damage layers, this fact confirmed the lack of sulphation process and therefore gypsum formation on the building surface, as it was revealed during the optical and scanning electron microscope observations.
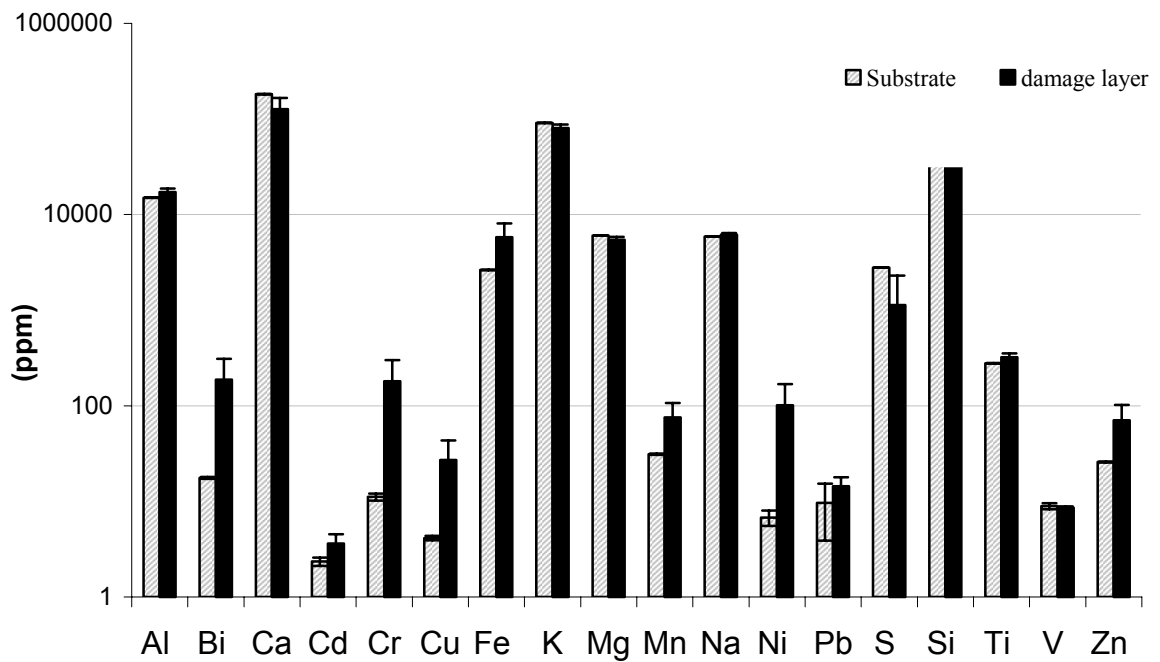
Figure 4.19. Mean element contents in substrate and damage layer taken from Chiesa dell'Autostrada del Sole.

The elaboration of one tailed t-test, at level $\alpha=0.05$, suggests the origin of the elements, from the substrate or from atmospheric deposition

.

Table 4.9. Elemental concentrations (ppm– µg metal/g crust) and corresponding standard deviation, ICP-OES analyses of samples from Chiesa dell'Autostrada del Sole.

Sample	Al	As	Ba	Be	Bi	Ca	Cd	Co	Cr	Cu	Fe	K	Li	Mg	Mn	Mo	Na	Ni	P	Pb	Pt	S	Sb	Se	Si	Sn	Sr	Ti	Tl	V	Zn	Zr
FICsub	15000	-	232	-	18	182412	2	-	11	4	2633	90756	8	6006	31	-	5880	7	-	10	2	2779	19	-	144243	-	126	277	-	9	26	15
FIC1+2	17588	-	205	-	178	123169	3	9	173	37	5262	95415	22	4719	71	-	6738	91	48962	29	3	1683	25	50	183860	-	88	358	-	13	69	16
FIC3	16766	-	156	-	198	130726	4	8	188	17	6379	65377	6	6210	80	-	5630	112	-	-	-	573	29	-	225265	-	103	284	-	4	72	31

Standard deviation

Sample	Al	As	Ba	Be	Bi	Ca	Cd	Co	Cr	Cu	Fe	K	Li	Mg	Mn	Mo	Na	Ni	P	Pb	Pt	S	Sb	Se	Si	Sn	Sr	Ti	Tl	V	Zn	Zr
FICsub	83	-	2	-	1	1297	1	-	1	1	10	50	1	65	1	-	27	1	-	6	1	42	2	-	665	-	1	2	-	1	1	1
FIC1+2	4	-	1	-	1	1277	1	1	2	1	7	36	1	23	1	-	48	1	2990	6	1	43	2	9	535	-	1	2	-	1	1	2
FIC3	48	-	1	-	3	1165	1	4	3	1	22	24	1	18	1	-	48	2	-	-	-	42	4	-	3080	-	9	1	-	1	1	2

Table 4.10. Differences between the mean concentrations of the elements in damage layer and substrate, and corresponding $t_{calculated}$ values calculated for samples from Chiesa dell'Autostrada del Sole; in bold are the positive significant differences found by one tailed t-test, α=0.05, N=4 for all samples (t_{table} = 2.78), except for sample FIC4, where N=2, t_{table}=4.3.

Sample	Al	As	Ba	Be	Bi	Ca	Cd	Co	Cr	Cu	Fe	K	Li	Mg	Mn	Mo	Na	Ni	P	Pb	Pt	S	Sb	Se	Si	Sn	Sr	Ti	Tl	V	Zn	Zr
FIC1+2	**2588**	-	-27	-	**160**	-59243	**1**	**9**	**162**	**33**	**2629**	4659	**5**	-1287	**40**	-	**858**	**84**	48962	**19**	1	-1096	**6**	50	**39617**	-	-38	**81**	-	4	**43**	1
FIC3	**1766**	-	-76	-	**180**	-51686	**2**	**8**	**177**	**13**	**3746**	-25379	-25	204	**49**	-	-250	**105**	-	-10	-2	-2206	**10**	-	**81022**	-	-23	7	-	-5	**46**	16

t calculated

Sample	Al	As	Ba	Be	Bi	Ca	Cd	Co	Cr	Cu	Fe	K	Li	Mg	Mn	Mo	Na	Ni	P	Pb	Pt	S	Sb	Se	Si	Sn	Sr	Ti	Tl	V	Zn	Zr
FIC1+2	54.16	-	-26.11	-	327.55	-56.39	4,57	9,31	154.41	180.08	378.48	13.03	151,51	-32.12	60.92	-	26.94	90.78	12,80	4.06	3,42	-31.53	4,44	6,88	80.35	-	-62,83	47.69	-	10.03	85.31	-
FIC3	31.91	-	-82.41	-	94.60	-51.35	2,82	3,34	101.56	42.19	272.07	-79.09	-35,12	5.21	79.25	-	-7.87	86.21	-	-0.55	-2,68	-64.58	4,35	-	44.54	-	-117,77	5.25	-	-8.17	72.08	-

Table 4.11. Enrichment factor (EF) for samples collected from Chiesa dell'Autostrada del Sole; in bold values of EF > 5.

Sample	Al	As	Ba	Be	Bi	Ca	Cd	Co	Cr	Cu	Fe	K	Li	Mg	Mn	Mo	Na	Ni	P	Pb	Pt	S	Sb	Se	Si	Sn	Sr	Ti	Tl	V	Zn	Zr
FIC1+2	1	-	0.8	-	**8.6**	0.6	1,2	-	**13.3**	**7.7**	1.7	0.9	2	0.7	1.9	-	1.0	**11.5**	-	2.6	1,4	0.5	1	-	1.1	-	1	1.1	-	1.2	2.28	1
FIC3	1	-	0.6	-	**10.1**	0.6	1,5	-	**15.1**	**3.7**	2.2	0.6	1	0.9	2.3	-	0.9	**14.7**	-	-	0,0	0.2	1	-	1.4	-	-	0.9	-	0.4	2.48	1

The results of student's t-test presented in Table 4.10, shows that Al, Bi, Cd, Co, Cr, Cu, Fe, Mn, Ni, Si, Ti, Zn have higher contribution in crusts than in substrate and theirs presence is probably connected to atmospheric deposition. This was verified by elaboration of enrichment factor EF, where Al was selected as a reference. There was accepted that if the value of EF is higher than 5, we can consider the element X in the crust due to external sources, in particular atmospheric deposition, and not to the original building material. The results of elaborated EF presented in Table 4.11, indicate that Bi, Cr, Cu, Ni origin from atmospheric deposition.

Table 4.12. The results from t-test and EF presenting elements coming from atmospheric deposition.

Method	Elements with atmospheric origin
t-test	Al, Bi, Cd, Co, Cr, Cu, Fe, Mn, Ni, Si, Ti, Zn
EF	Bi, Cr, Cu, Ni

Table 4.12 sums up the results from t-test and EF: in case of elements such as Bi, Cr, Cu, Ni, we can consider a sure atmospheric origin. The presence of Bi in this case is unclear. The elements Cr, Cu, Ni can be associated to vehicular emissions (Ondov et al., 1982; Monaci, et al., 2000; Caselles et al., 2002), that is closely linked to the motorway in neighbourhood of the building; and also to different anthropogenic activities (i.e. foundry). However, the presence of Cu can be also linked to the erosion of the roof.

4.2.4. Concluding remarks

The analyses of samples from Chiesa dell'Autostrada del Sole indicate the presence of aluminosilicate particles originating from combustion processes and trace elements of vehicular exhaust. Gypsum has not been identified in the samples collected from this building, this is due to the restorations work, regularly performed for the maintenance of the building, particularly surface cleaning. Due to this fact there were not performed further analyses such as XRD, DTA-TGA, IC, and CHNSO in order to qualify and quantify the composition of the damage layer.

4.3. Experimental data of Casa Galleria Vichi

4.3.1. Optical Microscope Observations

Optical microscope observation of transversal thin section of samples from sheltered areas (BOS2 and BOS10), indicated the presence of dark damage layers as it is shown in Figure 4.20 and 4.21. The black crusts appeared in an irregular shape with maximum thickness of 400 μm. It is composed of gypsum with frequently embedded black carbonaceous particles and iron oxides, presented in Figure 4.22. There were two sizes of carbonaceous particles small with diameter ranging from 15 μm to 25 μm and bigger with maximum diameter of 45 μm.
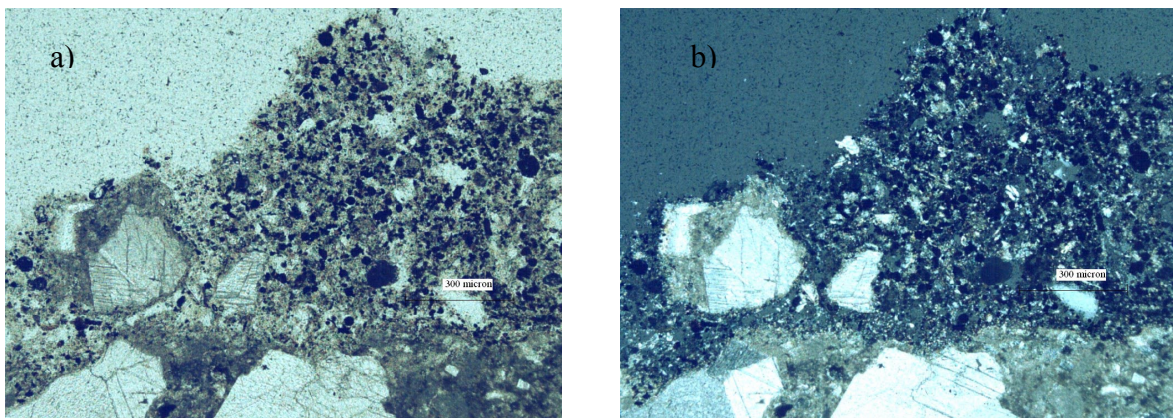
Figure 4.20. Optical micrographs (a) planed-polarised light, (b) cross-polarised light of damage layer in sheltered area of sample (BOS10), Casa Galleria Vichi (Florence).
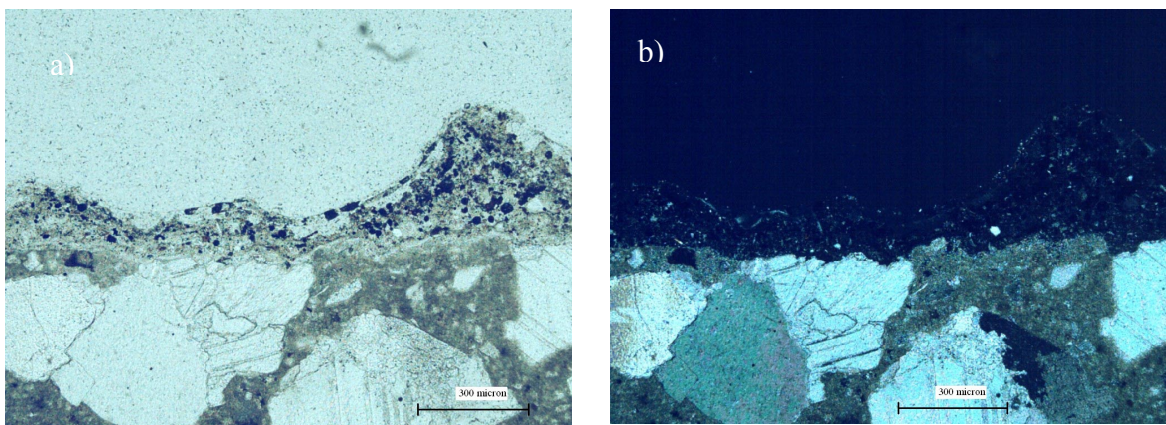
Figure 4.21. Optical micrographs (a) planed-polarised light, (b) cross-polarised light of damage layer in sheltered area of sample (BOS2), collected from Casa Galleria Vichi. Several black particles are clearly identifiable embedded in the gypsum matrix.
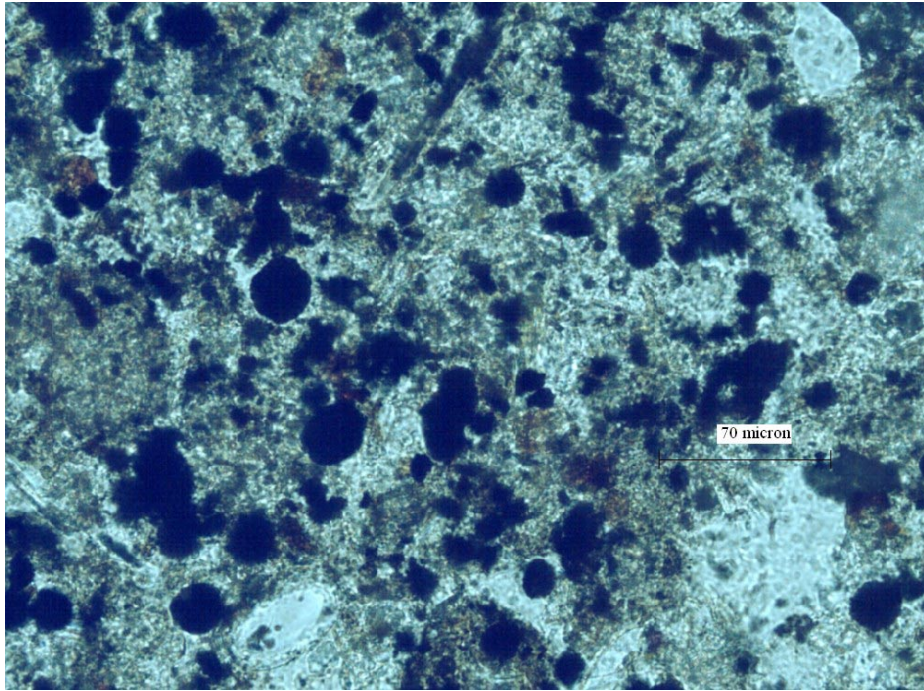
Figure 4.22. Optical micrograph (planed-polarised light) of damage layer in sheltered area (BOS10); black carbonaceous particles and yellow-orange iron oxides are observable.

Sporadically, there were identified transparent aluminosilicate particles of dimension 5-7 μm.

The mineralogical characterisation of the substrate showed that the material is a cement mortar. As for the other sites investigated, the aggregate is heterogeneous and poorly sorted. It is composed of monocrystalline and polycrystalline quartz, fragments of silicatic and carbonate stones, calcite, amorphous silica and crystals of feldspar.

4.3.2. Scanning Electron Microscope Observations

The SEM-EDX analysis performed on samples BOS2 and BOS7 presented in Figure 4.23, confirmed the optical microscope observations, indicating that gypsum, in both laminar and globular form, covered the external surface (Figure 4.23 a). The airborne particulate matter was observed embedded in gypsum matrix.
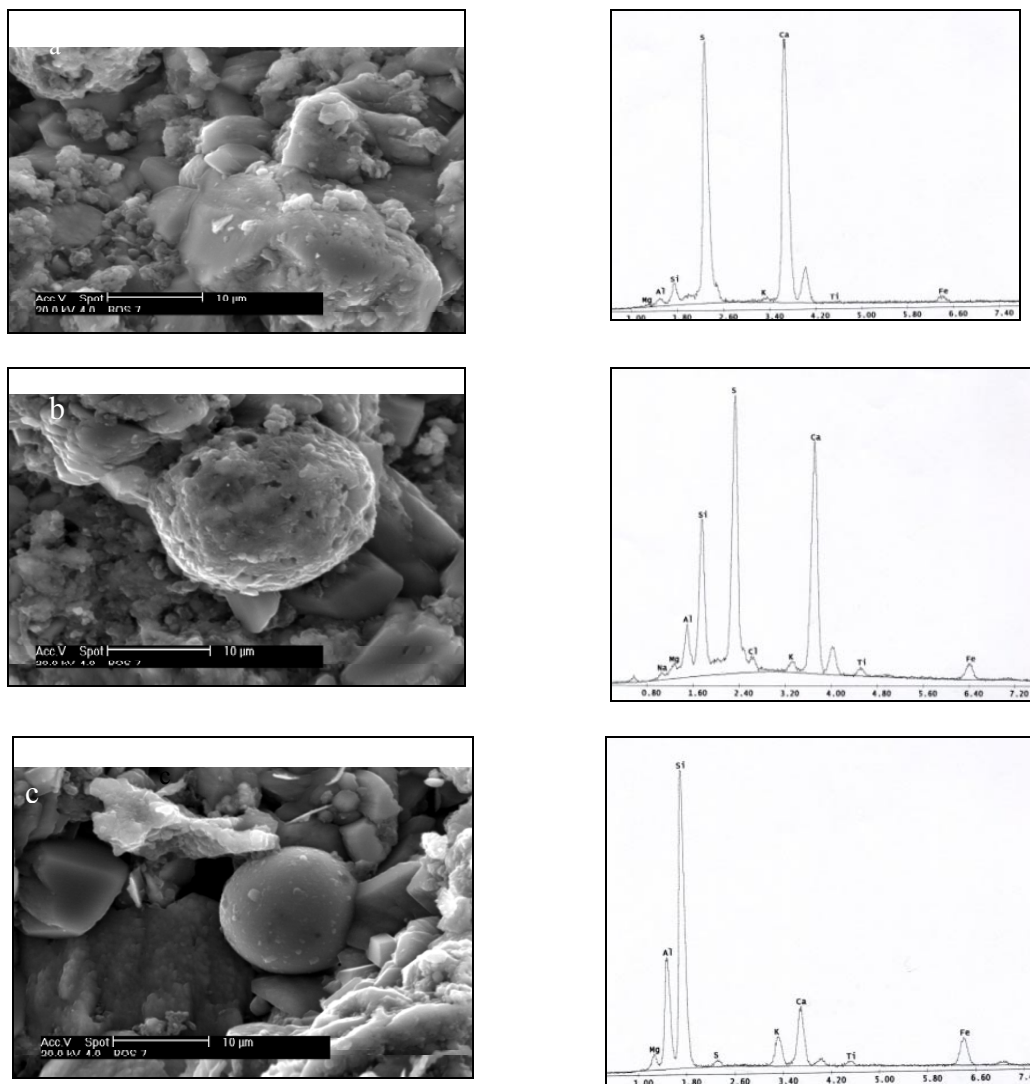
Figure. 4.23. Scanning electron micrographs (on the left) with relative EDX (on the right) of sample BOS7, showing: (a) surface covered by lamellar and globular gypsum, (b) carbonaceous and (c) aluminosilicate particles.

Spherical particles with spongy structure (Figure 4.23 b) and S as significant element are typical carbonaceous particles emitted by oil combustion (Bacci et al., 1983; Del Monte and Sabbioni, 1984).

There were also found spherical smooth particles (Figure 4.23 c), characterized by the presence of silicon and aluminium as the main elements with smaller amounts of Ca, S, K, Mg, Fe and Ti, representing aluminosilicate particles from combustion processes (Jabłońska et al., 2003).
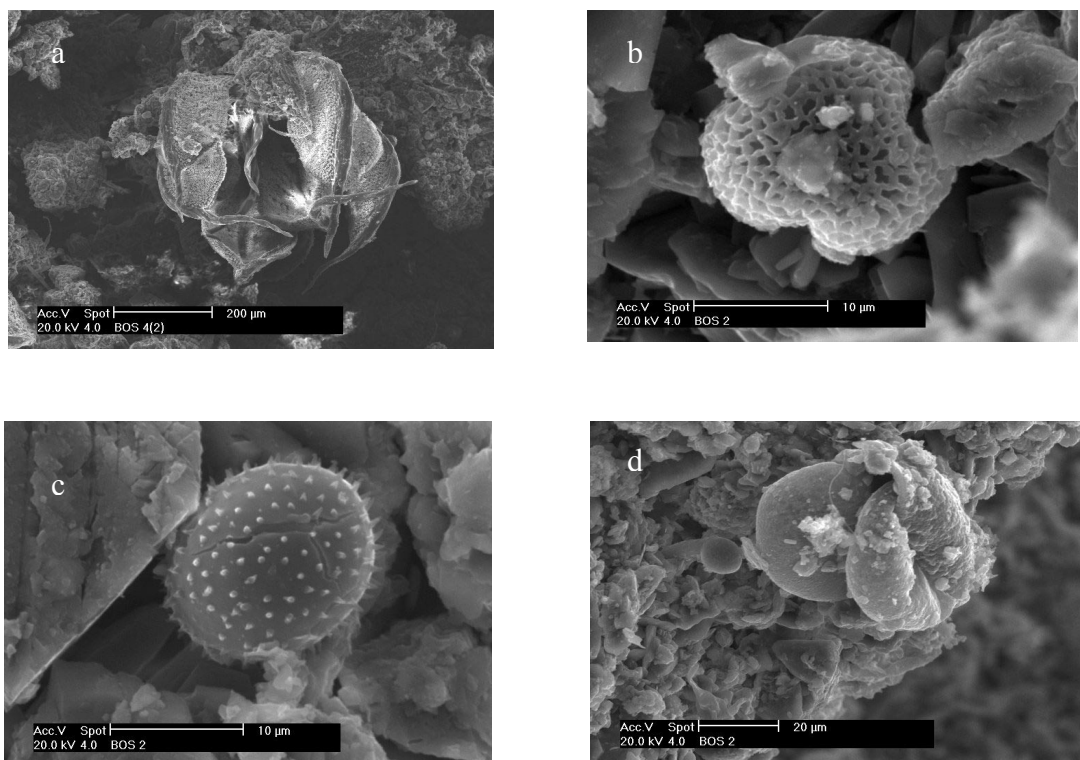
Figure 4.24. Scanning electron micrographs (a), (b), (c), (d) of biological particles on surface of the sample BOS2.

In case of sample from the top of the building (BOS2), frequently were observed biological particles as it is shown in Figure 4.24.

4.3.3. X-Ray Diffraction Analysis

The crystal phases of powdered sample were identified by X-ray diffraction analyses, the results are listed in Table 4.13. Sample BOS4(2) which is representative for the underlying material show that quartz and calcite are main mineral phases followed by feldspar and tracers of rutile (Figure 4.25).

Table 4.13. Main crystal phases revealed by X-ray diffraction in the analysed crusts and substrate collected on Casa Galleria Vichi (Florence).

Sample	Gypsum	Quartz	Calcite	Feldspars	Hematite	Ilmenite	Rutile
BOS4(2)[*]		+++++	++++	+			tr
BOS2	+	+	+++++	+			
BOS5	++	+++++	+	+	+	+	
BOS6	+++++	+++	+++	+		+	
BOS12		++	+++++			tr	
BOS14	+		+++++		tr		
BOS1516	+++	+	+++++		+	tr	

[a] +++++ main mineral present; ++++, +++ very abundant; ++ abundant; + present, tr tracers
[*] substrate

In general the minerals identified in samples of the damage layer are calcite, quartz and gypsum. The gypsum is more abundant in samples with black coherent damage layers (BOS6 or BOS1516). There was also detected presence of hematite, ilmenite and also feldspar.

The presence of quartz, calcite and feldspar is ascribable to the binder and aggregates of the concrete. The mineral phases such as gypsum, hematite, ilmenite identified in damage layers are connected to the atmospheric deposition. Gypsum is formed due to the interaction of atmospheric SO_2/H_2SO_4 with cement components (Martínez-Ramírez, et al., 1998). The main source of SO_2 in case of Casa Galleria Vichi is vehicular exhaust from traffic roads in surrounding area of the building, and fossil fuel combustion in domestic heating. The presence of hematite and ilmenite in damage layers of Florence site can be connected to oil fly ash (Chen, et al., 2004), but also to erosion of metal decorations on the building .
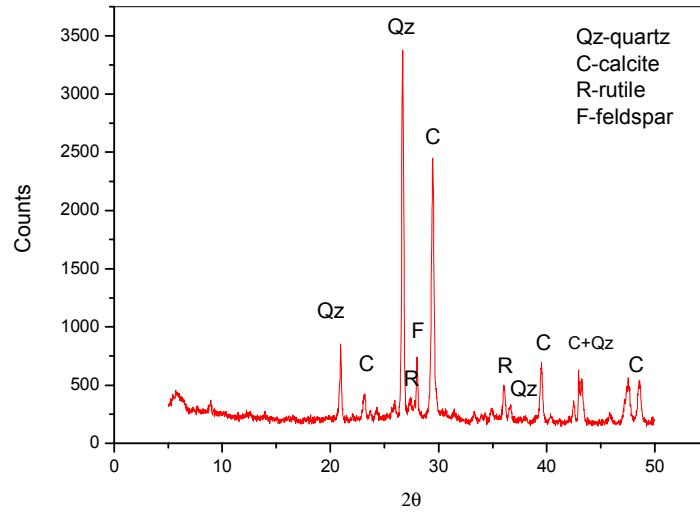
Figure 4.25. X- ray diffractogram of substrate, Casa Galleria Vichi (Florence).
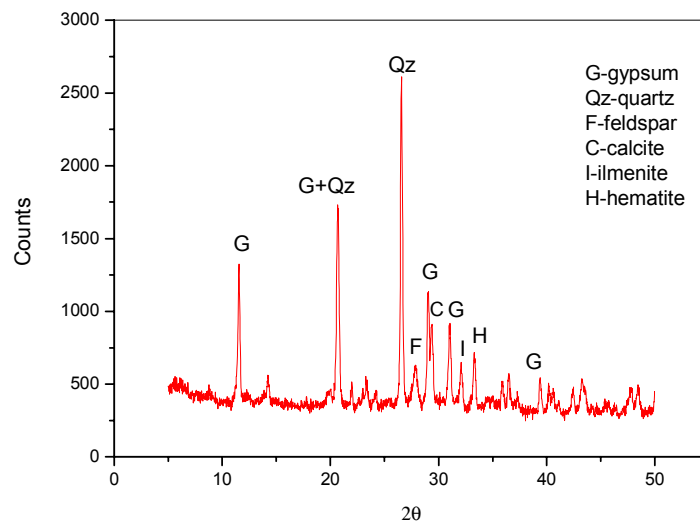
Figure 4.26. X- ray diffractogram of surface damage layer sample on the concrete façade, Casa Galleria Vichi in Florence.

4.3.4. Differential and Gravimetric Thermal Analysis

The differential and gravimetric thermal analyses (DTA-TGA) allowed to quantify gypsum and carbonates in collected samples, the results are presented in Table 4.14.

The results for sample BOS4_2 representing underlying material, show decarbonation of carbonates between 600 ºC and 850 ºC , with an amount of 25 %.

Table 4.14. Concentrations (%) of gypsum and carbonates in samples from Casa Galleria Vichi (Florence).

Sample	Gypsum[1]	Carbonates[2]
BOS4(2)[*]		25.09
BOS2	14.54	57.62
BOS5	32.97	7.43
BOS6	50.20	18.55
BOS12	9.06	70.28
BOS14	41.85	41.99
BOS1516	66.02	11.36

[*] substrate
[1] calculated as $CaSO_4 \cdot 2H_2O$, [2] calculated as $CaCO_3$

Considering samples of damage layer, gypsum (Figure 4.27) had significant amount in samples with coherent crust (BOS6, BOS14, BOS1516) ranging from 42 % to 66 %. The smaller amounts were in samples with incoherent deposit 9-33 % (BOS2, BOS5, BOS12). The higher concentration of gypsum in black coherent crusts was an effect of advance sulphation level and complete protection against rain wash out.
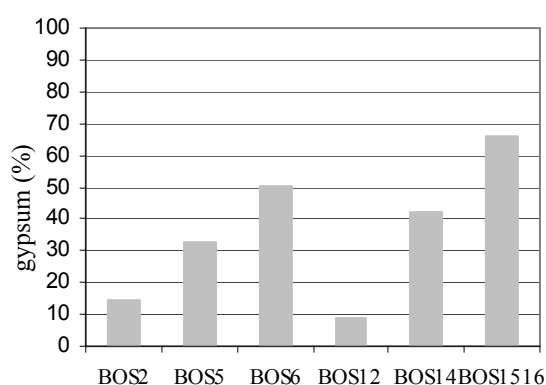
Figure 4.27. Concentration of gypsum (%) measured by DTA-TGA analyses in samples colleted from Casa Galleria Vichi.

Carbonates were also presented in variable amounts ranging from 7 % to 58 %, the decarbonation of them underwent in temperature between 600-850 °C.

Additionally in samples of crusts were observed two exothermic peaks within DTA curves corresponding to two steps of the loss of weight, an example is presented in Figure 4.28. The first peak occurred in the temperature range from 306 ºC to 320 ºC, the second peak was located between 431 ºC to 472 ºC. This peaks were correlated with CO_2 development due to carbon components oxidation (Bonazza et al., 2007), the first peak can be attributed to organic carbon coming from organic compounds in atmospheric aerosols. The second peak corresponds to elemental carbon which can origin from particles emitted into the atmosphere by combustion processes.
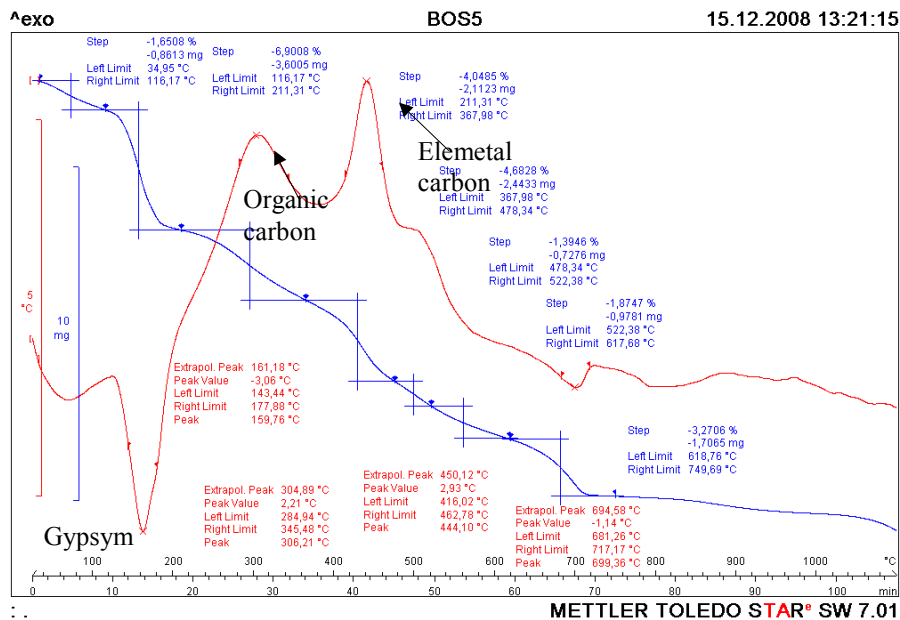
Figure 4.28. DTA-TGA graphs of black crusts collected on Casa Galleria Vichi.

4.3.5. Ion Chromatography data

The anion composition and concentrations were measured by ion chromatography, the results obtained on samples collected Casa Galleria Vichi are summarized in Table 4.15.

The mean anion concentrations for coherent and incoherent damage layers and also for substrate are presented in Figure 4.29. They show that sulphate ($SO_4^=$) had the highest concentration among all anions, with always higher contribution in damage layers. The strongest contribution of $SO_4^=$, was observed in samples of black coherent crusts with mean of 36 %, and lower in incoherent deposit with mean of 14 %. The higher concentration of sulphate in specimens of black crust is an effect of higher amounts of gypsum in those samples, as it was revealed during DTA-TGA analyses. This presence of $SO_4^=$ proves the importance of sulphation process, due to dry and wet deposition of SO_2 and consequent interaction with components of cement matrix.

Table 4.15. Anion concentration (ppm) measured by ion chromatography in damage layer and substrate collected.

Sample	$SO_4^=$	NO_3^-	NO_2^-	Br^-	Cl^-	CHO_2^-	$C_2H_3O_2^-$	$C_2O_4^=$
BOS4(2)[*]	7325	166	113	n.d.	363	286	2775	135
BOS1	421846	4823	148	1275	3100	2274	12098	5568
BOS3	98608	4460	363	710	3272	226	5688	2357
BOS5	122651	9950	626	n.d.	11616	168	7878	3102
BOS6	112250	2148	28	n.d.	1890	111	7878	3538
BOS8	206734	8141	28	n.d.	8715	117	7932	1285
BOS9	221166	7439	28	n.d.	7606	158	9490	1743
BOS10	389626	3285	36	n.d.	1835	126	8462	386
BOS12	25676	879	70	n.d.	1557	278	3706	3999
BOS13	202441	19003	70	n.d.	14796	184	11817	1561
BOS14	251455	3020	29	n.d.	1812	128	9791	1068
BOS1516	381331	3989	29	n.d.	2505	2095	9504	n.d

[*] substrate
n.d. = not detected.
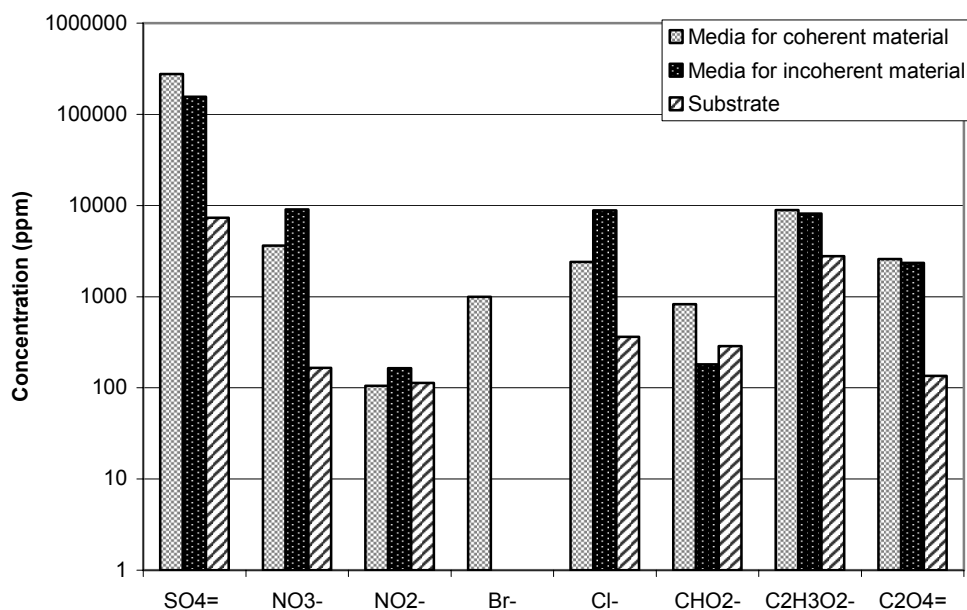
Figure 4.29. Mean concentration of anions in coherent crust, incoherent deposit and substrate samples collected at Casa Galleria Vichi**.**

The IC results indicate also the presence of marked amounts of organic anions such as formate (CHO_2^-), acetate ($C_2H_3O_2^-$), oxalate ($C_2O_4^=$). The most abundant among them is acetate with maximum concentration of 1.2 % in sample of black crust (BOS1) and the a minimum of 0.4 % in sample of incoherent material (BOS12). Oxalate appeared in lower amounts with mean concentration in damage layer of 0.2 %, followed by formate with mean of 0.05 %. The presence of organic anions is attributed to primary and secondary air pollutants, biological weathering and restoration treatments (Sabbioni et al., 2003). There is not available information about the restoration work performed on the Casa Galleria Vichi.

NO_3^- and NO_2^- were also found in considerable and variable amounts, with higher concentration of NO_3^-. Nitrogen oxides presence in this case could be connected to direct exposition of this building to motor exhaust, however due to the high solubility of salts formed due deposition of NO_x/HNO_3, the role of NO_x as damage factor is difficult to determine (Derry et al., 2001).

The presence of Cl^- (maximum concentration of 1.5 %) could be ascribed to marine aerosol deposition and also to fossil fuel combustion (Ondov et al., 1982; Arditsoglou and Samara, 2005).

4.3.6. Carbon compound Discrimination and Measurements

The carbon fraction measured during CHNSO analyses are presented in Table 4.16. The total carbon (TC) concentration in samples from Casa Galleria Vichi was ranging from 4 % to 17 % of total mass of samples. The mean concentration of TC in all samples was 9 %, which was higher then in samples from Centennial Hall, where mean of TC was 2 %.

The fractions of total carbon presented in Figure 4.30, indicated that non carbonate carbon (NCC) appeared in very variable amounts, from minimum of 29 % (BOS8) to maximum of 91 % of TC in sample of thick black crust (BOS1). The carbonate carbon (CC) predominated over NCC in samples BOS8 and BOS1516. This result is in agreement with DTA-TGA analyses, where the significant contribution of carbonates in damage layers from this building was verified. The presence of carbonate carbon in analysed samples is probably due to the nature of the sample, during sampling part of underlying material could have been collected.

Table 4.16. The TC, NCC, CC, EC and OC concentrations (%) and OC/EC ratio measured in damage layers collected on Casa Galleria Vichi.

Sample	TC[1]	CC[3]	NCC[2]	EC[2]	OC[3]	OC/EC
BOS1	3.68	0.32	3.36	3.01	0.35	0.12
BOS3	11.23	2.34	8.89	3.13	5.77	1.84
BOS5	10.03	4.18	5.85	2.64	3.21	1.22
BOS8	16.73	11.88	4.85	4.52	0.33	0.07
BOS10	8.82	1.87	6.95	2.04	4.91	2.41
BOS13	7.30	1.29	6.01	2.80	3.21	1.15
BOS1516	8.59	4.59	4.00	3.13	0.87	0.28

[1] measured on substrate, [2] measured on treated samples, [3] calculated

Elemental carbon (EC) (Table 4.16) was ranging from 2 % to 5 % of total mass of sample, this values were much higher and homogenous than in case of sample from Centennial Hall. Elemental carbon origins from combustion–generated aerosols, in case of Casa Galleria Vichi, surrounding by high car traffic, EC presence can be an effect of fossil fuel (mainly diesel) and domestic combustion (Kupiainen and Klimont, 2007).

Considering the organic carbon (OC), the values were very variable with maximum of 6 % in sample BOS3, which was supposed to be affected by biological attack. It is known that OC origins from incomplete combustion processes, secondary air pollutants, biological weathering and restoration treatment (there are not information about the restoration work

done). The contribution of organic carbon in total mass of sample was much higher in samples from Casa Galleria Vichi than ones from Centennial Hall. This fact can be connected to direct exposition of building to vehicular emission.

Figure 4.31 presents the EC and OC percentages with respect to NCC. Elemental carbon predominates over OC in samples of black crust (BOS1, BOS8, BOS1516), with contribution higher than 80 % of NCC. This was also noticed in the samples of black crust from Centennial Hall. The EC fraction is a product of combustion processes and it constitutes a quantitative index of carbonaceous particles embedded in black crust (Riontino et al., 1998).

In case of sample of grey crust (BOS5, BOS13) the OC/EC ratio was higher than 1.

The exception was sample of black damage layer BOS10 with the maximum value of OC/EC ratio of 2.41. Considering the concentrations of EC of 2 % and of sulphate of 39 %, indeed the sample has a typical composition of the black crust (gypsum and black carbonaceous particles). Therefore the high ratio of OC/EC indicates the prevailing contribution of mobile combustion sources in damage layer formation in this part of the monument.
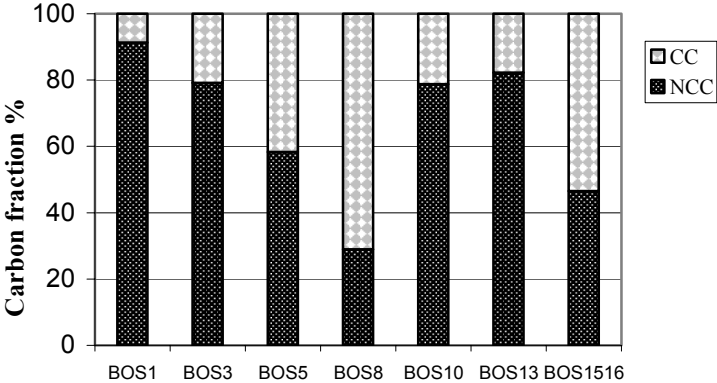
Figure 4.30. The non carbonate carbon (NCC) and carbonate carbon (CC) percentage fraction of total carbon in samples of damage layers collected from Casa Galleria Vichi (Florence).
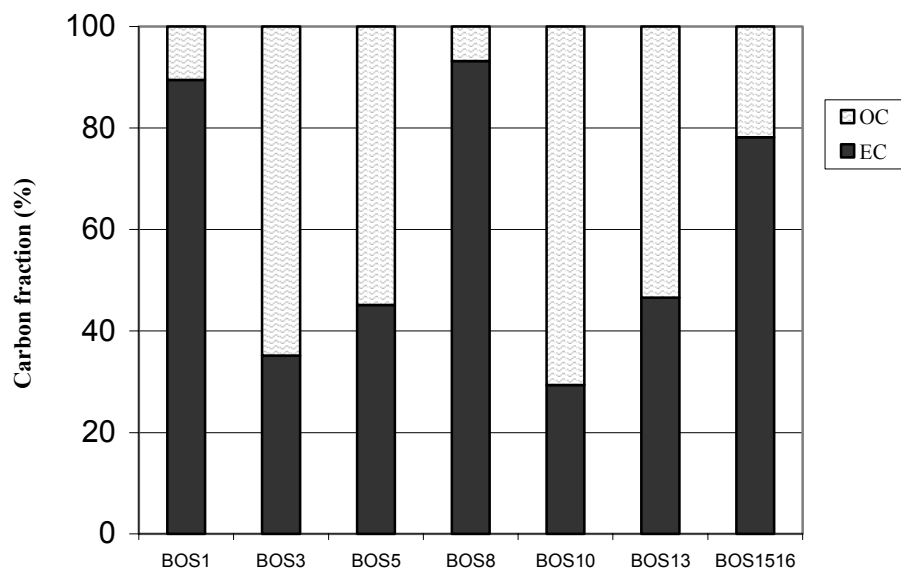
Figure 4.31. The percentage fraction of organic carbon (OC) and elemental carbon (EC) of NCC in sample of crusts from Casa Galleria Vichi.

4.3.7. Induce Coupled Plasma-Optical Emission Spectroscopy

The results achieved during ICP-OES analyses of damage layer and substrate are presented in Table 4.17. The mean concentration of the elements indicates higher contributions of almost all elements in damage layers than in substrates, with exception of Ca and Sr. The most abundant elements in all analysed samples were Si, Ca, S, Fe, Al, K, Na, and Mg. The maximum concentrations of S was observed in samples of black crust e.g. sample BOS1, BOS10 and BOS16, that finds great agreement with results from DTA-TGA, where in those samples was detected the highest amounts of gypsum, and results from IC with high concentration of $SO_4^=$.

Looking at Table 4.17, the two samples representative of the underlying material BOS4(2) (collected from dragon) and BOS7 (from façade) have different elemental concentration, this could be linked to the restorations work on the dragons and to the application of mortars different from the original material, but there is lack of information about the maintenance of the building. Keeping in mind this difference, for further elaboration, samples were divided into two groups, samples from dragons (BOS1, BOS3, BOS4(2)) and samples from façade BOS5, BOS7, BOS8, BOS9, BOS10, BOS13, BOS16.

Elaboration of t – test at level α=0.05, gave an indication about origin of elements (atmospheric deposition or substrate). The results of t-test presented in Table 4.18, pointed: that elements such Cu, Fe (only sample BOS3), Pb, S, Sn, Zn come from atmospheric deposit in case of sample from dragons; in sample collected from façade the elements with atmospheric origin can be Al, Ba, Cd, Co, Cr, Cu, Fe K, Na, Ni, Pb, S, Sb, Si, Sn, Ti, V and Mg, Mn, Zn (except sample of black coherent material, BOS10, BOS1516). In both cases, samples from dragons and samples from façade, Cu, Fe, Pb, S, Sn, Zn seem to origin from atmospheric deposition.

Principal components analyses (PCA) were performed for two groups of data: 1st group of all analysed samples (dragon and façade) and 2nd group of samples collected only from façade.

Table 4.17. The elements concentration (ppm– µg metal/g crust) and corresponding standard deviation, results from ICP-OES of samples from Casa Galleria Vichi, Florence.

Sample	Al	As	Ba	Be	Bi	Ca	Cd	Co	Cr	Cu	Fe	K	Li	Mg	Mn	Mo	Na	Ni	P	Pb	Pt	S	Sb	Se	Si	Sn	Sr	Ti	Tl	V	Zn	Zr
BOS4 (2)	13854	-	777	4	-	160055	4	105	71	62	21141	21865	32	6455	932	-	15608	40	615	59	-	-	29	32	261649	-	810	142	17	72	76	225
BOS1	5539	-	306	-	-	149884	1	37	31	138	7569	3698	8	2153	87	-	3601	15	422	336	-	133420	6	15	44310	1	521	53	9	36	318	37
BOS3	11522	-	324	1	-	169716	3	194	50	139	38249	9332	14	4783	427	-	6635	38	651	161	-	36156	16	16	106000	-	376	77	13	37	184	112
BOS7	5011	-	130	2	-	368702	-	26	17	114	5174	4162	14	5874	248	-	6150	6	256	207	-	47741	9	28	46188	-	850	24	17	23	296	42735
BOS5	7592	-	976	3	-	109688	4	209	192	1154	39123	17200	38	9252	624	-	19979	87	1883	635	-	61022	29	31	194711	4	499	253	31	119	568	272591
BOS8	7312	-	862	3	-	127231	4	167	129	605	31525	15471	30	7951	566	-	21521	63	1328	927	-	79069	24	26	192937	11	594	201	22	86	955	220760
BOS9	6139	-	1029	3	-	118928	4	215	197	988	40118	16000	33	8047	556	-	19053	84	1711	931	-	96346	30	23	198533	4	541	263	33	116	525	273784
BOS10	7661	-	658	2	-	232961	2	91	86	209	18749	8728	18	4568	212	-	8114	30	1000	606	-	138614	14	31	104847	1	605	121	21	70	223	118693
BOS13	7762	-	858	3	-	92439	4	202	173	708	32136	13773	34	8742	502	-	17181	75	1441	838	-	83636	26	37	143457	4	607	203	27	102	571	220120
BOS16	5150	-	495	2	-	189744	1	61	52	283	12606	6155	13	3267	139	-	6465	21	695	603	-	152938	11	37	68410	1	648	74	24	44	300	46713

Standard deviation

Sample	Al	As	Ba	Be	Bi	Ca	Cd	Co	Cr	Cu	Fe	K	Li	Mg	Mn	Mo	Na	Ni	P	Pb	Pt	S	Sb	Se	Si	Sn	Sr	Ti	Tl	V	Zn	Zr
BOS4 (2)	4454	-	82	1	-	25484	1	4	7,1	19	919	424	2	833	37	-	632,6	1	9	12	-	-	1	6	5177	-	52	12	2	3	30	38
BOS1	86	-	7	-	-	2678	1	1	0,7	4	133	61	1	36	2	-	60,8	1	16	16	-	3639	2	94	1350	1	15	1	4	4	4	2
BOS3	194	-	2	1	-	1661	1	5	0,7	4	484	58	1	30	5	-	15,2	1	5	3	-	232	1	11	381	-	3	1	4	1	4	1
BOS7	98	-	3	1	-	6274	-	1	1	1	76	1	1	20	3	-	146	1	5	6	-	339	1	12	797	-	8	1	5	1	4	1887
BOS5	40	-	1	1	-	1001	1	6	2	8	248	67	1	87	3	-	103	1	15	8	-	825	1	8	629	1	4	1	5	1	2	1299
BOS8	122	-	10	1	-	1178	1	1	2	8	388	169	1	34	3	-	271	1	9	15	-	580	1	10	4088	1	8	2	4	1	12	2548
BOS9	13	-	6	1	-	1362	1	3	1	11	29	182	1	82	5	-	44	1	16	6	-	952	1	20	3119	1	5	2	4	1	4	1952
BOS10	99	-	7	1	-	1358	1	2	1	1	85	98	1	4	1	-	8	1	8	7	-	1461	1	8	767	1	3	1	6	1	2	2938
BOS13	388	-	185	1	-	16696	1	8	2	5	7820	2883	1	116	3	-	4863	1	2	7	-	845	1	14	39131	1	33	35	1	2	13	8976
BOS16	103	-	4	1	-	3341	1	2	1	2	72	97	1	15	1	-	77	1	6	8	-	1617	1	10	558	1	4	1	4	1	2	1319

Table 4.18. Differences between the mean concentrations of the elements in damage layer and substrate, and corresponding $t_{calculated}$ values calculated for samples from Casa Galleria Vichi; in bold are the positive significant differences; t_{table} = 2.78 for all sample, except sample BOS13, where t_{table}=3.18.

Sample	Al	As	Ba	Be	Bi	Ca	Cd	Co	Cr	Cu	Fe	K	Li	Mg	Mn	Mo	Na	Ni	P	Pb	Pt	S	Sb	Se	Si	Sn	Sr	Ti	Tl	V	Zn	Zr
BOS1	-8315	-	-471	-3	-	-10171	-3	-68	-39	**76**	-13572	-18167	-24	-4302	-845	-	-12007	-26	-192	**277**	-	**133420**	-23	-17	-217338	**1**	-289	-89	-9	-36	**241**	-189
BOS3	-2332	-	-453	-3	-	9661	0	**89**	-21	**77**	**17108**	-12532	-18	-1672	-504	-	-8973	-3	**36**	**102**	-	**36156**	-13	-16	-155649	0	-434	-65	-4	-35	**108**	-113
BOS5	**2581**	-	**846**	**1**	-	-259014	**4**	**183**	**174**	**1041**	**33949**	**13038**	**24**	**3379**	**376**	-	**13830**	**81**	**1627**	**428**	-	**13282**	**20**	3	**148524**	**4**	-351	**229**	**14**	**96**	**272**	**229856**
BOS8	**2302**	-	**732**	**1**	-	-241471	**4**	**141**	**112**	**492**	**26350**	**11309**	**16**	**2077**	**318**	-	**15371**	**58**	**1072**	**720**	-	**31328**	**15**	-3	**146749**	**11**	-257	**178**	5	**63**	**659**	**178025**
BOS9	**1129**	-	**900**	**1**	-	-249773	**4**	**189**	**179**	**874**	**34943**	**11839**	**20**	**2174**	**308**	-	**12903**	**78**	**1455**	**724**	-	**48605**	**21**	-5	**152345**	**4**	-310	**239**	**16**	**93**	**229**	**231049**
BOS10	**2650**	-	**528**	0	-	-135741	**2**	**65**	**69**	**96**	**13575**	**4566**	**5**	-1306	-36	-	**1964**	**24**	**744**	**399**	-	**90874**	**5**	3	**58660**	**1**	-245	**97**	4	**47**	-73	**75957**
BOS13	**2751**	-	**728**	**1**	-	-276263	**4**	**176**	**156**	**595**	**26962**	**9611**	**20**	**2869**	**254**	-	**11031**	**69**	**1185**	**631**	-	**35895**	**17**	9	**97269**	**4**	-243	**180**	**10**	**79**	**275**	**177384**
BOS16	140	-	**365**	0	-	-178957	**1**	**35**	**35**	**170**	**7431**	**1994**	-1	-2607	-109	-	**315**	**15**	**439**	**396**	-	**105198**	2	9	**22223**	**1**	-202	**50**	7	**21**	4	**3978**

$t_{calculated}$

Sample	Al	As	Ba	Be	Bi	Ca	Cd	Co	Cr	Cu	Fe	K	Li	Mg	Mn	Mo	Na	Ni	P	Pb	Pt	S	Sb	Se	Si	Sn	Sr	Ti	Tl	V	Zn	Zr
BOS1	-3,2	-	-10,0	-38,4	-	0,0	-5,9	-25,7	-9,6	6,8	-25,3	-73,5	-22,3	-8,9	-39,9	-	-32,7	-26,6	-18,2	23,7	-	63,5	-25,0	-2,9	-70,4	9,7	-9,2	-13,1	-3,4	-22,7	13,6	-8,7
BOS3	-0,9	-	-9,6	-41,7	-	0,0	-0,6	23,8	-5,0	7,0	28,5	-50,7	-16,6	-3,5	-23,6	-	-24,6	-3,5	5,7	13,9	-	270,0	-38,0	-2,1	-51,9	3,9	-14,3	-9,5	-1,5	-22,8	6,1	-5,2
BOS5	42,2	-	458,5	23,1	-	-70,6	22,6	51,8	148,4	227,2	226,8	337,3	97,5	65,7	162,2	-	133,9	163,5	183,5	74,9	-	25,8	40,9	0,3	253,4	19,7	-66,3	269,6	3,5	186,7	108,0	173,8
BOS8	25,5	-	121,6	17,8	-	-65,5	22,0	190,0	117,1	104,2	115,5	116,2	63,0	91,3	131,6	-	86,5	115,7	187,1	77,6	-	80,7	26,0	-0,3	61,0	56,1	-39,7	160,1	1,4	125,4	90,0	97,3
BOS9	19,8	-	242,6	21,5	-	-67,4	17,0	116,4	362,6	140,4	747,6	112,8	77,0	44,6	98,7	-	146,5	103,4	147,1	150,4	-	83,3	40,8	-0,4	82,0	27,2	-56,2	236,7	4,4	168,9	76,0	147,4
BOS10	33,0	-	127,1	1,7	-	-36,6	9,9	58,6	167,7	117,5	206,6	80,9	39,1	-112,8	-19,3	-	23,3	35,3	141,5	75,1	-	105,0	7,2	0,3	91,8	9,1	-49,0	214,2	0,9	90,6	-30,3	37,7
BOS13	9,8	-	5,6	16,9	-	-22,4	13,3	32,8	90,5	159,5	4,9	4,7	43,1	34,5	99,7	-	3,2	109,3	374,0	100,7	-	57,1	26,4	0,7	3,5	31,7	-10,1	7,3	3,7	68,8	28,5	27,5
BOS16	1,7	-	120,2	-5,8	-	-43,6	6,2	30,2	71,2	110,0	122,8	35,6	-8,2	-181,1	-61,2	-	3,3	27,1	102,0	72,1	-	110,3	2,5	1,0	39,5	4,8	-39,1	125,9	2,0	42,2	1,5	3,0

Table 4.19. Enrichment factor (EF) for samples collected from Casa Galleria Vichi (Florence), in bold values of EF > 5.

Sample	Al	As	Ba	Be	Bi	Ca	Cd	Co	Cr	Cu	Fe	K	Li	Mg	Mn	Mo	Na	Ni	P	Pb	Pt	S	Sb	Se	Si	Sn	Sr	Ti	Tl	V	Zn	Zr
BOS1	1,0	-	1,0	-	-	0,7	0,4	0,9	1,1	**5,6**	0,9	0,4	0,6	0,8	0,2	-	0,6	0,9	1,7	**14,3**	-	-	0,5	1,2	0,4	-	1,6	0,9	1,3	1,3	**10,4**	0,4
BOS3	1,0	-	0,5	0,3	-	0,0	1,1	2,2	0,9	2,7	2,2	0,5	0,5	0,9	0,6	-	0,5	1,1	1,3	3,3	-	-	0,7	0,6	0,5	-	0,6	0,7	0,9	0,6	2,9	0,6
BOS5	1,0	-	**5,0**	1,0	-	0,2	-	**5,3**	**7,3**	**6,7**	**5,0**	2,7	1,8	1,0	1,7	-	2,1	**10,2**	4,9	2,0	-	0,8	2,1	0,7	2,8	-	0,4	**7,0**	1,2	3,4	1,3	4,2
BOS8	1,0	-	4,5	1,0	-	0,2	-	4,4	**5,1**	3,6	4,2	2,5	1,5	0,9	1,6	-	2,4	**7,7**	3,6	3,1	-	1,1	1,8	0,6	2,9	-	0,5	**5,8**	0,9	2,6	2,2	3,5
BOS9	1,0	-	**6,5**	1,2	-	0,3	-	**6,8**	**9,3**	**7,1**	**6,3**	3,1	2,0	1,1	1,8	-	2,5	**12,1**	5,5	3,7	-	1,6	2,7	0,7	3,5	-	0,5	**9,0**	1,6	4,1	1,4	5,2
BOS10	1,0	-	3,3	0,7	-	0,4	-	2,3	3,3	1,2	2,4	1,4	0,9	0,5	0,6	-	0,9	3,4	2,6	1,9	-	1,9	1,0	0,7	1,5	-	0,5	3,3	0,8	2,0	0,5	1,8
BOS13	1,0	-	4,3	0,9	-	0,2	-	**5,0**	**6,4**	4,0	4,0	2,1	1,6	1,0	1,3	-	1,8	**8,6**	3,6	2,6	-	1,1	1,9	0,8	2,0	-	0,5	**5,5**	1,0	2,9	1,2	3,3
BOS16	1,0	-	3,7	0,9	-	0,5	-	2,3	2,9	2,4	2,4	1,4	0,9	0,5	0,5	-	1,0	3,6	2,6	2,8	-	3,1	1,2	1,3	1,4	-	0,7	3,0	1,4	1,9	1,0	1,1
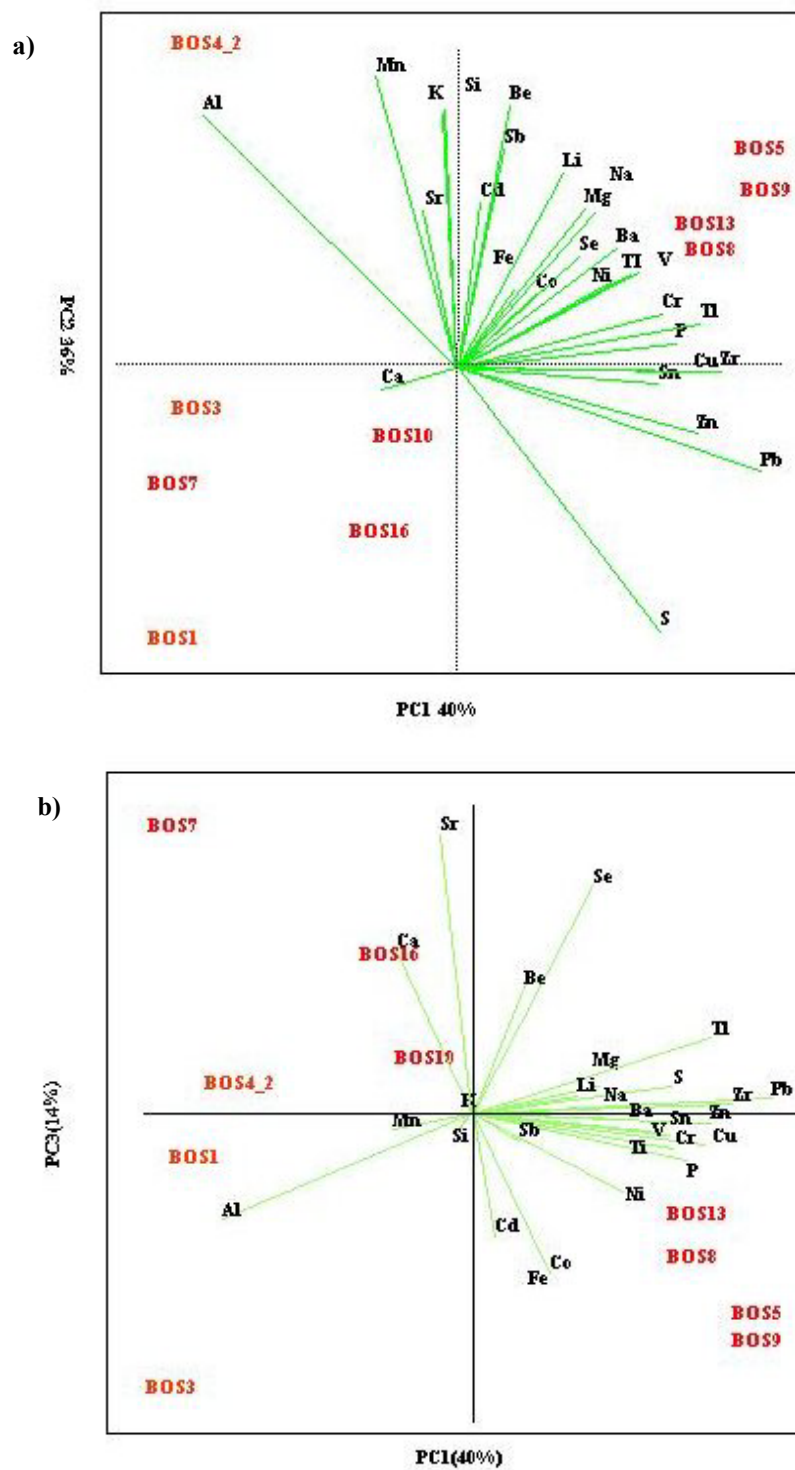
Figure 4.32. Principal components analyses, maps generated for results of ICP-OES, sample collected from façade and dragons of Casa Galleria Vichi, BOS7 substrate of façade, BOS4(2) substrate of dragon (a) PC1 verso PC2, (b) PC1 verso PC3.
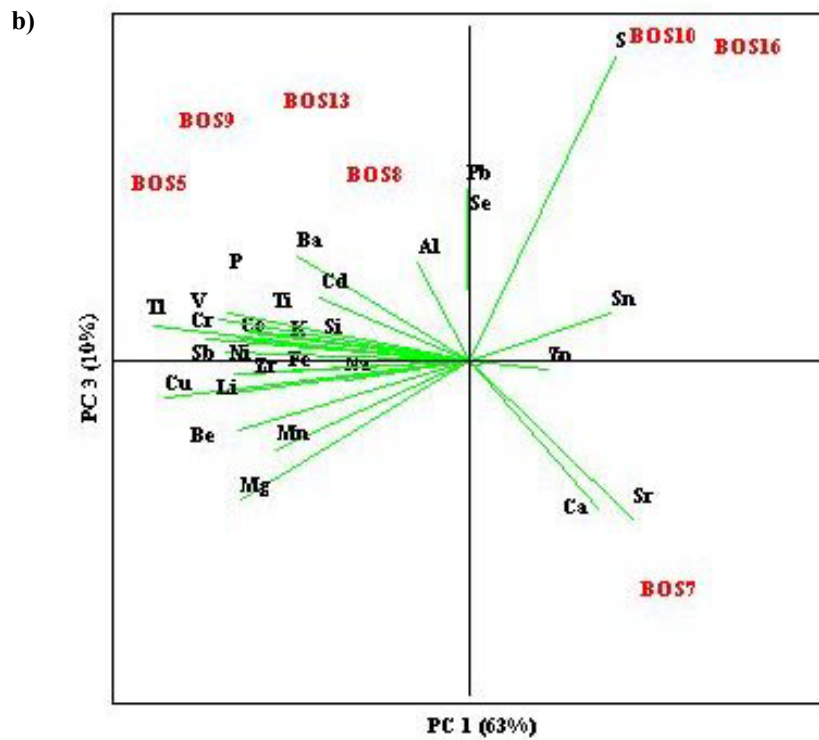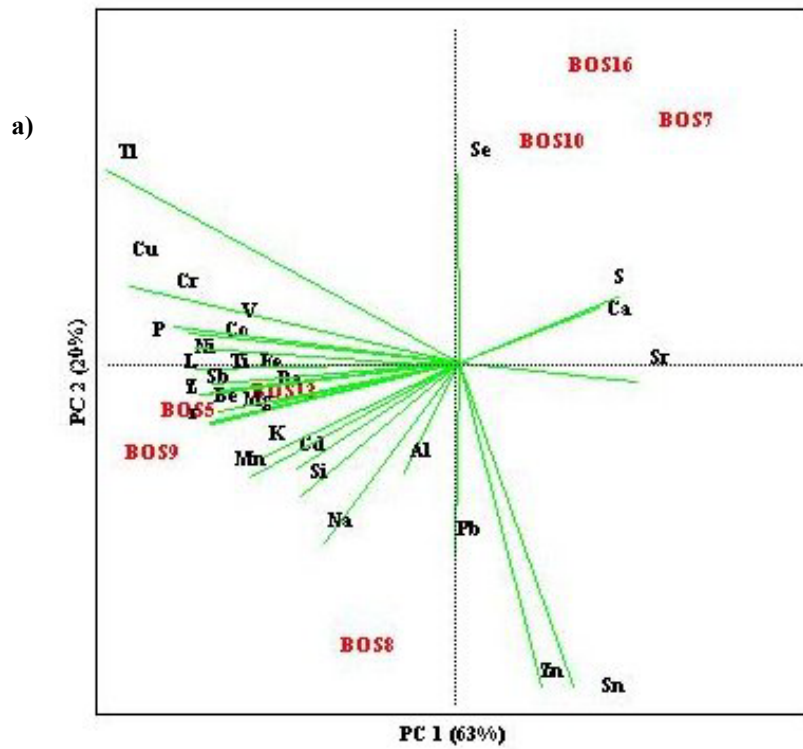
Figure 4.33. Principal components analyses, maps generated for results of ICP-OES, sample collected from façade of Casa Galleria Vichi, BOS7 substrate, (a) PC1 verso PC2, (b) PC1 verso PC3.

In Figures 4.32 a and 4.32 b are shown generated maps for all samples (from dragon and façade), with three rotated components, Figure 4.32 a: PC1 verso PC2; Figure 4.32 b: PC1 verso PC3, representing together 90 % of the total variance; PC1 of 40 %, PC2 of 36 % and PC3 of 14 %.

The most important dynamic in the system presented in Figure 4.32 is strong division between samples of dragons (BOS1, BOS3, BOS4(2)) and samples of façade BOS5, BOS7, BOS8, BOS9, BOS10, BOS13, BOS16. There is noticeable group of sample of incoherent deposit material (BOS5, BOS8, BOS9, BOS13) under influence of range of elements such Ba, Cd, Co, Cr, Cu, Fe, Li, Mg, Na, Ni, Sn, V, Zn, that is probably linked to particles and fly ash deposition .

The maps generated for 2nd group of samples, with three rotated components representing 93% of the total variance (PC1 of 63%, PC2 of 20%, PC3 of 10%) are presented in Figure 4.33 a (PC1 verso PC2), Figure 4.33 b (PC1 verso PC3). Considering the maps, there are observed three groups of elements with relation to incoherent deposit, coherent crust and substrate, especially visualized in Figure 4.33 b (PC1 vs PC3). The elements such as Ba, Cd, Co, Cr, Cu, K, Fe, Li, Ni, P, Ti, V are associated with samples of incoherent deposit (BOS5, BOS8, BOS9, BOS13), this fact is probably due to deposition of airborne particulate matter. Sulphur followed by Ca, Pb, Sn, Zn are observed in strong association with samples of black damage layers (BOS10, BOS16), where S and Ca can be related to gypsum.

In order to clarify the nature of the elements, originating from the substrate or atmospheric deposition, the enrichment factor (EF) was also elaborated, using Al as reference element.

The results of enrichment factor elaboration are shown in Table 4.19. There was adopted that if EF (X) > 5, the element X origins from atmospheric deposition, and not belonging to original building material. The elements with EF >5, in most of the samples, are Ba, Co, Cr, Cu, Fe, Ni, and Ti and therefore ascribe to atmospheric origin. The lack of EFs values in case of Cd, S, Sn is an effect of not detection those elements in substrate, makings EF impossible to calculate, however we can assumed them as elements with atmospheric origin.

Table 4.20. Results of t-test, PCA and EF of samples collected on Casa Galleria Vichi (Italy).

Method:	Elements with origin from atmospheric deposition
t-test	Al, Ba, Cd, Co, Cr, Cu, Fe, K, Li, Mg, Mn, Na, Ni, P, Pb, S, Sb, Si, Sn, Ti, V, Zn
PCA	Ba, Cd, Co, Cr, Cu, Fe, Ni, P, Pb, S, Sn, Ti, V Zn
EF	Ba, Cd, Co, Cr, Cu, Fe, Ni, P, Pb, S, Sn, Ti, Zn

Table 4.20 summarized the results from t-test , PCA and EF. The elements with atmospheric deposition and contribution of variety pollution emissions are Ba, Co, Cd, Cr, Cu, Fe, Ni, P, Pb, S, Sn, Ti, and V, Zn.

The elements such as Ba, Co, Cd, Cr, Cu, Fe, Ni, Pb, S, Sn, Ti, V, Zn can be tracers of particles from traffic emission, wear of brake lining materials and from combustion of fossil fuels in domestic heating (Monaci and Bargagli, 1997; Caselles et al., 2002; Geo et al., 2002; Arditsoglou and Samara, 2005). The presence of most of elements is due to motor exhaust, that fact underlines the direct impact of the traffic emissions, in roads around this building, on formation of damage layer.

4.3.8. Concluding remarks

The methodological approach followed for analysing the damage layers indicates that gypsum is the main product of deterioration, due to the interaction of the atmospheric sulphur compounds and cement matrix constituents. Furthermore, numerous carbonaceous and aluminosilicate particles were identified in the gypsum matrix of the damage layers. The composition of those black carbonaceous particles reflects theirs role in surface deterioration, elemental carbon causes darkening of the surface, and the metal content can act as catalytic support for the heterogeneous oxidation of SO_2. The effect of air pollutants was also reflected in anions and trace elements accumulated in the black crusts. The elaboration of the enrichment factor indicates that the main sources of air multi-pollutants deposited on the building are traffic emission and oil fossil fuels combustion of domestic heating.

Conclusion

The research activity focused on the impact of the air multi-pollutants on the 20th century architecture, through the diagnosis of the damage induced by gaseous air pollutants and particles on three European buildings mainly constructed in concrete: Centennial Hall, Wroclaw (Poland), Chiesa dell'Autostrada del Sole, Florence (Italy), and Casa Galleria Vichi, Florence (Italy).

The complete characterization of the damage layers present at the cement-based monuments selected was obtained for the first time. The results showed that gypsum is the main damage product at surfaces sheltered from rain run off at Centennial Hall and Casa Galleria Vichi. In addition the mineralogical observations and quantitative results highlighted that gypsum was more abundant in case of Centennial Hall (Wroclaw, Poland) than in Casa Galleria Vichi (Florence, Italy), being this directly linked to the location of the buildings. In fact, the Polish site is placed in one of the most polluted region in Europe by SO_2 and additionally coal power stations are in the neighborhood of the building. By contrast, gypsum has not been identified in the samples collected at Chiesa dell'Autostrada del Sole. It has to be underlined that this is connected to the restoration works, particularly surface cleaning, regularly performed for the maintenance of the building.

Furthermore, both carbonaceous and aluminosilicate particles were found embedded in gypsum matrix. It is known that carbonaceous particles cause the aesthetic impairment (blackening) of the building façade and, because of their heavy metal content, act as catalytic support for the heterogeneous oxidation of SO_2. The presence of carbonaceous particles is related to the combustion of fossil fuels in the power stations and domestic heating. The aluminosilicate particles origin from coal combustion, that in case of Centennial Hall emphasizes the impact of coal power station and coal use in domestic heating.

The discrimination of carbon fractions showed also a difference in concentration of elemental and organic carbon within the damage layer depending on the location. The elemental carbon had higher concentration in samples of black crusts from Centennial Hall than those collected at Casa Galleria Vichi, proving that fix combustion sources, such as electric power plants, predominate in EC emissions over mobile ones. Mobile sources

(traffic) are the major emitters of organic carbon in urban atmospheres. The damage layers collected at Casa Galleria Vichi had higher organic carbon, that is closely connected to traffic emission in front of the building. The quantification of carbon fractions is essential to identify the anthropogenic sources causing deterioration of the built heritage, including aesthetic damage of the surface (i.e. darkening).

The effect of air pollutants was also reflected in anion concentrations detected in the black crusts. Along sulphates and nitrates, there were detected significant amounts of organic anions (acetate, formate, oxalate); their presence, particularly that of the oxalate ion, which origin is still an open problem, allowed to exclude the contribution of the past surface treatments as possible source. The elaboration of elemental data (t-test, PCA, EF) allowed to identify the origin of elements present in the black crust, confirming that Casa Galleria Vichi is more affected by pollutants from traffic emission (e.g. Pb, Zn) and oil fly ash from domestic heating, while Centennial Hall deterioration is mainly caused by multi-pollutants emitted by coal combustion (e.g. As). The enrichment factor elaborations for the samples of Chiesa dell'Autostrada del Sole indicated that Bi, Cr, Cu, Ni arrive from atmospheric deposition and are probably linked to the traffic emissions from the highway in the neighborhood of the building.

In conclusion, SO_2 and particles emitted by combustion sources have been proved to have among the multi-pollutants the priority role in damage layer formation on the cement buildings investigated. Moreover, the results obtained showed the correlation between location of the building and the composition of the damage layer: Centennial Hall is mainly undergoing to the impact of pollutants emitted from the coal power station, whilst Casa Galleria Vichi is principally affected by pollutants from vehicular exhaust. This proves that the major role is played by local sources of pollutants in the damage process occurring on the cement surface. The quantification of EC and OC has been a key factor for the discrimination between fix and mobile combustion sources of pollutants mainly impacting on the buildings investigated. The application on the statistical techniques also allowed to identify the elements with atmospheric origin and to indicate the possible anthropogenic sources, revealing statistical methods as an useful tool for elemental data elaboration in the diagnosis of cultural heritage damage.

The investigation of the impact of air multi-pollutants on the cementitious materials, characterizing modern architecture is fundamental for planning the protection and

conservation of the 20th century built heritage. It has to be underlined that the modern architecture undergoes deterioration and requires to be restored as well as ancient one. In terms of heritage management, frequent surface cleaning should be adopted as building maintenance procedure, with complete removal of the black crusts, avoiding as much as possible the irreversible damage of the cement substrate. Additionally, air pollution monitoring, particularly SO_2 and particulate matter, and air quality control are essential for the preservation of modern built cultural heritage. In fact, the emission of carbonaceous particles has increased in recent years and SO_2 still requires to be controlled, even though the reduction of sulphur content in fossil fuels and the introduction of abatement systems in particular in some European regions. As a final point, the knowledge achieved during this research may also find an application in the construction sector, giving indications for example on the durability of the cement mortars.

References

Alexander, M.G., Mackechnie, J.R., Yam, W., 2007. Carbonation of concrete bridge structures in three South African location. Cement and Concrete Composition 29 (10), 750-759.

Arditsoglou, A., Samara, C., 2005. Levels of total suspended particulate matter and major trace elements in Kosovo a source identification and apportionment study. Chemosphere 59, 669-678.

Bacci, P., Del Monte, M., Longhetto, A., Piano, A., Prodi, F., Redaelli, P., Sabbioni, C., Ventura, A., 1983. Characterization of the particulate emission by a large oil fuel fired plant. Journal of Aerosol Science 14 (4), 557-572.

Bellmann, F., Stark, J., 2007. Prevention of thaumasite formation on concrete exposed to sulphate attack. Cement and Concrete Research 37, 1215-1222.

Benner, W.H., Brodzinsky, R., Novakov, T., 1982. Oxidation of SO_2 in droplets which contain soot particles. Atmospheric Environment 16, 1333-1339.

Bityukova, L., 2006. Air pollution effect on the decay of carbonate buildings stone in old town of Tallinn. Water, Air, and Soil Pollution 172, 239-271.

Blanco-Varela, M.T., Aguilera, J., Martínez-Ramírez, S., Puertas, F., Palomo, A., Sabbioni, C., Zappia, G., Riontino, C., Van Balen, K., Toumbakari, E.E., 2003. Thaumasite formation due to atmospheric SO_2–hydraulic mortar interaction. Cement and Concrete Research 25, 983-990.

Bonazza, A., Sabbioni, C., Ghedini, N., 2005. Quantitative data on carbon fractions in interpreting black crusts and soiling on European built heritage. Atmospheric Environment 39, 2607-2618.

Bonazza, A., Brimblecome, P., Grossi, C.M., Sabbioni, C., 2007. Carbon in black crust from the tower of London. Environmental Science and Technology 41 (12), 4199-4204.

Bonazza, A., Sabbioni, C., Ghedini, N., Hermosin, B., Jurado, V., Gonzalez, J.M., Saiz-Jimenez, C., 2007. Did smoke from the Kuwait oil well fires affect Iranian archaeological heritage? Environmental Science and Technology 41, 2378-2386.

Cachier, H., 1998. Carbonaceous combustions aerosol. In Harrison, R.M., Van Grieken, R. (Eds.), IUPAC Book on Atmospheric Particles. Wiley, New York, pp. 295-348.

Chang, C.F., Chen, J.W., 2006. The experimental investigation of concrete carbonation depth. Cement and Concrete Research 36, 1760–1767.

Caselles, J., Colliga, C., Zornoza, P., 2002. Evaluation of trace element pollution from vehicle emissions in petunia plants. Water, Air, and Soil Pollution 136, 1-9.

Chen, Y., Shah, N., Huggins, F.E., Huffman, G.P., 2004. Investigation of the microcharacteristics of $PM_{2.5}$ in residual oil fly ash by analytical transmission electron microscopy. Environmental Science and Technology 38, 6553–6560.

Collepardi, M., 2003. A state-of-the-art review on delayed ettringite attack on concrete. Cement and Concrete Composites 25, 401-405.

Collett, G., Crammond, N.J., Swamy, R.N., Sharp, J.H., 2004. The role of carbon dioxide in the formation of thaumasite. Cement and Concrete Research 34, 1599-1612.

Crammond, N., 2002. The occurrence of thaumasite in modern construction – a review. Cement and Concrete Composites 24, 393-402.

Czarnecki, L., Broniewski, T., Henning, O., 1996. Chemia w budownictwie (Chemistry building). Arkady, Warszawa.

Davidson, C.I., Wu, Y.L., 1989. Dry Deposition of Trace Elements. In: Pacyna, J.M., Ottar, B. (Eds.), Control and Fate of Atmospheric Heavy Metals, Volume 268. Kluwer Academic Publishers, Dordrecht, pp. 147-202.

De Santis, F., Allegrini, I., 1989. Determinazione di acido ossalico e di ossalati in atmosfera mediante tubi di diffusione. In The Oxalate Films: Origin and Significance in the Conservation of Works of Art. Centro CNR Gino Bozza, Milan, pp. 165-169.

Del Monte, M., Sabbioni, C., Vittori, O., 1981. Airborne carbon particles and marble deterioration. Atmospheric Environment 15 (5), 645-652.

Del Monte, M., Sabbioni C., 1983. Weddellite on limestone in the Venice environment. Environmental Science and Technology 17 (9), 518-522.

Del Monte, M., Sabbioni, C., 1984. Morphology and mineralogy of fly ash from a coal-fueled power plant. Archives for Meteorology, Geophysics, and Bioclimatology Series B35, 93-104.

Del Monte, M., Sabbioni, C., 1987. A study of the patina-called "scialbatura" on Roman Imperial marbles. Studies in Conservation 32, 114-121.

Del Monte, M., Sabbioni, C., Zappia, G., 1987. The origin of calcium oxalates on historical buildings, monuments and naturals outcrops. The Science of the Total Environment 67, 17-39.

Derry, D.J., Malati, M.A., Pullen, J.C., 2001. Effects of atmospheric acids on Portland cements. Journal of Chemical Technology and Biotechnology 76, 1049-1056.

Ekolu, S.O., Thomas, M.D.A., Hooton, R.D., 2006. Pessimum effect of externally applied chlorides on expansion due to delayed ettringite formation: Proposed mechanism. Cement and Concrete Research 36, 688-696.

Gabrisova, A., Havlica, J., Sahu, S., 1991. Stability of calcium sulphoaluminates in water solution with varoius pH values. Cement and Concrete Research 21, 1023-1027.

Gabrovšek, R., Vuk, T., Kaučič, V., 2006. Evaluation of the hydration of Portland cement containing various carbonates by means of thermal analysis. Acta Chimica Slovenica 53, 159-165.

Gao, Y., Nelson, E.D., Field, M.P., Ding, Q., Li, H., Sherrell, R.M., Gigliotti, C.L., Van Ry, D.A., Glenn, T.R., Eisenreich, S.J., 2002. Characterization of atmospheric trace elements on PM2.5 particulate matter over the New York—New Jersey harbor estuary. Atmospheric Environment 36, 1077-1086.

Ghedini, N., Gobbi, G., Sabbioni, C., Zappia, G., 2000. Determination of elemental and organic carbon on damaged stone monuments. Atmospheric Environment 34, 4383-4391.

Ghedini, N., Sabbioni, C., Bonazza, A., Gobbi, G., 2006. A chemical-thermal quantitative methodology for carbon speciation in damage layer on building surfaces. Environmental Science and Technology 40, 939-944.

Gorban, A., Kegl, B., Wunsch, D., Zinovyev, A., 2007. Principal manifolds for data visualisation and dimension reduction. Springer, Berlin – Heidelberg – New York.

Grounds, T., Midgley, H.G., Nowell, D.V., 1988. Carbonation of ettringite by atmospheric carbon dioxide. Thermochimica Acta 135, 347-352.

Hutchinson, A.J., Johnson, J.B., Thompson, G.E., Wood, G.C., Sage, P.W., Cooke, M.J., 1992. The role of fly-ash particulate material and oxide catalysts in stone degradation. Atmospheric Environment 26A (15), 2795-2803.

Jabłońska, M., Smołka–Danielewska, D. 2003. Aluminosilicate particles in fly ash and atmospheric dust. Mineralogical Society of Poland – special papers 22, 82-89.

Köhler, S., Heinz, D., Urbonas, L., 2006. Effect of ettringite on thaumasite formation. Cement and Concrete Research 36, 697-706.

Kupiainen, K., Klimont, Z., 2007. Primary emissions of fine carbonaceous particles in Europe. Atmospheric Environment 41 (10), 2156-2170.

Lanting, R.W., 1986. Black smoke and soiling. In: Lee, S.D., Schneider, T., Grant, L.D., Verkerk, P.J. (Eds.), Aerosols: Research, Risk Assessment and Control Strategies: Proceedings of the Second US-Dutch International Symposium May 1995, Lewis Publishers, Williamsburg VA, pp. 923–932.

Ma, B., Gao., X., Byars, E.A., Zhou, Q., 2006. Thaumasite formation in a tunnel of Bapanxia Dam in Western China. Cement and Concrete Research 36, 716-722.

Mankiewicz, R., 2000. The Story of Mathematics. Princeton University Press.

Marinoni, N., Pellizon Birelli, M., Rostagno, C., Pavede, A., 2003. The effects of atmospheric multipollutants on modern concrete. Atmospheric Environment 37, 4701-4712.

Martínez-Ramírez, S., Thompson, G.E., 1998. Dry and wet deposition studies of the degradation of cement mortars. Materiales de Construcción 48, 15–31.

Martinez-Ramirez, S., 1999. Influence of SO_2 deposition on cement mortar hydration. Cement and Concrete Research 29, 107-111.

Martinez-Ramirez, S., Thompson, G.E., 1999. Wet deposition studies of hydraulic mortars. Materials and Structures 32, 606-610.

Martinez-Ramirez, S., Zamarad, A., Thompson, G.E., Moore, B., 2002. Organic and inorganic concrete under SO_2 pollutant exposure. Building and Environment 37 (10), 933-937.

Massey, S.W., 1999. The effects of ozone and NO_x on the deterioration of calcareous stone. The science of the Total Environment 227, 109-121.

Monaci, F., Bargagli, R., 1997. Barium and other trace metals as indicators of vehicle emissions. Water, Air, and Soil Pollution 100, 89-98.

Monaci, F., Moni, F., Lanciotti, E., Grechi, D., Bargagli, R., 2000. Biomonitoring of airborne metals in urban environments: new tracers of vehicle emission, in place of lead. Environmental Pollution 107 (3), 321-327.

Morselli, L., Olivieri, P., Brusori, B., Passarini, F., 2003. Soluble and insoluble fractions of heavy metals in wet and dry atmospheric depositions in Bologna, Italy. Environmental Pollution 124 (3), 457-469.

Morselli, L., Bernardi., E., Vassura, I., Passarini, F., Tesini, E., 2008. Chemical composition of wet and dry depositions in an urban environment: local, regional and long-range influences. Journal of Atmospheric Chemistry 59, 151-170.

Nagy, S., Rychlicki, S., Siemek, J., 2006. Impact of inactive hard-coal mines processes in Silesian Coal Basin on greenhouse gaseous pollution. Acta Geologica Polonica 56 (2), 221-226.

Nishikawa, T., Suzuki, K., Ito, S., Sato, K., Takebe, T., 1992. Decomposition of synthesized ettringite by carbonation. Cement and Concrete Research 22, 6-14.

Okochi, H., Kameda, H., Hasegava, S., Saito, N., Kubota, K., Igawa, M., 2000. Deterioration of concrete structures by acid deposition – an assessment of the role of rainwater on deterioration by laboratory and field exposure experiments using mortars specimens. Atmospheric Environment 34, 2937-2945.

Ondov, J.M., Zoller, W.H., Gordon, G.E., 1982. Trace element emission on aerosols from motor vehicles. Environmental Science and Technology 16, 318-328.

Ozga, I., Bonazza, A., Tittarelli, F., Bernardi, E., Favoni, O., Ghedini, N., Morselli, L., Sabbioni, C., 2009. Environmental damage in XXth century architecture. In: Brebbia C.A. (Ed.), Structural Studies, Repairs and Maintenance of Heritage Architecture XI. WIT Press, Ashurst Lodge, pp. 581-591.

Ozga, I., Ghedini, N., Bonazza, A., Morselli, L., Sabbioni, C., 2009. The importance of atmospheric particle monitoring in the protection of cultural heritage. In: Brebbia, C.A., Popov, V. (Eds.), Air Pollution XVII. WIT Press, Ashurst Lodge, pp. 259-269.

Pade, C., Guimareas, M., 2007. The CO_2 uptake of concrete in a 100 year perspective. Cement and Concrete Research 37, 1348-1356.

Pavlik, V., 1994. Corrosion of hardened cement paste by acetic and nitric acids. Part I: calculation of corrosion depth. Cement and Concrete Research 24, 551-562.

Pavlík, V., Bajza, A., Rouseková, I., Unčik, S, Dubĭk, M., 2007. Degradation of concrete by flue from coal combustion. Cement and Concrete Research 37, 1085-1095.

Petri, M., Kawalec, M., 1998. Beton do naprawy (Concrete to repair). Renowacje 1, 11-13.

Rampazzi, L., Andreotti, A., Bonaduce, I., Colombini, M.P., Colombo, C., Toniolo, L., 2004. Analytical investigation of calcium oxalate films on marble monuments. Talanta 63, 967–977.

Riontino, C., Sabbioni, C., Ghedini, N., Zappia, G., Gobbi, G., Favoni, O., 1998. Evaluation of atmospheric deposition on historic buildings by combined thermal analysis and combustion techniques. Thermochimica Acta 321, 215-222.

Rodriguez-Navarro, C., Sebastian, E., 1996. Role of particulate matter from vehicle exhaust on porous building stones (limestone) sulfation. The Science of Total Environment 187, 79-91.

Romer, M., 2003. Steam locomotive soot and the formation of thaumasite in shotcrete. Cement and Concrete Composition 25, 1173-1176.

Rossi Manaresi, R., 1996. Oxalate patinas and conservation treatments. In: Realini, M., Toniolo, L. (Eds.), Proceedings of the Second International Symposium on The Oxalate Films in the Conservation of Works of Art. EDITEAM, Milan, pp. 111–127.

Querol, X., Alastuey, A., López-Soler, A., Mantilla, E., Plana, F., 1996. Mineral composition of atmospheric particulates around a large coal-fired power station. Atmospheric Environment 30, 3557-3572.

Sabbioni, C., Zappia, G., 1991. Oxalate patinas on ancient monuments: the biological hypothesis. Aerobiologia 7, 31-37.

Sabbioni, C., 1992. Characterization of atmospheric particles on monuments by scanning electron microscopy/energy dispersive X-ray analyses. In: Electron Microscopy, Volume 2. EUREM 92, Granada, Spain, pp. 773–777.

Sabbioni, C., Zappia, G., 1992. Decay of sandstone in urban areas correlated with atmospheric aerosol. Water, Air, and Soil Pollution 63, 305-316.

Sabbioni, C., Zappia, G., 1992. Atmospheric-derived element tracers on damaged stone. The Science of the Total Environment 126, 35-48.

Sabbioni, C., 1995. Contribution of atmospheric deposition to the formation of damage layers. The Science of the Total Environment 167, 49-55.

Sabbioni, C., Zappia, G., Ghedini, N., Gobbi, G., Favoni, O., 1998. Black crust on ancient mortars. Atmospheric Environment 32, 215-223.

Sabbioni, C., Zappia, G., Riontino, C., Blanco-Varela, M.T., Aguilera, J., Puertas, F., Van Balen, K., Toumbakari, E.E., 2001. Atmospheric deterioration of ancient and modern hydraulic mortars. Atmospheric Environment 35, 539-548.

Sabbioni, C., Bonazza, A., Zappia, G., 2002. Damage on hydraulic mortars: the Venice Arsenal. Journal of Cultural Heritage 3, 83-88.

Sabbioni, C., Ghedini, N., Bonazza, A., 2003. Organic anions in damage layer on monuments and buildings. Atmospheric Environment 37, 1261-1269.

Saiz-Jimenez, C., 1989. Biogenic vs anthropogenic oxalic acid in the environment. In The Oxalate Films: Origin and Significance in the Conservation of Works of Art. Centro CNR Gino Bozza, Milan, pp. 207-214.

Saiz-Jimenez, C., 1993. Deposition of airborne organic pollutants on historical buildings. Atmospheric Environment 27B, 77-85.

Saiz-Jimenez, C., 1995. Deposition of anthropogenic compounds on monuments and their effects on airborne microorganisms. Aerobiologia 11, 161–175.

Sersale, R., Frigione, G., Bonavita, L., 1998. Acid depositions and concrete attack: main influences. Cement and Concrete Research 28 (1), 19-24.

Sims, I., Huntley (nèe Hartshorn), S.A., 2004. The thaumasite form of sulphate attack-breaking the rules. Cement and Concrete Composites 26, 837-844.

Sokal, R.R., Rohlf, F.J. (Eds), 1994. Biometry: the principles and practices of statistics in biological research. W.H. Freeman & Co Ltd.

Stark, J., Bollmann, K., 2002. Investigation into delayed ettringite formation in concrete. Proceedings of the 9th International Congress on the chemistry of cement, New Delhi, India pp. 348–354.

Steiger, M., 2003. Salts and crusts. In: Brimblecombe, P. (Ed.), The Effects of Air Pollution on the Built Environment. Imperial College Press, London, pp. 133-181.

Thaumasite Expert Group, 1999. The thaumasite form of sulfate attack: Risks, diagnosis, remedial works and guidance on new construction. Department of the Environment, Transport and the Regions, Rotherham, UK.

Turpin, B.J., Huntzicker, J.J., 1995. Identification of secondary organic aerosol episodes and quantitation of primary and secondary organic aerosol concentrations during SCAQS. Atmospheric Environment 29, 3527-3544.

Van Balen, K., Toumbakari, E.E., Blanco-Varela, M.T., Aguilera, J., Puertas, F., Palomo, A., Sabbioni, C., Riontino, C., Zappia, G. (Eds.), 2003. Environmental deterioration of ancient and modern hydraulic mortars. Protection and conservation of European cultural heritage. Office for Official Publications of the European Communities, Luxemburg.

Veniale, F., Setti, M., Rodriguez-Navarro, C., Lodola, S., Palestra, W., Busetto, A., 2003. Thaumasite as decay product of cement mortar in brick masonry of a church near Venice. Cement and Concrete Composition 25, 1123-1129.

Werynski, B., 2006. Mineralne spoiwa budowlane (Mineral binders). In: Stefanczyk, B. (Ed.), Budownictwo ogolne volume 1. Materialy i wyroby budowlane. Arkady, Warszawa, pp. 241-291.

Yates, T., 2003. Mechanism of air pollution damage to brick, concrete and mortar. In: Brimblecombe, P. (Ed.), The Effects of Air Pollution on the Built Environment. Imperial College Press, London, pp. 110-118.

Zappia, G., Sabbioni, C., Gobbi, G., 1993. Non-carbonate carbon content on black and white areas of damaged stone monuments. Atmospheric environment 27A (7), 1117-1121.

Zappia, G., Sabbioni, C., Riontino, C., Gobbi, G., Favoni, O., 1998. Exposure tests of building materials in urban atmosphere. The Science of the Total Environment 224, 235-244.

Zivica, V., Bajza, A., 2001. Acid attack cement based materials – a review. Part 1. Principle of acidic attack. Construction and Building Materials 15, 331-340.